

NUMERICAL STUDY OF CRASHWORTHINESS
ON HONEYCOMB FILLER SUBJECTED TO
IMPACT LOADING

TAN SZE PEI

UMP

MASTER OF SCIENCE

UNIVERSITI MALAYSIA PAHANG

UNIVERSITI MALAYSIA PAHANG

DECLARATION OF THESIS AND COPYRIGHT

Author's Full Name : TAN SZE PEI

Date of Birth : 19 SEPT 1990

Title : NUMERICAL STUDY OF CRASHWORTHINESS ON
HONEYCOMB FILLER SUBJECTED TO IMPACT
LOADING

Academic Session : SEM 1 2019/2020

I declare that this thesis is classified as:

- CONFIDENTIAL (Contains confidential information under the Official Secret Act 1997)*
- RESTRICTED (Contains restricted information as specified by the organization where research was done)*
- OPEN ACCESS I agree that my thesis to be published as online open access (Full Text)

I acknowledge that Universiti Malaysia Pahang reserves the following rights:

1. The Thesis is the Property of Universiti Malaysia Pahang
2. The Library of Universiti Malaysia Pahang has the right to make copies of the thesis for the purpose of research only.
3. The Library has the right to make copies of the thesis for academic exchange.

Certified by:

(Student's Signature)

900919-01-6408

New IC/Passport Number
Date:

(Supervisor's Signature)

DR. SITI NADIAH BT MOHD SAFFE

Name of Supervisor
Date:

NOTE : * If the thesis is CONFIDENTIAL or RESTRICTED, please attach a thesis declaration letter.

SUPERVISOR'S DECLARATION

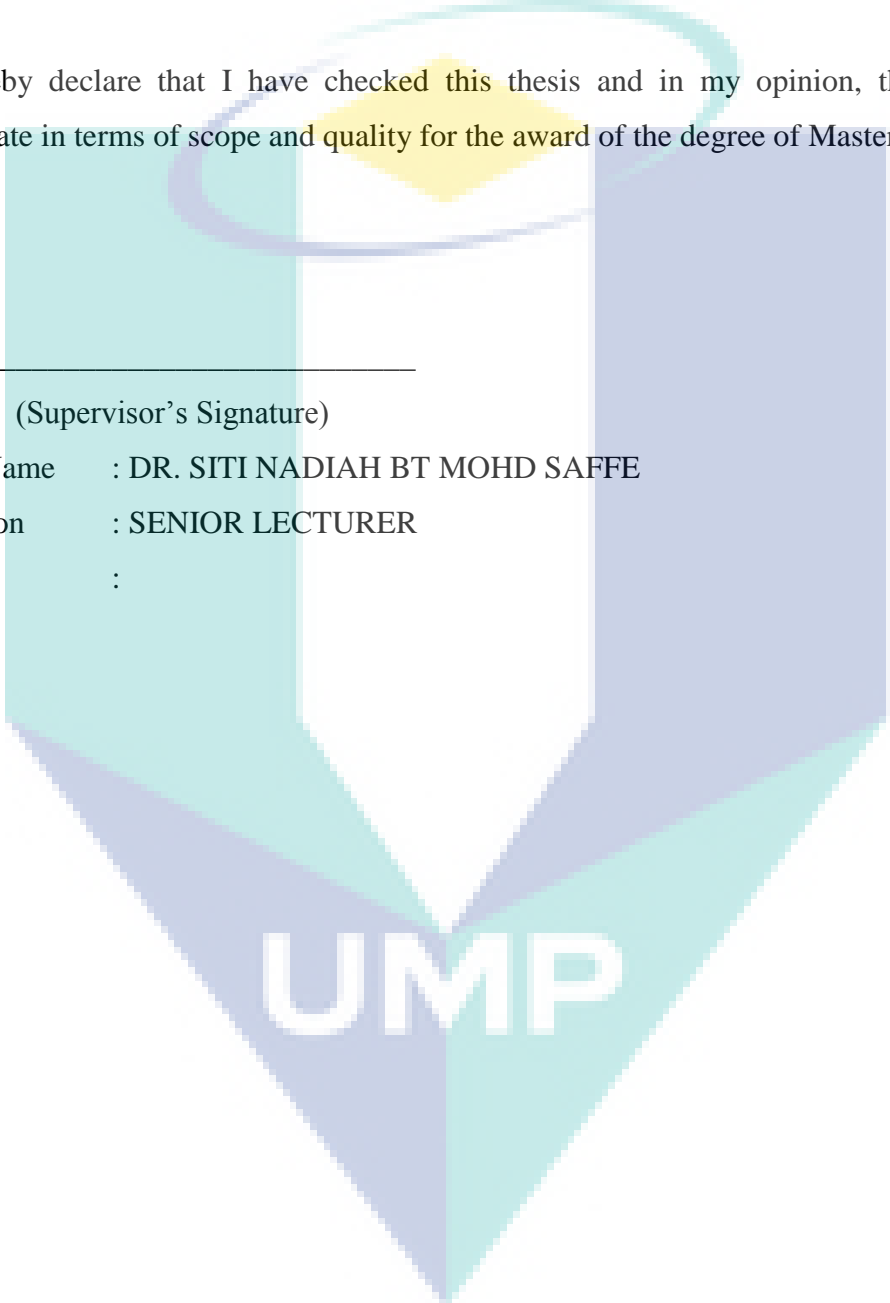
I hereby declare that I have checked this thesis and in my opinion, this thesis is adequate in terms of scope and quality for the award of the degree of Master of Science.

(Supervisor's Signature)

Full Name : DR. SITI NADIAH BT MOHD SAFFE

Position : SENIOR LECTURER

Date :



UMP

STUDENT'S DECLARATION

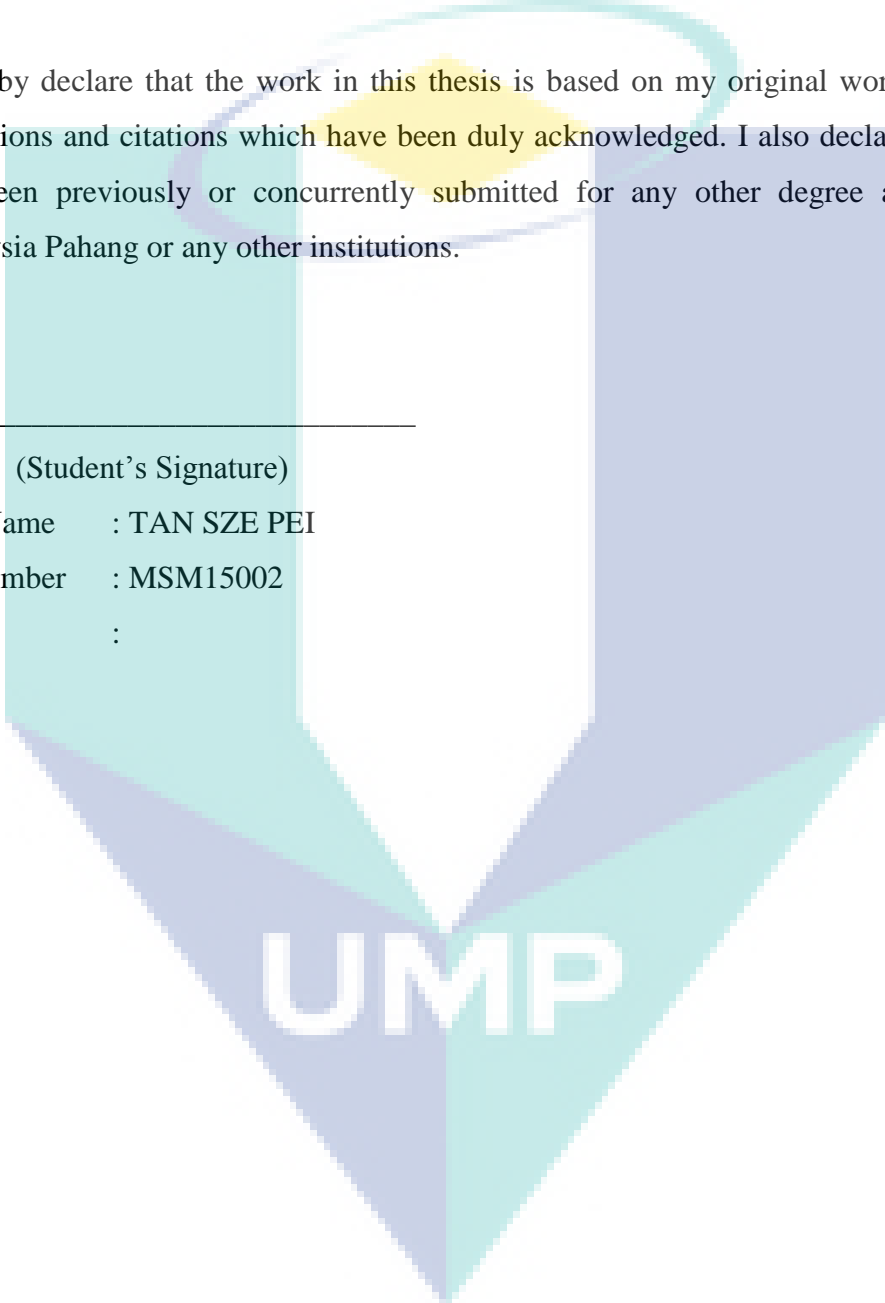
I hereby declare that the work in this thesis is based on my original work except for quotations and citations which have been duly acknowledged. I also declare that it has not been previously or concurrently submitted for any other degree at Universiti Malaysia Pahang or any other institutions.

(Student's Signature)

Full Name : TAN SZE PEI

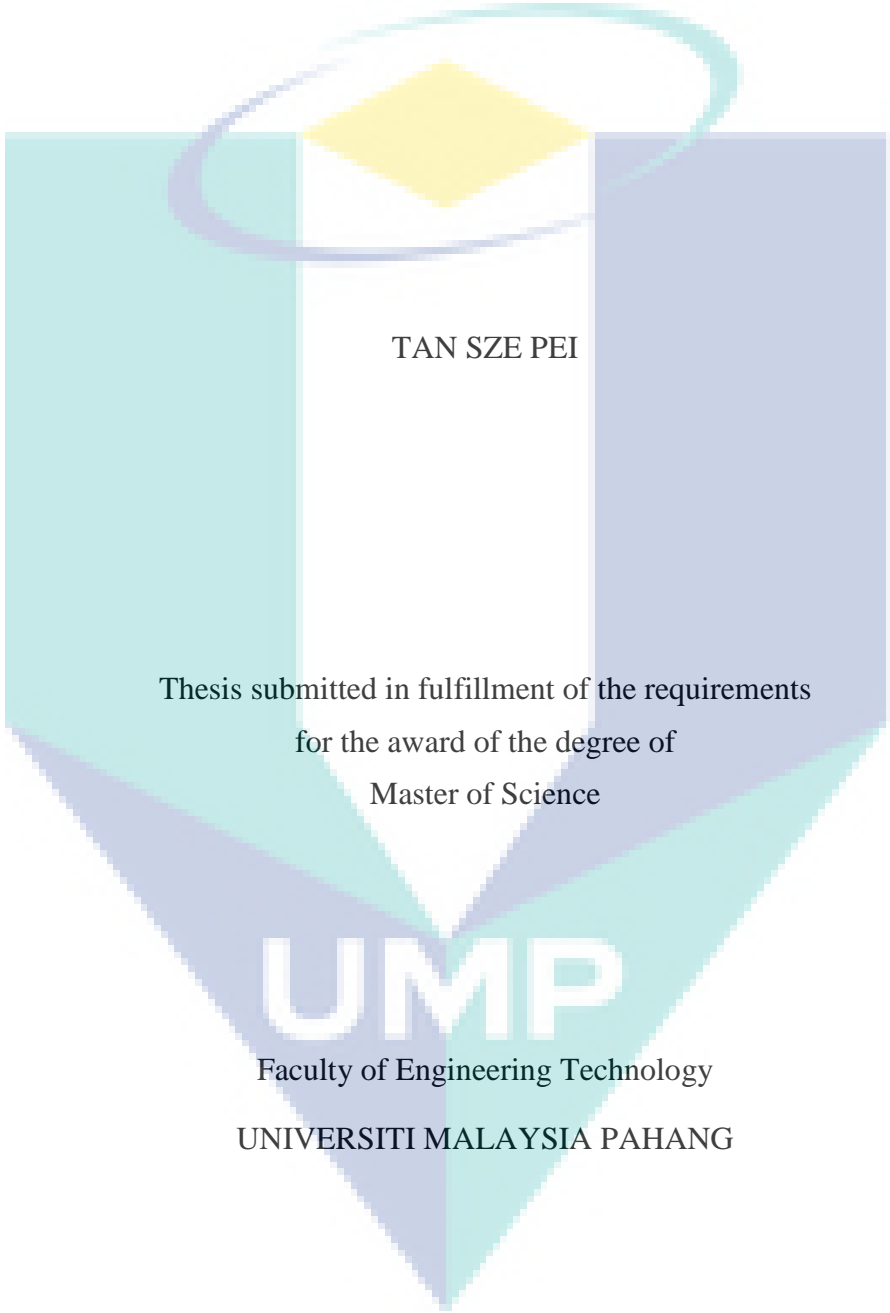
ID Number : MSM15002

Date :



UMP

NUMERICAL STUDY OF CRASHWORTHINESS ON HONEYCOMB FILLER
SUBJECTED TO IMPACT LOADING



TAN SZE PEI

Thesis submitted in fulfillment of the requirements
for the award of the degree of
Master of Science

UMP

Faculty of Engineering Technology

UNIVERSITI MALAYSIA PAHANG

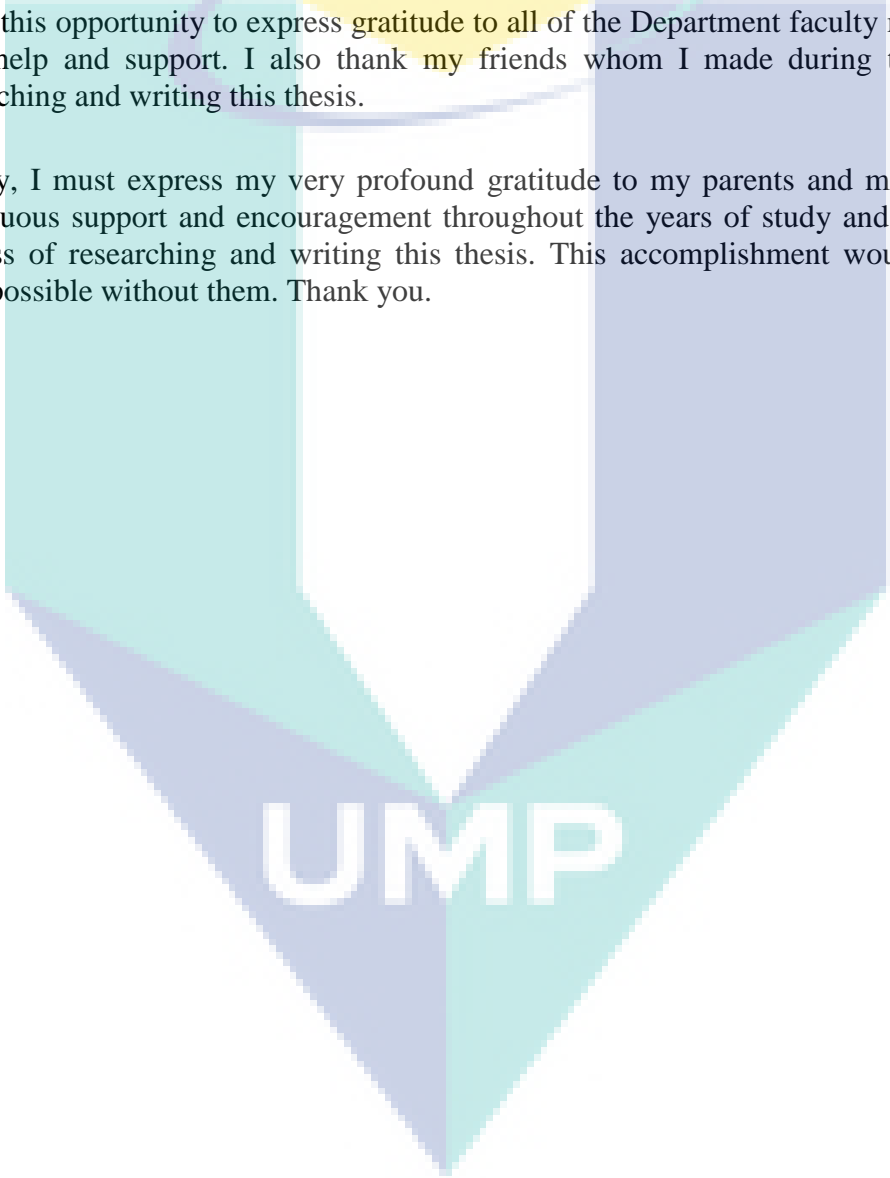
DECEMBER 2019

ACKNOWLEDGEMENTS

I would like to thank my supervisor Dr. Siti Nadiah bt Mohd Saffe of the Faculty of Technology Engineering at Univerity Malaysia Pahang. The door to Dr. Siti office is always open whenever I ran into a trouble spot or had a question about my research or writing. She consistently allowed this thesis to be my own work, but steered me in the right direction whenever she thought I needed it. I would also like to thank my co-supervisor Madam Siti Aishah bt Rusdan and Madam Nurul Nadiah for the encouragement and help whenever I needed it throughout my entire length of study.

I take this opportunity to express gratitude to all of the Department faculty members for their help and support. I also thank my friends whom I made during the years of researching and writing this thesis.

Finally, I must express my very profound gratitude to my parents and my family for continuous support and encouragement throughout the years of study and through the process of researching and writing this thesis. This accomplishment would not have been possible without them. Thank you.

The logo of Universiti Malaysia Pahang (UMPA) is a large, downward-pointing arrow shape. It is composed of several overlapping geometric shapes in shades of teal, light blue, and yellow. The letters 'UMPA' are written in white, bold, sans-serif font across the bottom of the arrow.

UMPA

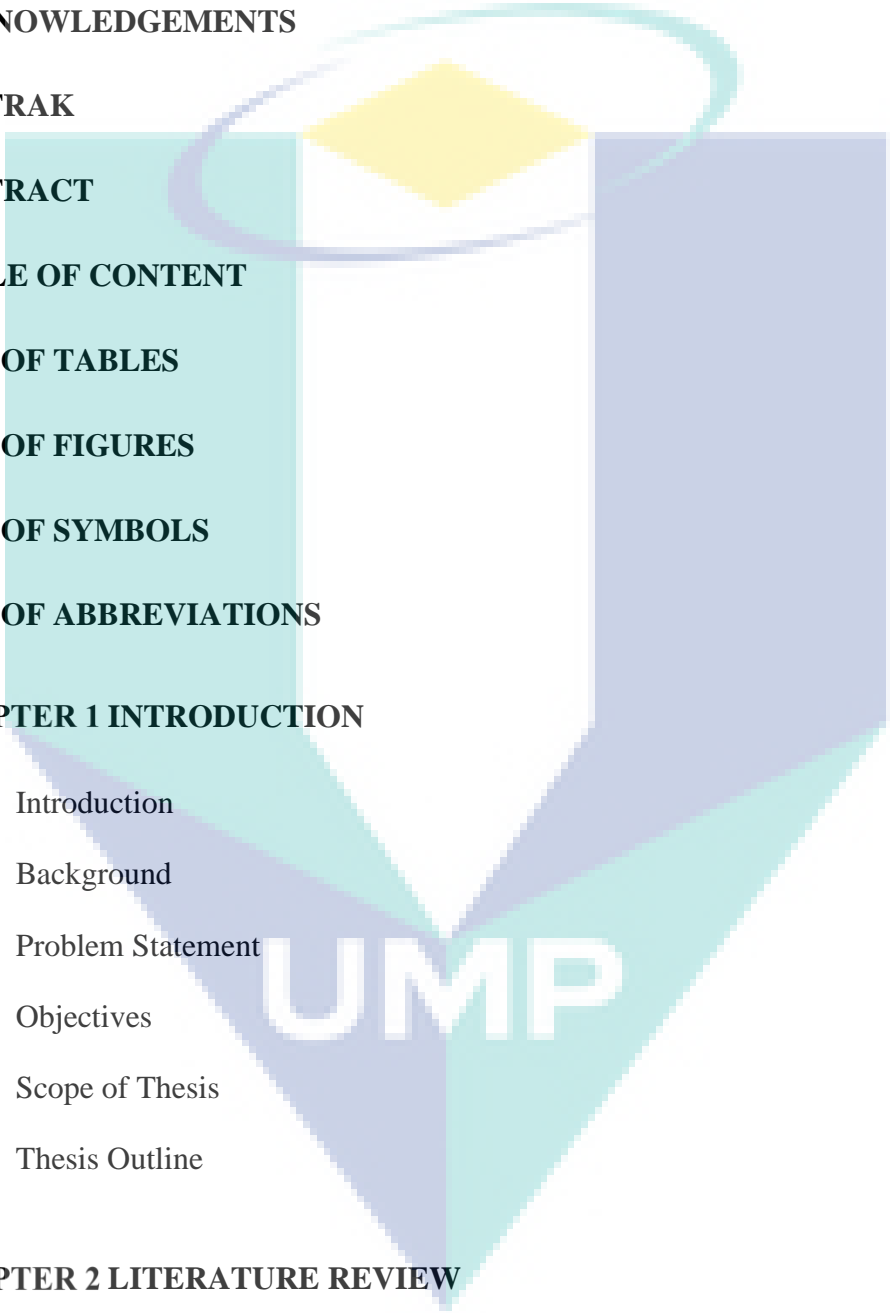
ABSTRAK

Pengisi sarang lebah adalah komponen yang baik bagi peralatan penyerapan tenaga untuk struktur kereta. Banyak kajian berkenaan pengisi sarang lebah di bawah impak hadapan beban paksi telah dijalankan dan dicadangkan di dalam kajian literatur. Namun, apabila kemalangan sebenar terjadi, pelanggaran bukan sahaja datang daripada impak hadapan (beban paksi), malah dari pelbagai sudut (beban serong). Oleh itu, ketahanan pelanggaran daripada pelbagai sudut yang paling penting di dalam rekaan keselamatan kenderaan. Kriteria ketahanan pelanggaran yang dikenali sebagai penyerapan tenaga (EA) dan penyerapan tenaga khusus (SEA) adalah berkait dengan parameter pemuatan. Keselamatan merupakan satu ciri keutamaan di dalam reka bentuk sesebuah penyerap tenaga. Walau bagaimanapun, tidak mengenakan berat berlebihan ke atas penyerap tenaga juga menjadi perhatian pengeluar. Hal ini adalah kerana semakin ringan sesebuah kenderaan, semakin sedikit bahan bakar yang digunakan untuk lebih mesra alam. Objektif utama kajian ini adalah untuk mengkaji prestasi pengisi sarang lebah dengan rekabentuk keratan rentas yang berbeza dengan ketebalan yang dikenakan pada sudut impak pemuatan yang berbeza. Penyiasatan ini dijalankan secara Finite Element (FE) menggunakan perisian ABAQUS. Penyiasatan dilaksanakan dengan mengenakan impak dinamik terhadap semua model FE pengisi sarang lebah. Penyiasatan numerikal mengkaji tindak balas tiga reka bentuk geometri pengisi iaitu pengisi sarang lebah berbentuk bulatan, heksagon dan struktur berbilang sel. Diameter bagi setiap satu sel pengisi sarang lebah ditetapkan kepada 10.4 mm. Tiga ketebalan berbeza bagi setiap sel berukuran $t = 0.06$ mm, 0.12 mm dan 0.18 mm telah dikaji. Semua model dijalankan dengan menggunakan impak dinamik beban paksi dan beban serong yang bersudut $\theta = 0^\circ, 10^\circ, 20^\circ$ dan 30° . Bahan logam yang digunakan terhadap setiap model adalah aloi aluminium AA6060-T4. Berdasarkan rekabentuk struktur tersebut, pengisi sarang lebah berbentuk heksagon adalah reka bentuk yang terbaik. Keputusan bagi EA, SEA dan CFE untuk pengisi sarang lebah berbentuk heksagon ialah 120% lebih tinggi berbanding pengisi sarang lebah berbentuk bulatan dan 230 % lebih tinggi daripada pengisi berbilang sel. Berdasarkan keputusan analisa ini boleh dirumuskan bahawa apabila ketebalan pengisi sarang lebah meningkat, maka prestasi kriteria crashworthiness juga meningkat. Apabila ketebalan meningkat daripada 0.06 mm ke 0.12 mm, EA dan CFE meningkat lebih kurang 290 % dan SEA meningkat lebih kurang 150 %. Apabila ketebalan bertambah daripada 0.12 mm ke 0.18mm, EA, SEA dan CFE masing-masing meningkat lebih kurang 170 %, 120 % dan 190 %. Apabila ketebalan bertambah daripada 0.06 mm ke 0.18, EA, SEA dan CFE masing-masing juga dianggarkan meningkat sebanyak 500 %, 170 % dan 550 %. Peningkatan tersebut adalah lebih tinggi daripada nisbah ketebalan iaitu sebanyak 200 % bagi peningkatan daripada 0.06 mm ke 0.12 mm, 150 % bagi peningkatan daripada 0.12 mm ke 0.18 mm dan 300 % bagi peningkatan 0.06 mm ke 0.18 mm. Akhir sekali, beban paksi dan beban sarang pengisi sarang lebah bersudut $\theta = 0^\circ - 30^\circ$ juga dikaji. Keputusan menunjukkan prestasi EA dan SEA menurun apabila sudut, θ meningkat. Kesimpulannya, keseluruhan keputusan menunjukkan pengisi sarang lebah berbentuk heksagon adalah model terbaik dari segi geometri, ketebalan dan sudut pemuatan.

ABSTRACT

Honeycomb filler is known as a good filler for energy absorbing devices in car. Many types of research about honeycomb filler under axial impact had been done and proposed in the literature. However, when it comes to the real situation in an accident, a collision is not only coming from a frontal impact (axial loading). A collision might also come from a different angle (oblique loading). Therefore, crashworthiness in several impact angles are important concern in designing a safe vehicle. The crashworthiness criteria, namely energy absorption (EA) and specific energy absorption (SEA) are related to loading parameters. Safety is the main concern in designing an energy absorber. However, reducing the extra weight caused by the energy absorber is also one of the concerns for manufacturers. This is because the lighter the weight the vehicle has the lesser fuel is consumed to be eco-friendly. In this study, the main objective is to study the performance of honeycomb fillers by different cross-sectional design versus thickness subjected to different angles of impact loading. The investigation is carried out by Finite Element (FE) simulation using ABAQUS software. The investigations of all FE models are carried out by the dynamic impact test. Numerical investigation studies the reaction of three types of honeycomb filler geometric designs which are circular honeycomb filler, hexagon honeycomb filler and multicell. The diameter of every single cell for honeycomb filler is fixed at 10.4 mm. Three different thicknesses of every cell are investigated which are $t = 0.06$ mm, 0.12 mm, and 0.18 mm. All models are carried out by dynamic impact with both axial and oblique loading which $\theta = 0^\circ, 10^\circ, 20^\circ,$ and 30° . The material assigned to all models is aluminium alloy AA6060-T4. According to simulation result in this study, hexagon honeycomb filler is the best structural design. The result of EA, SEA, and CFE of hexagon honeycomb filler is 120 % higher than circular honeycomb filler and 230 % higher than multicell filler. The crashworthiness is influenced by the thickness of honeycomb filler, the thickness of honeycomb filler increased, then crashworthiness criteria performance increased. When thickness increased from 0.06 mm to 0.12 mm, the EA and CFE increased by approximately 290 % and SEA increased by approximately 150 %. When thickness increased from 0.12 mm to 0.18 mm, the EA, SEA, and CFE increased by approximately 170 %, 120 % and 190 %, respectively. When thickness increased from 0.06 mm to 0.18 mm, the EA, SEA, and CFE increased by approximately 500 %, 170 %, and 550 %, respectively. The increment is much higher than the aspect ratio of thickness of 200 %, 150 %, and 300 % respect to 0.06 mm to 0.12 mm, 0.12 mm to 0.18 mm, and 0.06 mm to 0.18 mm. Lastly, the axial loading and oblique loading of honeycomb fillers with angles, $\theta = 0^\circ - 30^\circ$ are studied. Results showed that the performance of EA and SEA decreased when angles, θ increased. In conclusion, the overall result showed that hexagon honeycomb filler is the best model in terms of geometry, thickness, and angle of loading.

TABLE OF CONTENT

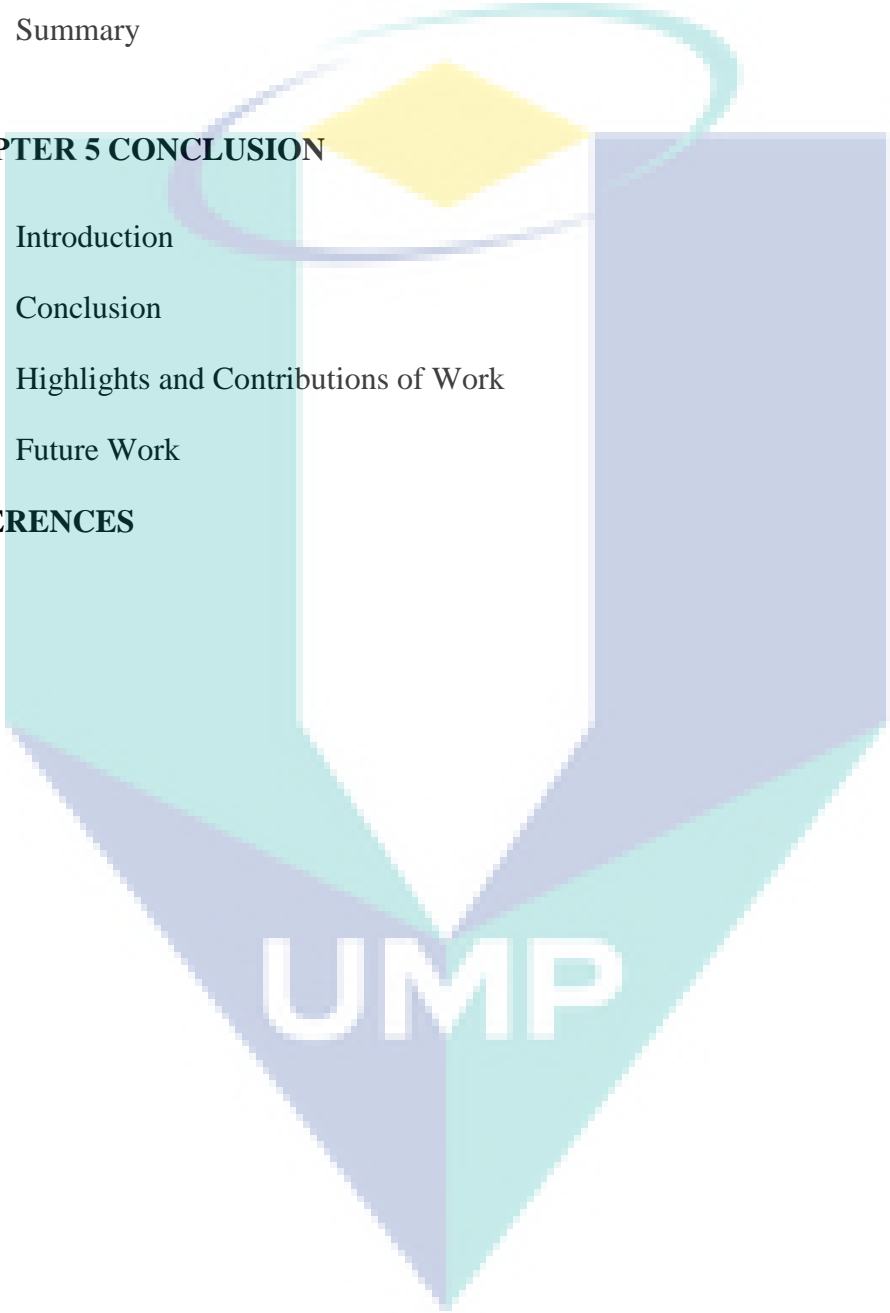


DECLARATION	
TITLE PAGE	
ACKNOWLEDGEMENTS	ii
ABSTRAK	iii
ABSTRACT	iv
TABLE OF CONTENT	v
LIST OF TABLES	ix
LIST OF FIGURES	x
LIST OF SYMBOLS	xii
LIST OF ABBREVIATIONS	xiii
CHAPTER 1 INTRODUCTION	1
1.1 Introduction	1
1.2 Background	1
1.3 Problem Statement	2
1.4 Objectives	3
1.5 Scope of Thesis	3
1.6 Thesis Outline	4
CHAPTER 2 LITERATURE REVIEW	6
2.1 Introduction	6
2.2 Overview	6
2.3 Types of Collision during Car Crash	9

2.3.1	Impact at Different Angle	10
2.3.2	Rollover	12
2.4	Crashworthiness Evaluation of Energy Absorber	12
2.4.1	Total Energy Absorption (EA)	13
2.4.2	Specific Energy Absorption (SEA)	14
2.4.3	Peak Crush Force (PCF)	14
2.4.4	Mean Crush Force (MCF)	14
2.4.5	Crush Force Efficiency (CFE)	15
2.4.6	Stroke Efficiency (SE)	15
2.5	Failure Mode	16
2.5.1	Axial Collapse of Columns	16
2.5.2	Bending Collapse of Columns	20
2.5.3	Modes of Collapse under Axial and Oblique Loading	23
2.6	Principles of Structure Design of Energy Absorber	24
2.6.1	Irreversible Energy Conversion	25
2.6.2	Constant and Stable Crush Force	25
2.6.3	Long Stroke	25
2.6.4	Light Weight with High Specific Energy Absorption Capacity	26
2.7	Previous Work	27
2.7.1	Energy Absorber for Axial Loading	27
2.7.2	Energy Absorber for Oblique Loading	30
2.7.3	Filler of Energy Absorber	31
2.8	Finite Element Application in Crashworthiness	36
2.8.1	Nonlinear Dynamic Explicit Analysis	36
2.8.2	Dynamic Effect on the Crash Resistance	37
2.9	Data Verification	39

2.10	Summary	43
CHAPTER 3 RESEARCH METHODOLOGY		44
3.1	Introduction	44
3.2	Research Plan	44
3.3	Finite Element Model	46
3.3.1	Preliminary Study	46
3.3.2	Design Approach	48
3.3.3	Material Characteristic	50
3.3.4	Boundary Condition	52
3.3.5	Interaction	53
3.3.6	Meshing	55
3.3.7	Steps	57
3.4	Honeycomb Thickness Design and Impact Angles	58
3.5	Summary	59
CHAPTER 4 RESULTS AND DISCUSSION		61
4.1	Introduction	61
4.2	Effect of Geometry	61
4.2.1	0 Degree	61
4.2.2	10 Degrees	63
4.2.3	20 Degrees	64
4.2.4	30 Degrees	66
4.2.5	Overall Result	67
4.3	Effect of Thickness	69
4.3.1	0 Degrees	69

4.3.2	10 Degrees	73
4.3.3	20 Degrees	77
4.3.4	30 Degrees	80
4.3.5	Overall Result	84
4.4	Summary	85
CHAPTER 5 CONCLUSION		87
5.1	Introduction	87
5.2	Conclusion	87
5.3	Highlights and Contributions of Work	90
5.4	Future Work	90
REFERENCES		92

A large, semi-transparent watermark of the UMPA logo is centered on the page. The logo consists of a shield-like shape with a yellow diamond at the top, a white vertical bar in the center, and a teal and blue gradient at the bottom. The letters 'UMP' are written in white across the bottom of the shield.

UMP

LIST OF TABLES

Table 2.1	General road accident data in Malaysia (2007-2017)	8
Table 2.2	Collapse modes of square columns under axial loading	18
Table 2.3	Comparison of explicit and implicit integration techniques	37
Table 2.4	Geometry details and material properties for aluminum	40
Table 2.5	True stress-strain data of the aluminum alloy	40
Table 2.6	The details of the validation models	41
Table 2.7	Strain hardening data for AA6060 T4	41
Table 2.8	FE simulation and experimental solution of empty circular tubes	42
Table 3.1	Comparison of FE simulation and experimental data of preliminary study	48
Table 3.2	Design variable of parameter on angle of loading	58
Table 3.3	Honeycomb thickness and labelling of models	59
Table 3.4	Design variables and labelling of models subjected to angle of loading	60
Table 4.1	The result of honeycomb filler versus geometry at 0 degrees	62
Table 4.2	The result of honeycomb filler versus geometry at 10 degrees	63
Table 4.3	The result of honeycomb filler versus geometry at 20 degrees	64
Table 4.4	The result of honeycomb filler versus geometry at 30 degrees	66
Table 4.5	Summary of honeycomb filler versus geometric and structure subjected by different angle of loading	69
Table 4.6	Result of honeycomb filler versus thickness at 0 degrees impact loading	70
Table 4.7	Result of honeycomb filler versus thickness at 10 degrees impact loading	74
Table 4.8	Result of honeycomb filler versus thickness at 20 degrees impact loading	77
Table 4.9	Result of honeycomb filler versus thickness at 30 degrees impact loading	81
Table 4.10	Summary of result for honeycomb filler influenced by thickness versus angle of loading	84
Table 5.1	Aspect ratio of model versus thickness in every angle of loading	89

LIST OF FIGURES

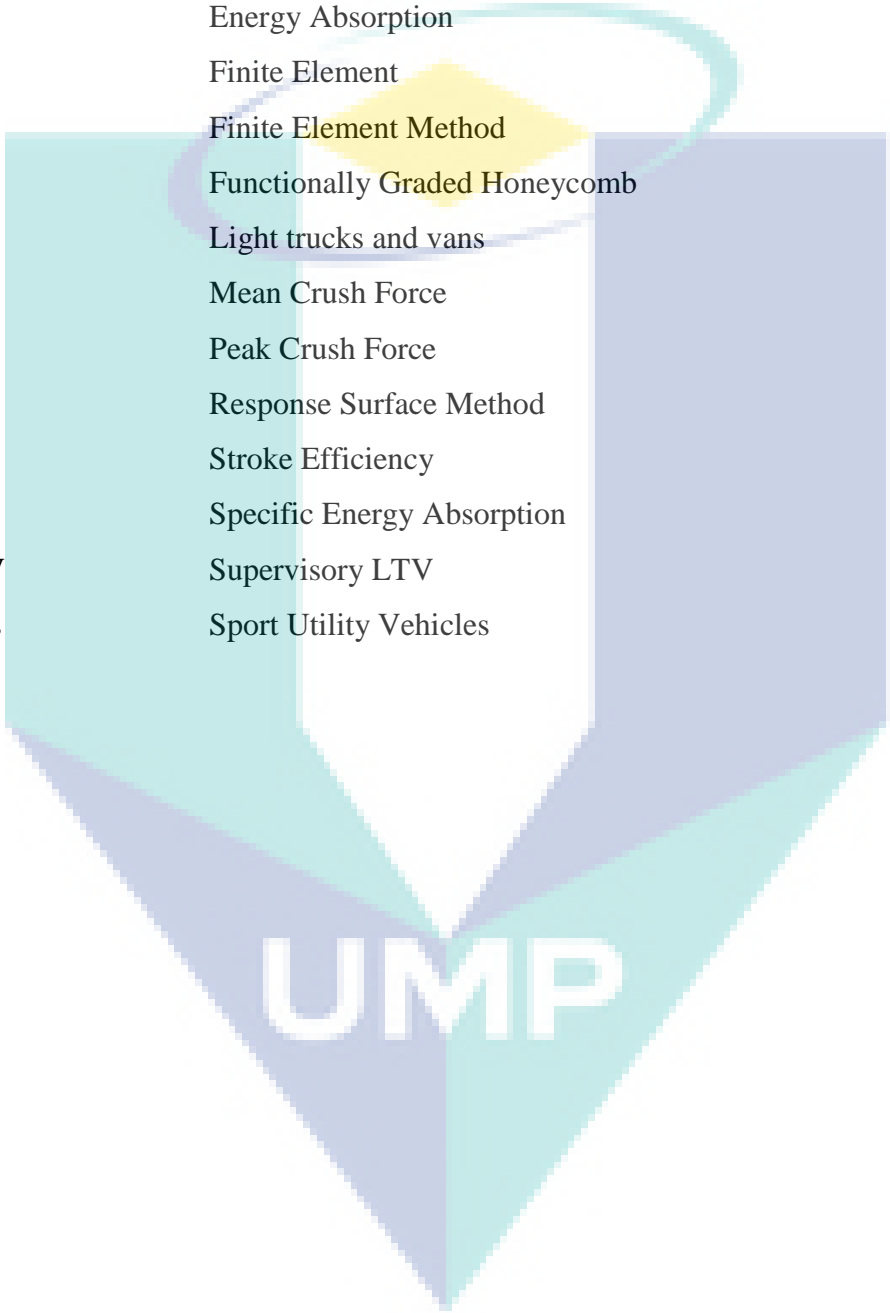
Figure 1.1	Structural of vehicle	2
Figure 2.1	The number of newly registered vehicles in Malaysia from year 1998 - 2018	8
Figure 2.2	Statistical analysis probability of crash direction	10
Figure 2.3	Possible frontal test conditions	11
Figure 2.4	Force-displacement graph for energy absorbing devices	13
Figure 2.5	Superfolding-elements: (a) type I (b) type II	17
Figure 2.6	Analysis of bending collapse of columns by Kecman: (a) typical hinge collapse mechanism (b) cross section at the hinge (c) theoretical model (d) development stages of hinge	21
Figure 2.7	Analysis of bending collapse of columns by Wierzbicki: (a) simplified collapse mode of a column in bending and (b) the collapse mode superposed on the deformed FE mode	22
Figure 2.8	Types of oblique crushing: (a) angled loading, (b) off-axis loading	23
Figure 2.9	Illustration of (a) type A and (b) type B patterns.	28
Figure 2.10	Cross-sectional geometry of multicell prismatic columns, (a) Chen & Wierzbicki (2001), (b) Kim (2002), (c) Zhang et al. (2006), (d) Zhang & Cheng (2007), (e) Hou et al. (2008), (f) Zhang et al. (2009), (g) Najafi & Rais-Rohani (2011), (h) Zhang & Zhang (2013).	35
Figure 3.1	The adopted research methodology approached	45
Figure 3.2	Force-Displacement response of FE model (a) Gameiro's model (b) preliminary study	47
Figure 3.3	Absorbed energy response of FE model (a) Gameiro's model (b) preliminary study	47
Figure 3.4	Honeycomb material direction	48
Figure 3.5	Cross-sectional view of the honeycomb fillers (mm) (a) hexagon honeycomb filler (b) circular honeycomb filler and (c) multicell filler	49
Figure 3.6	FE model of hexagon honeycomb filler with the angle of θ , 20°	50
Figure 3.7	Setting of material properties with unit (a) density (tonne/mm ³) (b) young's modulus (N/mm ²) (c) yield stress (%) and plastic strain (MPa)	51
Figure 3.8	Boundary condition of (a) bottom plate (b) top plate	52
Figure 3.9	Setting of velocity for top plate (mm/s)	53
Figure 3.10	Setting of impact load for top plate (tonne)	53
Figure 3.11	Interaction of honeycomb, top and bottom plate (a) constraint setting set as tie (b) surface contact of both top and bottom plate with honeycomb	54
Figure 3.12	Contact property setting of (a) friction coefficient (b) hard contact	55

Figure 3.13 Surface contact between master and slave	55
Figure 3.14 Setting of mesh size: 0.4 mm	56
Figure 3.15 Setting of mesh type	57
Figure 3.16 Setting of mesh element	57
Figure 3.17 Setting of step	58
Figure 3.18 Setting of thickness and integration point (mm)	59
Figure 4.1 Force displacement of honeycomb filler at 0 degrees of impact loading	62
Figure 4.2 Force displacement of honeycomb filler at 10 degrees of impact loading	63
Figure 4.3 Force displacement of honeycomb filler at 20 degrees of impact loading	65
Figure 4.4 Force displacement of honeycomb filler at 30 degrees of impact loading	66
Figure 4.5 Overall performance of honeycomb filler when angle of loading	68
Figure 4.6 Effect of thickness on EA across geometric design when $\theta = 0$ degrees	70
Figure 4.7 Effect of thickness on SEA across geometric design when $\theta = 0$ degrees	71
Figure 4.8 Effect of thickness on CFE across geometric design when $\theta = 0$ degrees	73
Figure 4.9 Effect of thickness on EA across geometric design when $\theta = 10$ degrees	74
Figure 4.10 Effect of thickness on SEA across geometric design when $\theta = 10$ degrees	75
Figure 4.11 Effect of thickness on CFE across geometric design when $\theta = 10$ degrees	76
Figure 4.12 Effect of thickness on EA across geometric design when $\theta = 20$ degrees	78
Figure 4.13 Effect of thickness on SEA across geometric design when $\theta = 20$ degrees	79
Figure 4.14 Effect of thickness on CFE across geometric design when $\theta = 20$ degrees	80
Figure 4.15 Effect of thickness on EA across geometric design when $\theta = 30$ degrees	81
Figure 4.16 Effect of thickness on SEA across geometric design when $\theta = 30$ degrees	82
Figure 4.17 Effect of thickness on CFE across geometric design when $\theta = 30$ degrees	83

LIST OF SYMBOLS

Fds	Area under the load-displacement
m	Mass of the component
h	Thickness of shell
C	Material-dependent constant
D	Diameter
D_{shell}	Diameter of the shell
E	Energy absorbed
M_0	Column wall flow stress
c	Width of the column
H	Half-fold length
d	Crushing distance
d_{max}	Effective crushing distance
$\sigma_{0.2}$	0.2% plastic strain
σ_{Ult}	Ultimate stress
σ_0	Flow stress
β	Hinge rotation angle
P_d	Dynamic crash force
P_s	Static crash force
V_0	Initial impact velocity
σ_0^d	Dynamic flow stress
σ_0^s	Static flow stress
P	Material constants determined from the dynamic tensile tests
$^\circ$	Degree of angles
θ	Angle of loading
r	Radius
t	Thickness
s	Displacement

LIST OF ABBREVIATIONS



CAE	Computer-Aided Engineering
CFE	Force Efficiency Crush
CO ₂	Carbon dioxide
EA	Energy Absorption
FE	Finite Element
FEM	Finite Element Method
FGH	Functionally Graded Honeycomb
LTVs	Light trucks and vans
MCF	Mean Crush Force
PCF	Peak Crush Force
RSM	Response Surface Method
SE	Stroke Efficiency
SEA	Specific Energy Absorption
SLTV	Supervisory LTV
SUVs	Sport Utility Vehicles

CHAPTER 1

INTRODUCTION

1.1 Introduction

This chapter will describe the basic background, problem statement, objectives and scope of research. The background of research will be discussed in the first part of the chapter. Problem statement of the research will be discussed in Chapter 1.3. Later, objectives of the research will be mentioned in Chapter 1.4. The scope of the research will be discussed next. Lastly, thesis outline will go through before starting of Chapter 2, Literature Review.

1.2 Background

The expression “crashworthiness” gives a proportion of the capacity of a structure and any of its parts to secure the occupants in survivable accidents. Back to early historical of vehicle basic advancements, vehicle bodies were manufactured from wood, and the objective of crashworthiness was to prevent vehicle deformations much as could be expected. Throughout the years, the body structures evolved to incorporate progressive crush zones to absorb part of the crash kinetic energy by plastic deformations. At present, vehicle bodies are manufactured fundamentally of stepped steel panels and assembled using various securing techniques. Designers make vehicles to provide occupant insurance by maintaining integrity of the passenger compartment and by simultaneously controlling the crash deceleration pulse to fall below the upper limit of human tolerance. An accident deceleration pulse with an early peak in time and a gradual decay is more beneficial for protection of a restrained occupant. Consequently, the objective of crashworthiness is improving vehicle structure that can dissipate the kinetic energy by controlling vehicle deformations while maintaining satisfactory space

so that the residual crash energy can be managed by the restraint systems to reduce crash loads transfer to the vehicle occupants.

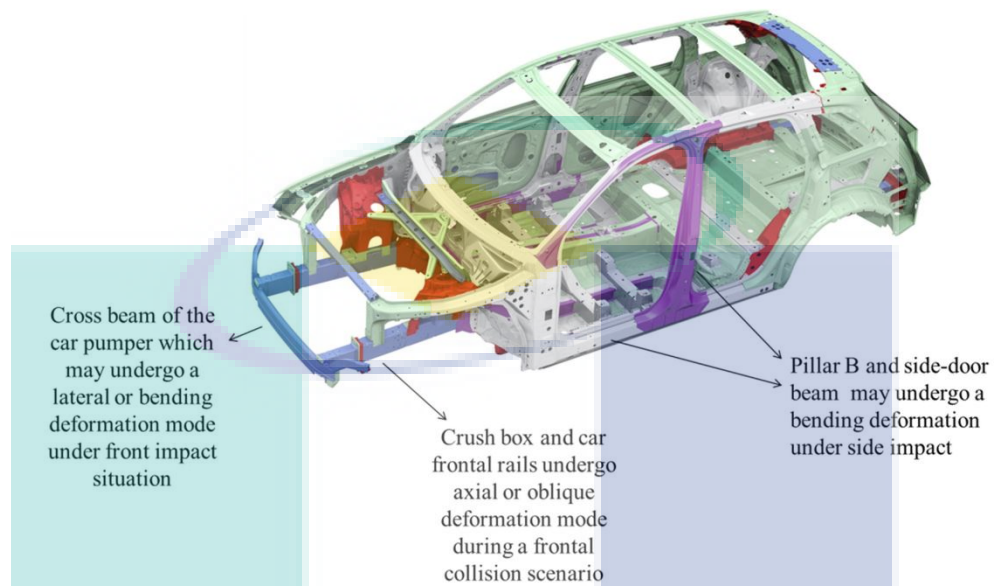


Figure 1.1 Structural of vehicle

Source: Baroutaji et al. (2017)

1.3 Problem Statement

Lightweight vehicle is the challenge for the car manufacturer in the design of the modern era. Only by reducing the weight of the vehicle will make the vehicles have low fuel consumption and emissions. Hence, the concern for the crashworthiness of lighter vehicles that the fatality rates of occupants of the lighter vehicle (Evans, 2001), all things considered, a few times higher than the occupants of the heavier vehicle in a multivehicle accident (Evans, 1989; Tolouei et al., 2013). The increased incorporation of both passive and active energy-absorbing devices gives rise to an increase in the weight of the vehicle. This is proved by the fact that historically for a specific car model, the ratio of overall vehicle mass to “body-in-white” mass has increased (Wallentowitz & Adam, 1996).

For the solutions to these competing design objectives of security and eco-friendly lie at the beginning of innovative designs and materials. Aluminium is material used in the replacing on conventional mild steel engine cradle. The new design proved that a weight reduction of 34%, while still meeting crashworthiness requirements (Triantos & Michaels, 1999). Furthermore, another challenge of the car manufacturer is

to improve the safety of the vehicle during the crash. The energy absorber played an important role to protect passengers. To improve the performance of energy absorber, an extensive study on thin-walled structural is carried out. Aluminium honeycomb is utilized as filler in structural crash components. The crash responds in the mode of collapse is observed, resulting in a further increase in energy absorption per unit weight. The finite element (FE) method has been utilized in the automotive industry to study crashworthiness for quite a long while (Wallentowitz & Adam, 1996). The FE method takes into account the improvement of various structure design configurations, more test to carry out on evaluation in a much shorter time, and at a significantly lower cost than testing.

The energy absorber with filler is presenting that improved the performance of energy absorption. Even though the frontal impact is the domain of the study yet the different angle of impact collision is also the concern during design. In this research, a different type of fillers with different thickness of models impacted by different angles collision has been proposed.

1.4 Objectives

The objectives of this research are as below:

- To evaluate an efficient energy absorber of honeycomb filler of the structures subjected to dynamic impact loading of different angles. The efficiency is evaluated based on the crashworthiness criteria namely energy absorption (EA), specific energy absorption (SEA) and crush force efficiency (CFE) value.
- To determine the influence of different thickness of honeycomb filler on the performance of EA, SEA and CFE.

1.5 Scope of Thesis

This study focuses on the energy absorption capability of honeycomb filler. The honeycomb filler is subjected to frontal dynamic impact loading with different angles, which are axial and oblique impact, 0° , 10° , 20° and 30° . Various geometrical designs of honeycomb filler will be investigated and evaluated by using crashworthiness performance indicator analysis. In terms of geometric structure designs which are

hexagon, circular and multicell. Three different thicknesses of every cell are investigated which $t = 0.06$ mm, $t = 0.12$ mm and $t = 0.18$ mm are investigated. The study will be carried out by simulation using ABAQUS software. The crashworthiness criteria EA, SEA and CFE are related to loading parameters.

Simulation by finite element method has been known as a powerful technology for performance of system functioning. The study focuses on simulation test only with limited experimental data for verification. These data are taken from available experimental data in literatures. The literatures are from Gameiro and Cirne (2007) also Zarei and Kröger (2008). This simulation was performed by ABAQUS dynamic-explicit code. Similar works were conducted by other researches such as Sun et al. (2016), Xiang & Du (2017), Yin et al. (2011) and Zhang et al. (2016). For that, the simulation used in this study is acceptable.

Regarding this study, there are three types of geometrical design of honeycomb filler for this study. From previous study, circular honeycomb filler was found to perform better than hexagon honeycomb filler in in-plane compression loading test (Oruganti & Ghosh, 2008).

1.6 Thesis Outline

This thesis is divided into five chapters. The organizing of chapters as follows:

Chapter 1: Introduction

A brief background of this research is given in this chapter. This chapter includes the background and problem statement in order to justify the motivation for this research, as well as the objectives and scope of this research. The organization of the thesis is given at the end of this chapter.

Chapter 2: Literature Review

A concise review of literature relevant to this research is presented in this chapter. The main purpose of this review is to gain a sound understanding on the fundamentals of the type of collision during car accident, crashworthiness performance indicator analysis and failure mode of energy absorber. This review is essential to

identify the gaps in the current body of knowledge as well as to justify the rationale for carrying out this research.

Chapter 3: Methodology

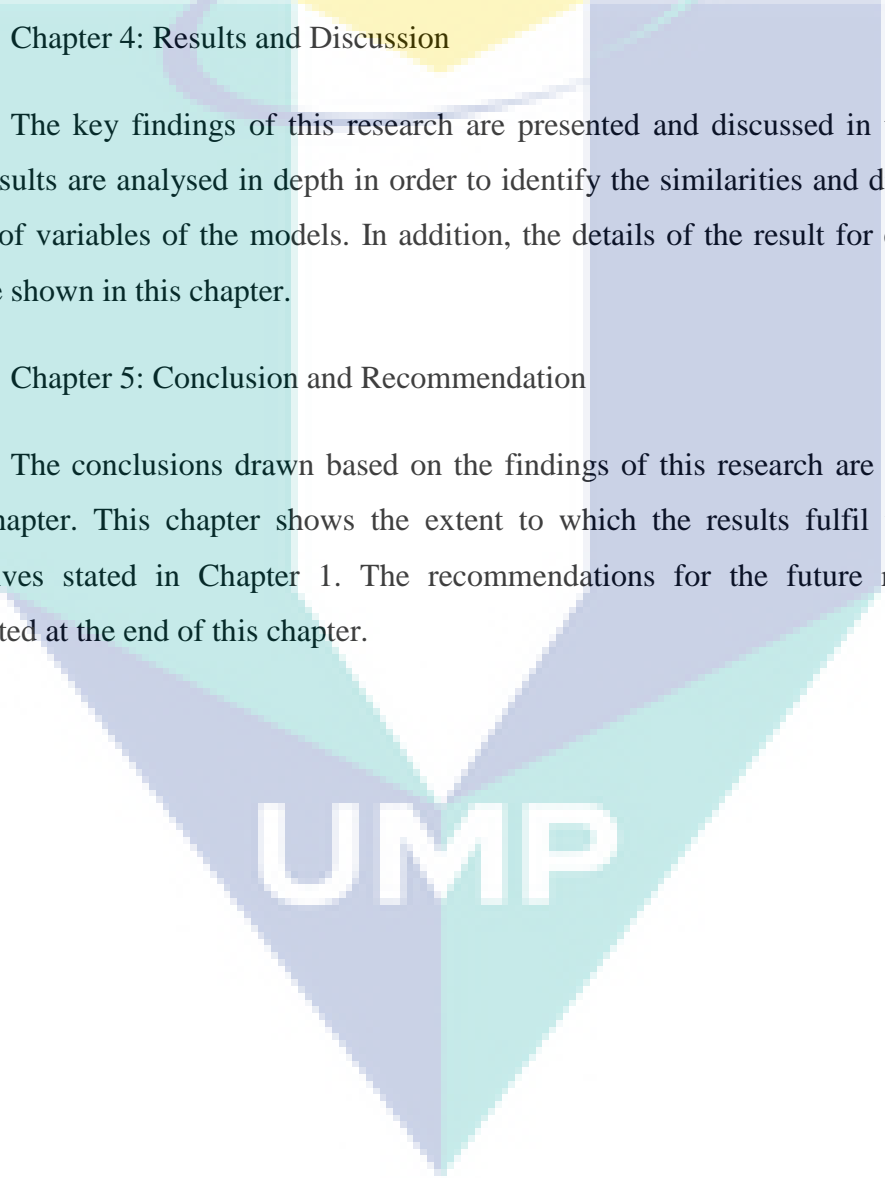
The methodology used to meet the objectives of this research is described in detail in this chapter, the procedure used for the FE simulations, designation of the proposed model and validation model to be carried out.

Chapter 4: Results and Discussion

The key findings of this research are presented and discussed in this chapter. The results are analysed in depth in order to identify the similarities and differences in effect of variables of the models. In addition, the details of the result for every model will be shown in this chapter.

Chapter 5: Conclusion and Recommendation

The conclusions drawn based on the findings of this research are presented in this chapter. This chapter shows the extent to which the results fulfil the research objectives stated in Chapter 1. The recommendations for the future research are presented at the end of this chapter.

The logo for UIMP (Universiti Malaysia Perlis) is a large, stylized letter 'V' shape. The left side of the 'V' is light blue, the right side is light purple, and the bottom point is a darker blue. The letters 'UIMP' are written in white, bold, sans-serif font across the center of the 'V' shape.

UIMP

CHAPTER 2

LITERATURE REVIEW

2.1 Introduction

This chapter will review the crashworthiness of energy absorber. Various designs and angles of loading conditions on energy absorber are presented as the following chapters. Crashworthiness is the most important criteria in designing a safety vehicle, so, the types of collisions, crashworthiness evaluation, failure modes and principal of structure design on energy absorber are included in this part. Next, the energy absorber regarding the axial loading and oblique loading in terms of geometry parameters and materials of the previous research are reviewed. In addition, the geometric structural and parameter designs are studied to understand the performance and relation under loading. Lastly, the data verification and finite element application in crashworthiness are reviewed and expressed.

2.2 Overview

Crashworthiness is an approach that gives protection to human in a vehicle. This approach is to reduce injury to the occupant during an accident. In this technique, the structural and materials to be utilized are capable of providing superior performance in energy absorption and retained post-crushing integrity over a long displacement during the crash (Zhou et al., 1991).

In perspective of crashworthiness, dissipating kinetic energy during impact is the vital concern in the design of vehicle. Many researches work into crashworthiness had been done since 1960s particularly in the car and military industries (Lu & Yu, 2003). Johnson & Reid (1978) summarized the studies of energy absorbers in 1970s and proposed that the metallic structural components can dissipate energy whilst undergoing

plastic deformation. In spite of the fact that passenger safety had improved fundamentally since 1966, when federal motor vehicle standards were first enacted, new challenges exist with user and manufacturer pressure to develop “green” or eco-friendly cars such as, low emission of carbon dioxide (CO₂) and fuel-efficient. The most immediate strategy for reducing fuel consumption and CO₂ emissions is to reduce the weight of the vehicle. New vehicle structures will incorporate space frame technology. Space frames are composed of thin-walled components that are formed to meet at nodes.

In an accident, the thin-walled components of the space frame retain energy through a combination of bending and collapse (Langseth & Hopperstad, 1996). The crash response of structure during impact is the design involving a non-linear and highly complex investigation. In the other hand, the frontal collisions are considered here because in compare to other modes of collision such as side-impact, rear and roll-over, the frontal collision impact has a higher fatality rate (Witteman, 1999). The adequate energy absorbed by the crashworthy structure is able to minimize the serious injuries or prevent permanent brain damage to the passenger (Carruthers et al., 1998; Jacob et al., 2003). Consequently, the design of the structures for controlling a collapse could consider a factor of lighter weight which is more efficient than the most heavier structure on the design of catastrophic failure, for example, metals (Jacob et al., 2002).

Vehicle is an essential part of our life as a need and pleasure. The development of the civilisation in this world had increased the demand for vehicles. Based on the data from World Health Organization, WHO (2015), the quantity of these vehicles is expanding year by year through globe. From year 2010 to 2013, there had been 16 % increase in the quantity of vehicles on the world’s streets around the world. In 2014 alone, a record 67 million passenger cars are newly registered. In Malaysia, the quantity of newly registered vehicles for the last 20 years is increasing consistently as in Figure 2.1. Then, technology in transportation is improved and prompted gigantic and higher speed vehicles. On the off chance that the passengers are involved in an accident, the damage to passenger and cargo will be more serious as these vehicles convey higher kinetic energy during crash. According to WHO, the report presented that the quantity of death cases around the world during road accident had levelled at 1.25 million a year. It caused a huge impact on health and development. In any case, there is something that

the country should be concerned of, that are increase in fatalities and injuries due to collision of vehicles and crashworthiness and vehicle safety.

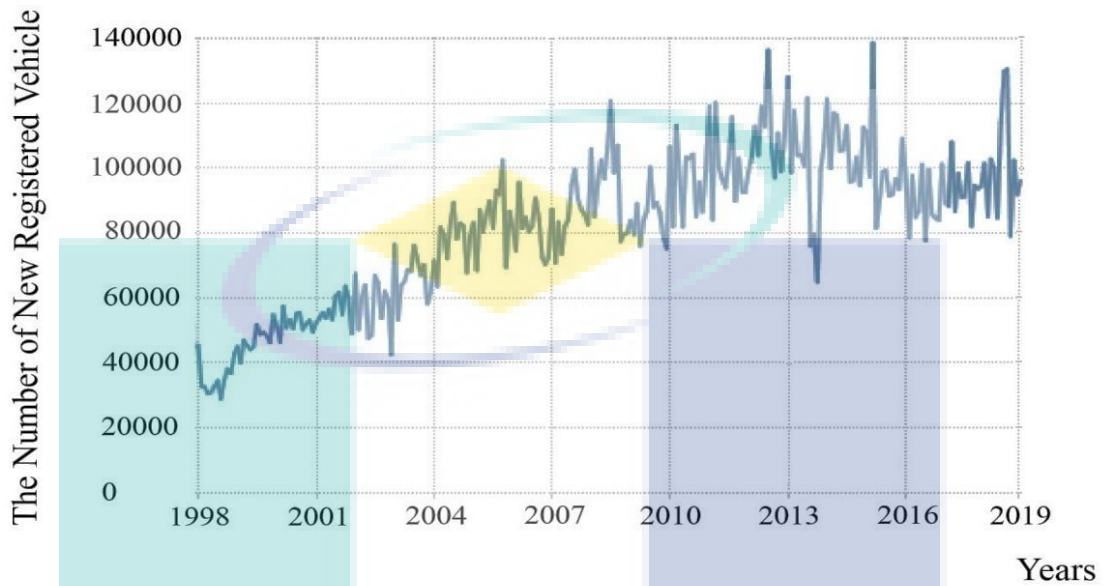


Figure 2.1 The number of newly registered vehicles in Malaysia from year 1998 - 2018

Source: Trading Economics (2019)

Table 2.1 General road accident data in Malaysia (2007-2017)

Year	Road Crashes	Road Deaths	Serious Injury	Minor Injury	Total Death and Injured
2007	363,319	6,282	9,273	18,444	33,999
2008	373,071	6,527	8,868	16,879	32,274
2009	397,330	6,745	8,849	15,823	31,417
2010	414,421	6,872	7,781	13,616	28,269
2011	449,040	6,877	6,328	12,365	25,570
2012	462,423	6,917	5,868	11,654	24,439
2013	477,204	6,915	4,597	8,388	19,900
2014	476,196	6,674	4,432	8,598	19,704
2015	489,606	6,706	4,120	7,432	18,258
2016	521,466	7,152	4,506	7,415	19,073
2017	533,875	6,740	3,310	6,539	16,589

Source: Ministry of Transport Malaysia (2017)

Figure 2.1 showed the new registered vehicles in Malaysia from year 1998 to 2018. Meanwhile, Table 2.1 showed the report of general road accident data in Malaysia from year 2007 to 2017. According to the data in Figure 2.1, the newly registered vehicles in Malaysia were increasing yearly in last 10 years. Simultaneously, there is an increasing trend of road accident cases reported by Ministry of Transport

Malaysia. However, the total number of fatalities and injuries during road accident decreased from 33,999 cases to 16,589 cases between years 2007 to 2017. It had reduced 50 % of cases compared to last 10 years.

From Table 2.1, the number of death during accident was averagely 6,700 cases. Thus, the number of serious injury and minor injury cases reported found decreased over the years. For serious injury case, that was decreased from 9,273 cases to 3,310 cases. There was decreased from 27 % to 18 % compared to total number death and injury. For minor injury case, that was decreased from 18,444 cases to 6,539 cases. There was decreased from 54 % to 39 % compared to total number death and injury.

This showed the effort of the research on crashworthiness are improving and maturing over the year. This effort reduced the injured and fatalities of passenger during accident. Therefore, extensive study of the energy absorption application is very important features on crashworthiness.

2.3 Types of Collision during Car Crash

Typically, there are two modes of car accidents: (i) impact from any direction (front, rear, left, and right side) and (ii) rollover. All crashworthiness features are designed for these typical accident modes. For example, crumple zones and airbags for frontal and rear impact mode where side impact zones for side impact mode. The probability of different collision types are shown in Figure 2.2 as published by Mercedes-Benz in 1994 (Wallentowitz & Adam, 1996). The reports for earlier models of Mercedes-Benz (Pletschen et al., 1990) and the U.S. Department of Transportation's National Highway Traffic Safety Administration, NHTSA 2014 annual report (National Highway Traffic Safety Administration - NHTSA, 2015) show a very similar accident probability distribution.

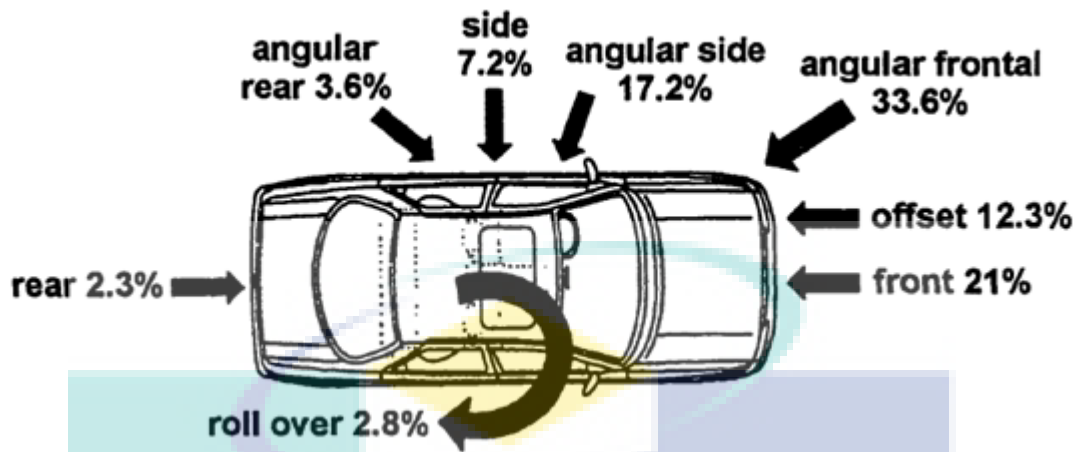


Figure 2.2 Statistical analysis probability of crash direction
 Source: Wallentowitz & Adam (1996)

2.3.1 Impact at Different Angle

Frontal Impact

The available reports indicate that frontal collision is the predominant type of collision for all vehicle types in either single or multiple vehicle collisions, accounting for approximately 50 % of all accidents. Due to the high impact speed and, consequently, high impact forces and energy, frontal collision is also considered the most severe. However, this type of collision only accounts for slightly more than 30 % of all severe and fatal injuries. In a majority of situations, frontal impact will not be a head-on full-width impact (Figure 2.2). Rather, a certain offset or oblique incidence will exist. In a full-width impact, energy absorption of the structure is maximized, and the integrity of the occupant compartment is maintained, except for in the case of very high-speed crashes. In an offset impact, a smaller area of the structure, on one side of a vehicle's front end, will experience all the crash energy. The difference between these two types of impact needs to be taken into account when conducting tests for improving crashworthiness. This is because the full-width impact test results in high occupant compartment decelerations and it is very demanding on the restraining systems (airbag, seat belts, etc.), while the offset test is very demanding on the structure for the higher energy absorption and prevention of intrusion into occupant compartment. By introducing the offset test in the early 1980s, for instance, and taking into account the crashworthiness of the vehicle under offset impacts in designing their vehicles,

Mercedes Benz was capable of reducing the percentage of fatalities in frontal collisions (Pletschen et al., 1990). Several different frontal test conditions and crash modes are shown in Figure 2.3. Four basic test configurations are used to represent different frontal collision situations where the impact is distributed or localized, oblique or head-on, offset or centred. These configurations can represent a collision with the fixed object, another vehicle, or both other important styles.

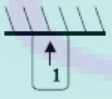
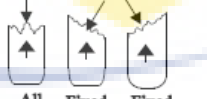
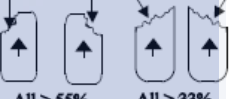
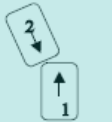
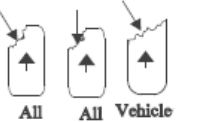
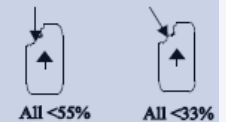
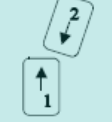
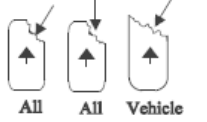
Test	Configuration	Crash Modes (Intrusion/Pulse)	% of Frontals	Crash Modes (Pulse Only)	% of Frontals
Frontal Barrier FMVSS No. 208 + - 30 Degrees		 All Fixed Object Fixed Object	21.7 %	 All > 55% Overlap All > 33% Overlap	74 %
Left Offset (0 to 30 Degrees)		 All All Vehicle	33.8 %	 All < 55% Overlap All < 33% Overlap	~13%
Right Offset (0 to 30 Degrees)		 All All Vehicle	35.3 %	 All < 55% Overlap All < 33% Overlap	~13 %
L. Obl./R. Off. R. Obl./L. Off. (+ - 30 Degrees)		 All All	8.8 %		

Figure 2.3 Possible frontal test conditions

Source: Stucki et al. (1998)

Side Impact

Side collisions between 1980 and 2001 yielded a 24 % decrease in fatality rate per million cars registered Malaysia. Although considerable, this number is still much lower than the decrease of 52 % in the case of frontal collisions for the same period. Reports also indicate that, more than 50 % of deaths are assigned to side collisions, which is 20 % more than in 1980. The primary reason for this great fatality of side collisions is the increasing size-mismatch between the LTVs and passenger cars, causing nearly 60 % of deaths in side collision to be the result of LTV-car collisions. In order to simulate this most severe case of impact by LTV, the standard side impact test is conducted perpendicular to the driver's side of the vehicle using a barrier that

accounts for the vehicle height and the specific shape of LTVs' front ends. However, side impact collisions remain very complex and require research input in order to improve crashworthiness and aggressivity of vehicles in side collisions (Summers et al., 2001).

Rear Impact

Rear impact collisions account for only 1 % - 3 % of vehicle accident fatalities. This is because this type of crash has the lowest probability of happening and because the speeds at which the collision occurs are low. Typical test configurations for this case are either rear-bumper-to-pole test at 5 mph or front-to-rear two-vehicle collision with both vehicles moving at similar speeds. The factor that affects the crashworthiness in rear collisions is the variability in possible configurations due to the considerable change in height of car's rear end caused by braking, number of passengers, and baggage, among others.

2.3.2 Rollover

The number of passenger-vehicle occupant fatalities in rollovers had increased by 5 % from 2001 to 2002. Although the number of fatalities in passenger cars had been declining since 1980, the great increase in the number of supervisory LTV (SLTV) rollover fatalities causes the above increase as well as contributes to nearly half of the increase in all occupant fatalities. The reason for SUVs being prone to rollover lies in their relatively high centre of gravity as compared to their width. Once rolled over, the roof of an SUV crashes inward due to insufficient support. This usually causes injuries to the head and neck regions of the occupants.

2.4 Crashworthiness Evaluation of Energy Absorber

Crashworthiness is an important parameter in designing a vehicle. During a crash, a vehicle is designed to absorb the energy from the impact of a collision. It acts as a protection to the occupants in the vehicle from the collision during a crash. The crumple zones of vehicle absorb the energy from the impact and deflect it away from the occupants. To meet these requirements, the advanced and lightweight engineering materials are the first choice in the technology of crashworthiness.

Several performance indicators have been developed to evaluate the effectiveness of energy absorbing device component for crashworthiness applications. An ideal energy absorber would be capable of attaining maximum load immediately and maintaining it for the entire length of the component. The goal to design an efficient energy absorbing device is to maximize its stroke. This is to have its total energy absorption (EA) absorbed by component, and to have high specific energy absorption (SEA) capability. Meanwhile, the performance of peak crush force (PCF) and mean crush force (MCF) are important as well. The crush force efficient (CFE) would express the relation of MCF and PCF. Lastly, stroke efficiency (SE) determines the maximum efficiency displacement of component along with the original length. These parameters are defined as below (Tarlochan, 2007). Figure 2.4 showed a force-displacement graph of energy absorbing device. This graph showed details of crashworthiness parameters such as total energy absorbed, peak crush force and average crush force.

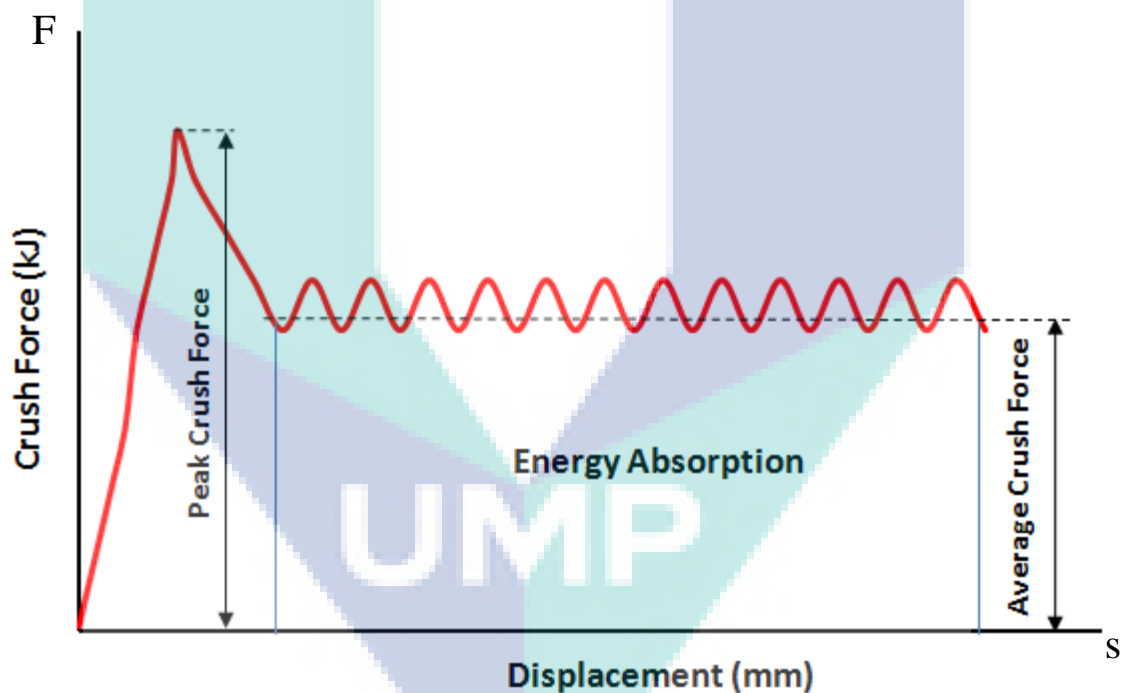


Figure 2.4 Force-displacement graph for energy absorbing devices
Source: Djamaluddin et al. (2015)

2.4.1 Total Energy Absorption (EA)

Total energy absorption, EA is an important key of crashworthiness parameter to analyse performance of the energy absorber. EA defined as the area under force-displacement curve or the maximum absorbed internal energy by the energy absorber

during impact. Therefore, if higher EA value means that the energy absorber can absorb more energy. This is a desirable condition in the automobile industry. Following equation showed the calculation of EA by using:

$$EA = \int_0^{d_{max}} Fds \quad 2.1$$

where d_{max} is effective axial crushing distance and Fds is area under the load-displacement. This formula is derived from Figure 2.4.

2.4.2 Specific Energy Absorption (SEA)

Specific energy absorption, SEA is also another important key crashworthiness parameter to analyse performance of the energy absorber after EA. SEA is required to examine the geometry and material discrepancy in the test specimens. The SEA defined as the energy absorbed per unit mass of material as given in equation below:

$$SEA = \frac{EA}{m} \quad 2.2$$

where m is the crushed mass of the component.

2.4.3 Peak Crush Force (PCF)

Peak crush force, PCF is the highest load required to cause significant permanent deformation and distortion onto a component. It is important in this research for two reasons. Firstly, during a low-speed and low-energy impacts, it is desirable that no permanent deformation takes place, as this would be considered damage to the structure. Secondly, peak crush force is often the maximum load observed in the useful stroke of the energy absorbing device because it has a direct influence on the loading of occupants in a vehicle.

2.4.4 Mean Crush Force (MCF)

Mean crush force, MCF also known as average crush load. The mean crush force is defined as the energy absorbed divided by the crushing distance (d) (Johnson &

Soden, 1977) MCF is a ratio of the energy absorbed in the crush zone (Figure 2.4) to the crush distance in the crush zone.

$$\text{MCF} = \frac{EA}{d} \quad 2.3$$

2.4.5 Crush Force Efficiency (CFE)

The mean crush force and peak crush force are important parameters to be determined as they are directly related to the deceleration that will be experienced by the occupants in a vehicle. The best way to quantify this is to define a ratio between mean crush force, MCF to peak crush force, PCF. And this ratio is termed as crush force efficiency, CFE. If the ratio is close to unity, the absorber is crushing at a value close to the peak crush force, hence minimizing the changes in deceleration as desired. On the other hand, if this ratio is away from unity, it indicates that there are rapid changes in the deceleration and this is dangerous to have in designing a vehicle.

$$\text{CFE} = \frac{\text{MCF}}{\text{PCF}} \quad 2.4$$

2.4.6 Stroke Efficiency (SE)

During a load displacement response of a crash component, the load will start to rise steeply due to densification at the particular maximum crush displacement. Thus, this maximum displacement is the useful displacement of the component. Meanwhile, geometry efficiency of an energy absorbing device is therefore defined as the ratio of the maximum displacement to the total length of the component. This is known as stroke efficiency.

$$\text{SE} = \frac{d_{max}}{d} \quad 2.5$$

2.5 Failure Mode

The primary concerns in this study are the axial mode of collapse and bending mode of collapse of structural components. In the other hand, the modes of collapse under combined loading will be discussed. Also, in this discussion, we refer specifically to metallic structural components.

2.5.1 Axial Collapse of Columns

The “pioneering” study in plastic folding of tubular structures was carried out by (Alexander, 1960) In his study, an approximate theory for the collapse of thin cylindrical shells under axial loading was derived. Alexander assumed that the shell collapsed in the form of a “concertina” with straight-sided convolutions. The work that is required to deform a metal in one such convolution is used to cause bending at circular joints and stretch the metal between the joints. If this work is equated to the work done by the mean collapse load, a solution of the type:

$$P_m = Ch^{1.5}\sqrt{D_{shell}} \quad 2.6$$

is obtained, where h is the thickness of the cylindrical shell, C is the material-dependent constant, and D_{shell} is the diameter of the shell. The main kinematic assumption made in this model is that one fold is formed at a time. Wierzbicki proposed several improvements to this solution (Wierzbicki and Bhat, 1986; Wierzbicki et al., 1992). In Wierzbicki and Bhat (1986), the stationary plastic hinges were replaced by moving hinges resulting in a more realistic deformed shape with improved prediction of the mean crush load. In (Tomasz Wierzbicki et al., 1992), the assumption was made that two folding waves were being created in an active crush zone. Two cases were compared in that case. First, a model with two straight elements constrained by stationary hinges was analysed and the final solution compared favourably with that in equation 2.6. In the second case, a more realistic deformed shape and a more accurate prediction for mean load were obtained by using two “S” shapes super folding elements. The solution was in the form given by the above equation, except for the constant C which was approximately 40 % higher than in the Alexander’s solution. This model was also capable of predicting the existence of intermediate peaks in the load-displacement response.

The super folding element was initially developed by Wierzbicki and Abramowicz (1983) as a two-degree of freedom corner element. They used this element to represent the deformed section of a prismatic column undergoing quasi-static compression loading. Their resulting theoretical analysis represents the basis for studying the progressive crushing of square and rectangular columns. Abramowicz and Jones (1986) had further extended this work to include the dynamic crushing strength of columns, as well as the experimental validation of the proposed theory.

$$E_1 = M_0 \left(\frac{8.880Hb}{h} + 2\pi c + \frac{4.592H^2}{b} \right) \quad 2.7$$

$$E_2 = M_0 \left(\frac{2\pi H^2}{h} + 2\pi c + \pi H \right) \quad 2.8$$

where $M_0 = \sigma_0 h^2 / 4$, σ_0 is column wall flow stress, h is wall thickness, E_i is defined in Figure 2.5, c is the width of the column, and b is the radius of toroidal shell element in the proposed kinematically admissible velocity field. Two basic types of superfolding-elements for square columns are shown in Figure 2.5. The energy absorbed in these basic element types is given by following equation (Hayduk & Wierzbicki, 1984; T. Wierzbicki & Abramowicz, 1983) :

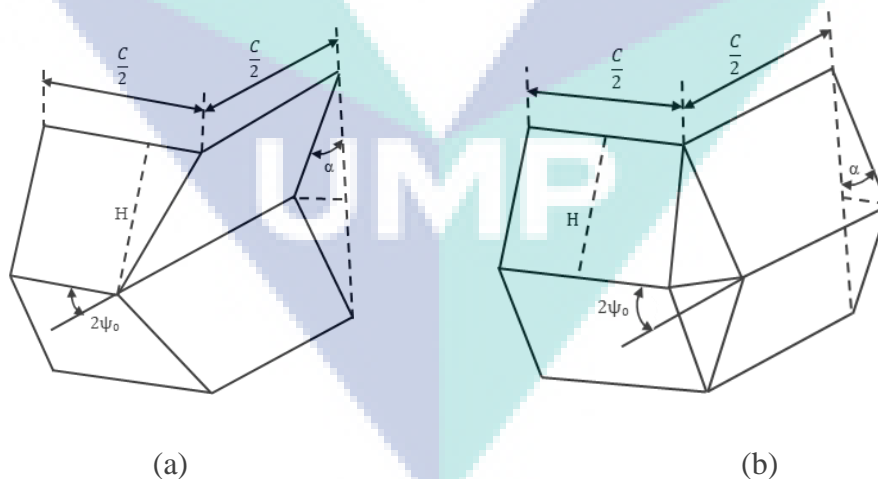


Figure 2.5 Superfolding-elements: (a) type I (b) type II
Source: Abramowicz & Jones (1986)

Idealized collapse behaviour of square tubes can be predicted through the combinations of these two basic types of superfolding-elements (SE). The mean

collapses load for the column can then be determined by first equating the internal energy given as a summation of E_1S and E_2S to the external work, and then minimizing the expression with respect to b and H . Table 2.2 lists four idealized modes of collapse and theoretically predicted mean collapse loads and half-fold lengths for a square column that failed in one of these collapse modes.

Table 2.2 Collapse modes of square columns under axial loading

Collapse mode	SE combination	Predicted mean collapse load (P) and half-fold length (H)	
Symmetric	4 type I (1 layer)	$MCF = M_0(52.22(c/h)^{1/3})$ $H = 0.99c^{2/3}h^{1/3}$	2.9a 2.10b
Asymmetric Mixed A	6 type 1 + 2 type II (2 layers)	$MCF = M_0(42.92(c/h)^{1/3} + 3.17(c/h)^{2/3} + 2.04)$ $H = 0.78c^{2/3}h^{1/3}$	2.11a 2.12b
Asymmetric Mixed B	7 type I + 1 type II (2 layers)	$MCF = M_0(45.90(c/h)^{1/3} + 1.75(c/h)^{2/3} + 1.02)$ $H = 0.86c^{2/3}h^{1/3}$	2.13a 2.14b
Extensional	4 type II (1 layer)	$MCF = M_0(32.64(c/h)^{1/3} + 8.16)$ $H = c^{1/2}h^{1/2}$	2.15a 2.16b

Source: Abramowicz & Jones (1986)

The MCF values in Table 2.2 are determined using the effective axial crushing distance of a column, d_{max} . The values for d_{max} are theoretically predicted by idealizing the deformation at the comers as the bending of a metal sheet about two orthogonal axes (Abramowicz, 1983). With slight modifications made based on the experimental observations (Abramowicz & Jones, 1984), the effective crushing distance is found to be:

$$\frac{d_{max}}{2H} = 0.73 \quad 2.17$$

for the symmetric collapse mode, while for the other three collapse modes:

$$\frac{d_{max}}{2H} = 0.77 \quad 2.18$$

These values are in agreement with earlier experimental results for empty columns (Ohkubo et al., 1974). Furthermore, if the column is stiffened from the inside, it can be proven that these values will become smaller (Abramowicz, 1983). Using equations 2.9 - 2.15, it is shown that the extensional mode of collapse will be the controlling mode for narrow, thick, square tubes ($c/h \leq 7.5$) while for wide, thin tubes ($c/h \geq 40.8$), the symmetric mode will prevail. For the width-to-thickness ratio between these two values, it is likely that the imperfections in the material, whether in the form of material flaws or intentionally introduced beneficial imperfections (Hui, 1986), will play a significant role in the onset of buckling. The strain hardening effects were taken into account in the above analysis through the use of energy equivalent flow stress, σ_0 , as defined in (Tomasz Wierzbicki & Abramowicz, 1989). This expression has to be corrected when materials other than mild steel are analysed.

The aluminium spaceframe concept had become a very attractive option in the mid '90s as a result of the need to better address environmental issues. In order to be able to absorb the same amount of energy, aluminium components used in structures need to be thicker than their steel counterparts due to their lower yield and ultimate strength. Combined with their generally lower ductility, this increase in thickness might lead to premature failure of material during deformation. Despite all this, weight savings of as much as 25 %, while keeping the adequate crashworthiness, have been reported when replacing the more conventional steel structures with aluminium. Prior to the study by Langseth and Hopperstad, there was limited reported experimental data for crushing aluminium. They performed extensive experimental and finite element analyses on the static and dynamic axial crushing of thin-walled aluminium extrusions (Langseth & Hopperstad, 1996; Langseth et al., 1999). In these studies, AA6060 square tubes in two different tempers of T4 and T6 with a slenderness range of $31.4 \leq c/h \leq 43.3$ were examined. In all the quasi-static cases, the progressive symmetric mode of deformation was observed. The mean collapse load was predicted within ± 10 % using equation 2.9a and the flow stress, σ_0 taken as the mean value between stress at 0.2 % plastic strain, $\sigma_{0.2}$, and the ultimate stress, σ_M :

$$\sigma_0 = 0.5(\sigma_{0.2} + \sigma_M) \quad 2.19$$

Alternative flow stress expressions for materials showing strain hardening are:

$$\sigma_0 = \sqrt{\frac{\sigma_y \sigma_u}{n+1}} \quad 2.20$$

$$\sigma_0 = 2.23^n \frac{\sigma_u}{n+1} \left[\frac{2}{n+2} \right]^{2/3} \left[\frac{h}{c} \right]^{(4.n)/9} \quad 2.21$$

as suggested by Santosa et al. (2000) and Hanssen et al. (2000), respectively. In the above equations, n represents the strain hardening exponent of the column-wall material and σ_y is material yield strength.

2.5.2 Bending Collapse of Columns

The bending collapse of thin-walled columns is usually localized at plastic hinges while the other sections of the column behave as rotating rigid bodies. The resistance to collapse drops significantly after this localized collapse at relatively small displacements, as can be seen from Figure 2.6. This will result in a low energy absorption efficiency of columns in pure bending. A first comprehensive study of deep bending collapse of prismatic columns was made by Kecman (1983). From extensive experimental study on rectangular columns with 27 different sections, he observed four distinct phases in the hinge development: (i) forming of a “bulge” in the web without apparent rolling deformation (A_1 in Figure 2.6d), (ii) rolling deformation (A_2 in Figure 2.6d), (iii) “jamming” of the rolling deformations and creation of new bending lines (A_3 in Figure 2.6d), (iv) two buckled halves coming in contact followed by the total jamming of the original hinge and the initiation of an adjacent secondary hinge. The theoretical analysis that Kecman developed was based on the second phase in the hinge development. The nominal value of energy absorbed at a hinge consists of eight different energies generated through the bending along lines or groups of lines (Figure 2.6c) and is given as:

$$E(\beta) = \sum_1^8 E_i(\beta) \quad 2.22$$

where E is the absorbed energy and β is the hinge rotation angle. The theoretical approach suggested by Kecman is semi-empirical since the so-called “rolling radius” has to be experimentally determined. A similar approach based on the kinematics

method of plasticity that involves determining the proper folding mechanism with stationary and moving hinges was developed independently by (Abramowicz, 1981). However, Kecman's study showed very good agreement between theoretical predictions and experimental results for the wide range of sections, while no experimental validation was given for Abramowicz's approach.

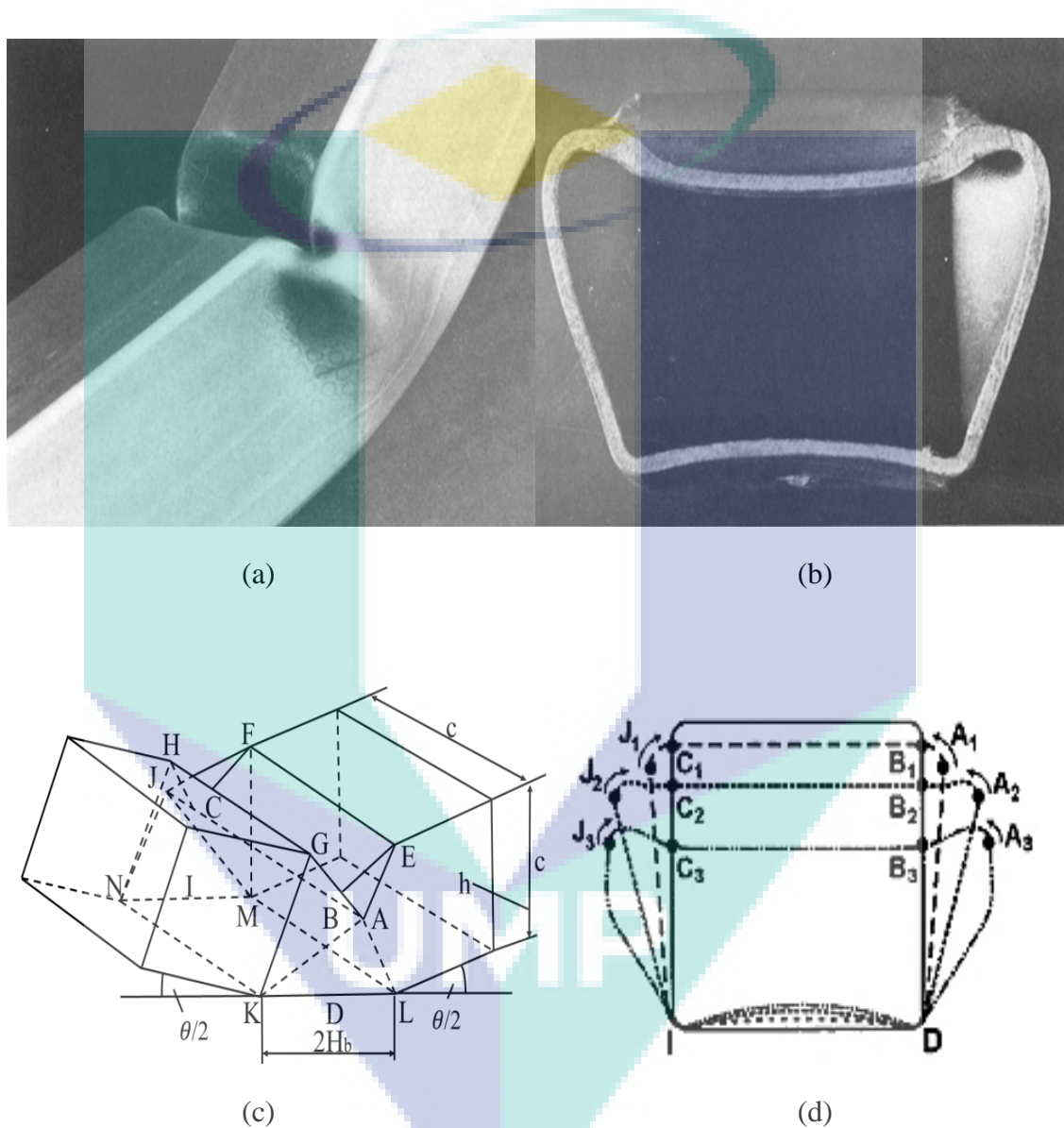


Figure 2.6 Analysis of bending collapse of columns by Kecman: (a) typical hinge collapse mechanism (b) cross section at the hinge (c) theoretical model (d) development stages of hinge

Source: Kecman (1983)

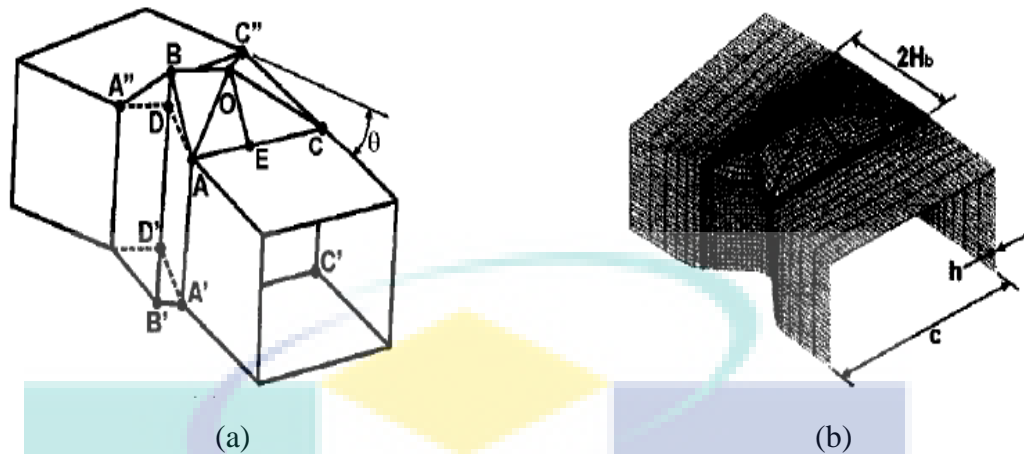


Figure 2.7 Analysis of bending collapse of columns by Wierzbicki: (a) simplified collapse mode of a column in bending and (b) the collapse mode superposed on the deformed FE mode

Source: Wierzbicki et al., (1994)

The methods above were further extended by Wierzbicki et al. (1994) as Figure 2.7. They first generated numerical solutions for square prismatic columns with three different width-to-thickness ratios using high accuracy FE models (very dense mesh) in ABAQUS. They also extended the concept of super folding element to develop a superbeam element. The simplified geometry of this element is shown in Figure 2.7b. The closed-form solution for the moment-rotation characteristic was derived by considering the superbeam element subjected to an eccentric force acting at the centre of the compression flange. Furthermore, they showed that bending performance indicators could in this case be derived from the performance indicators of identical columns subjected to axial crushing. The half-length of the fold in bending was observed to be higher than that in the axial compression and was expressed as:

$$H_b = 1.276c^{2/3}h^{1/3} \quad 2.23$$

Kim and Wierzbicki have used a similar approach of first generating a large set of numerical results in order to describe the behaviour of square and rectangular beams subjected to more complex biaxial bending (Kim & Wierzbicki, 2000) and simultaneous compression and bending (Kim & Wierzbicki, 2001). The authors concluded that general moment-rotation characteristics that were observed in planar bending can also be observed in biaxial bending. However, the behaviour observed for

combined compression and bending differed somewhat from the typical bending response in that after the peak point was reached, the load decayed dramatically.

2.5.3 Modes of Collapse under Axial and Oblique Loading

An energy absorbing structure will seldom be subjected to only pure axial or pure bending collapse during an actual crush event. Rather, both axial loading and moment will be generated in the structure causing oblique loading conditions. It is important to understand what happens to the structure during oblique impact since the bending collapse of components does not match crashworthiness design targets due to the low energy absorbing capacity. Limited studies in this area have been carried out until now.

Kim & Wierzbicki (2001) identified two types of oblique crushing: off-axis crushing and angled crushing (Figure 2.8). They found that tested E-glass/polyester pultruded tubes generally absorbed more energy in the angled loading, which they argued was due to the existence of static friction in the angled crushing in contrast to the dynamic friction in the off-axis crushing. In addition, the difference in energy absorption was observed to be greatly dependent upon the angle of impact.

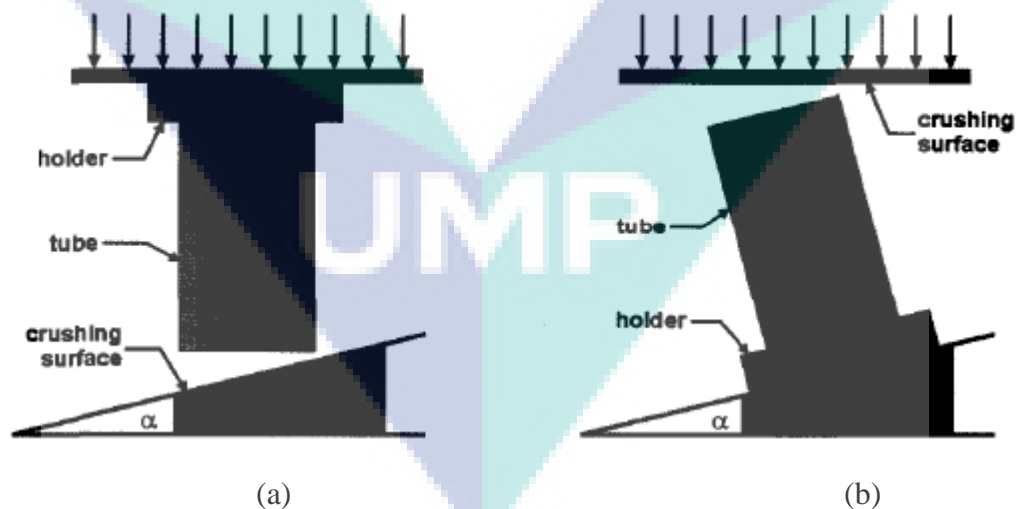


Figure 2.8 Types of oblique crushing: (a) angled loading, (b) off-axis loading
Source: Kim & Wierzbicki (2001)

Han & Park (1999) used the angled loading type (Figure 2.8a) in their numerical analysis of oblique loading of mild steel square columns. The columns were impacted

on an inclined wall at a speed of 30 mph assuming frictionless condition. Their results showed that there exists an angle, termed critical angle, at which the transition took place from axial to bending collapse mode. They used normalized numerical results from multiple cases to derive the approximate expressions for mean collapse load and critical load angle for the steel tubes modelled. Oblique crushing through off-axis loading (Figure 2.8b) was used by Reyes et al. (2002) in their experimental and numerical study on aluminium extrusions. All the tested columns experienced global bending collapse with a mode of deformation at the hinge that depended on both load angle and thickness. The fractional analysis they conducted showed that the thickness was the dominant parameter, though temper and length also had considerable effects. This importance of thickness differs somewhat from the conclusions made by Han & Park (1999), primarily due to the selection of geometry and impact conditions.

Crutzen et al. (1996) indicated a possible solution to the unwanted bending failure during oblique impact. They observed that the specimen could accommodate the oblique impact, i.e. fail in the more desirable progressive buckling rather than bending, if the mass and stiffness were redistributed along with the specimen length. They numerically observed the improvements in the collapse mode if the variable thickness columns or the variable cross-section columns are used instead of straight columns. Earlier, Reid & Reddy (1986) did an experimental and analytical study on the tapered mild steel sheet metal tubes loaded axially and obliquely. They concluded that these tubes withstand oblique impact loads as effectively as axial loads, and that such tubes were preferable to straight tubes since they were less likely to fail by global buckling in off-axis impact.

2.6 Principles of Structure Design of Energy Absorber

What is Energy Absorber? Energy absorber is a system that converts fully or partially of kinetic energy (KE) into another form of energy. The energy converted is either reversible or irreversible (Alghamdi, 2001). Meanwhile, the role of an absorber in crashworthiness is to absorb the majority of the kinetic energy during the impact in an irreversible manner. It is to ensure human injuries and equipment damages are reduced to lowest rate.

The axial loading is the most efficient mode of deformation and it is also the most difficult to attain. A structure that starts to deform axially can suddenly buckle in the global bending mode, causing a significant drop in the capacity of the structure to absorb the impact energy. This behaviour may completely alter the crash performance of the structures; hence it is important to understand the mechanics of this transition so that proper measures can be taken to avoid it. Therefore, the objectives of good structural crashworthiness design are irreversible energy conversion, constant and stable crush force, long stroke, and light weight with high specific energy absorption capacity (Lu & Yu, 2003).

2.6.1 Irreversible Energy Conversion

During collision, an impact energy hits to the vehicle by crush force. An important fundamental of design for the structure and the materials used should be able to absorb as much of the impact energy which is free from elastic strain energy. If the vehicle is designed as elastic strain energy, the structure returns to original shape after undergoing a maximum compression due to release of the elastic energy. This causes the vehicle rebounded like a spring. Hence, it is completely desirable to have inelastic energy absorption during collision to avoid the "spring back" effect.

2.6.2 Constant and Stable Crush Force

To minimize the changes in deceleration during collision, the crush force on the vehicle due to impact should remain almost constant and keep below a threshold value. Rapid changes in deceleration can cause brain injuries as indicated by the high impact collision. The energy absorbing device ideally should possess a rectangular force displacement characteristic.

2.6.3 Long Stroke

Dissipating kinetic energy during a crush is very important. Most of the kinetic energy is dissipated in terms of work done by the impact force to crush the structure to a particular distance. Most of this work, which is the crush force times the magnitude of the displacement of the structure, is converted into inelastic strain energy of the structure. So, when an energy absorbing device is designed to have a long stroke (i.e. larger useful crush distance) and high energy absorption, it is able to minimize the

injury of the occupant in the vehicle by reducing the intrusion of the structure into the occupant's compartment. Hence, this may retain a survival space for the occupants.

2.6.4 Light Weight with High Specific Energy Absorption Capacity

As we know, the crashworthiness is an important issue in a design of a vehicle. The additional features may be designed and added to the existing structure. These may increase the weight of the vehicle which in return increases the fuel consumption. Hence to reduce or minimize the impact on the overall weight of the vehicle, energy absorbing devices should be light in weight yet possessing high specific energy absorption capabilities.

Aluminium is the material that meets the objectives on both light weight and high energy absorption. Aluminium is the third most plentiful component on earth. Aluminium is strong, light weight and a flexible material. It is light weight and gives the strength of steel at a third to a large portion of the weight. Around the globe aluminium is turning into the choice for long range structures over steel frames for some reasons including the numerous environmental advantages of its materials impression. It will likewise review the most recent research by the Aluminium Association on the sustainability of aluminium from mining to reusing. This industry is resolved to improve industry energy consumption, lower emissions, reduce land resource used and maximize sustainability. Lightweight aluminium structures can weigh anywhere from 35 percent to as much as 80 percent less than steel, yet provide equivalent strength. Since aluminium is extrudable, it very well may be designed to put the material just where it is structurally required. The utilization of aluminium is increasing throughout the world for many uses. It is ideal automotive industries and has contributed to the reduction of emissions and transportation costs as a component in automobile manufacturing. Choosing aluminium as the structure for these new geometric structures and spaceframes decreases material consumption and has numerous environmental benefits. Aluminium products will continue to develop and be re-used for centuries.

2.7 Previous Work

2.7.1 Energy Absorber for Axial Loading

A lot of works had been done in understanding the energy absorption capabilities of energy absorber under axial loading scenario. Analytical, numerical and experimental studies on axial structural collapse had mainly focused on understanding and analysing the mode of collapse, the peak force, the mean force, and the energy-absorption characteristics. Most of the studied were studied on geometry and material used in designing energy absorber.

Thin-walled tube with simple geometrical profile has received the most attention in axial crushing studies. Langseth & Hopperstad (1996) studied the static and dynamic behaviour of square thin-walled tubes subjected to axial loading by varying the temper, wall thickness and impact velocity. The wall thickness was 1.8, 2.0 and 2.5 mm, while the impact velocity was in the range of 8 to 20 m/s. The behaviour between static and dynamic tests was also compared. The results showed that the mean load ratio between dynamic and static test was a decaying function with respect to the axial displacement which indicated a strong inertia effect to the straight square tube. Jensen et al. (2004) carried out static and dynamic tests to study the effect of geometry and impact velocity on the behaviour of axially loaded square thin-walled extrusions. From this study, the inertia effect was observed by varying the length of the tube. The results showed that more energy was absorbed in the progressive buckling mode than in the global bending mode. Zhang et al. (2007) introduced patterns to the surface of thin-walled square tubes to improve energy absorption capacity under axial compressive loads. Two types of patterns were constructed whereby pattern A was aimed at triggering the extensional mode while pattern B was intended to develop new collapse mode. Numerical results showed that pattern A absorbed 15 % - 32.5 % while pattern B absorbed 54 % - 93 % energy compared with the conventional tubes. Figure 2.9 showed the representative model of pattern A and pattern B.

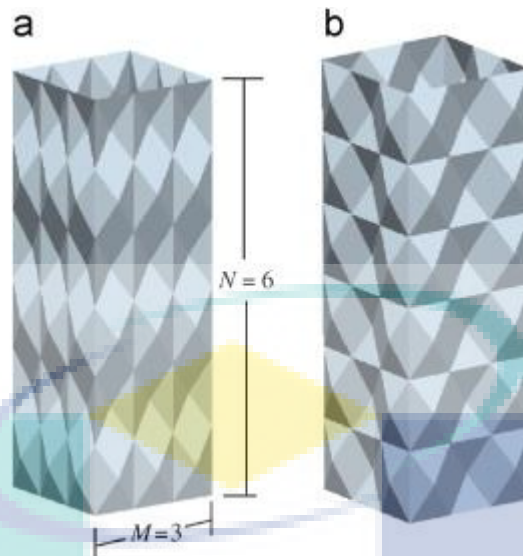


Figure 2.9 Illustration of (a) type A and (b) type B patterns.
Source: Zhang et al. (2007)

Besides square thin-walled tubes, cylindrical tubes also attract researcher's attention due to their high stiffness and strength, low weight, and ease of manufacturing process which contribute to a low cost of energy absorber devices (Alghamdi, 2001). Most of the past literature of thin-walled circular tubes were related to study the tube's collapse behaviour and derivation of the empirical model. Alexander (1960) was the first person who computed the mean crush force for cylindrical tubes and the tubes deforming in concertina mode. Also, empirical expression was derived by other researchers (Abramowicz & Jones, 1984; Abramowicz & Jones, 1986) to propose an improved model which there was a formula surprisingly applicable to both axisymmetric and non-axisymmetric modes (Guillow et al., 2001). Galib and Limam (2004) performed an experimental and numerical study of the crash behaviour of circular tubes and compared it with the available analytical solutions. It showed a good agreement between them and some effect of geometrical imperfection were made. Among many pieces of literature on the circular tube, work of Salehghaffar et al. (2010) was found to study the geometrical side. They designed two new structures of circular tubes which the first design was a rigid steel ring which was press-fitted on top of circular aluminium tubes, while the second design was some wide grooves that were cut from the outer surface of steel circular tubes. The finding proved that the suggested structural designs can improve energy absorption characteristics of circular tubes significantly under axial loading.

Tapered or frusta tubes have been considered desirable impact energy absorber due to desirable constant mean crush load-deflection response under axial loading (Reid & Reddy, 1986). However, relatively few studies have been reported on the energy absorption performance of such tubes compared with straight tubes. Singace et al. (2001) investigated the influence of end constraints of circular frusta and found out that frusta was more stable as a structure as compared to cylinders. However, this study was meant for ship protection. Besides those tubes, rectangular or square tapered tubes also have been given focus recently. Nagel & Thambiratnam (2004) compared the energy absorption response of straight and tapered thin-walled rectangular tubes by varying wall thickness, taper angle, impact mass and impact velocity. The results indicated that the energy absorption response of tapered tubes can be controlled via its wall thickness and taper angle. Ahmad & Thambiratnam (2009) investigated the effect of foam filling on the dynamic response and energy absorption characteristics of thin-walled conical tubes using finite element simulations. Results indicated that the foam filler stabilized the crushing process. Mirfendereski et al. (2008) investigated the axial crushing of foam-filled tapered thin-walled rectangular tube and find that foam density had no significant effect on the initial peak load but had increased the mean load, the absorbed energy and the crush force efficiency as the foam density increased.

There are many more researches that are still actively studying on axial crushing of energy absorber including the geometrical behaviour of multicell column (Chen & Wierzbicki, 2001; Kim, 2002; Zhang & Cheng, 2007), multi-tubes (Aktay et al., 2008), multi-corner thin-walled columns (Yucheng Liu, 2008), effect of trigger mechanisms on tubes (Daneshi & Hosseinipour, 2002), and usage of various foam fillers inside tubes (Avallé et al., 2001; Gameiro & Cirne, 2007; Seitzberger et al., 2000). Besides, selection of materials is also important in the study of the axial crushing of energy absorber. Steel has been extensively used in energy-absorbing structures (Gameiro & Cirne, 2007; Mantena & Mann, 2003; Salehghaffari et al., 2010; Seitzberger et al., 2000) due to low prices combined with excellent ductility. But the need to reduce structural components mass has increased in recent years (Tisza & Czinege, 2018). Hence, the use of aluminium tubes has been frequently promoted (Gameiro & Cirne, 2007; Kim, 2002). However, research on both materials is still going on until now. On the other hand, Structural optimization is also creating interest nowadays to seek for the optimal design. Latest optimal design works are found to seek for multi-corner columns (Yucheng Liu,

2008), foam-filled beam (Bi et al., 2010; Li et al., 2019; H. R. Zarei & Kröger, 2008), conical frusta (Sheriff et al., 2008; Shiravand & Asgari, 2019), partially tapered rectangular tubes (Asanjarani et al., 2017; Shariatpanahi et al., 2008), and multicell sections (Hou et al., 2008; Zhou et al., 2019).

2.7.2 Energy Absorber for Oblique Loading

Baroutaji et al. (2017) had summarized most of the work been done by other researchers. Not much effort was found in designing energy absorber for oblique loading. Based on 61 types of tube section model had been studied, there were only 11 out of 61 models investigated. Han and Park (1999) studied the crushing behaviour of thin-walled square columns subjected to oblique loads and found out that there was critical load angle at which transition took place from the axial collapse mode to the bending collapse mode. The critical load angles are about 6.0° and 6.7° for each model, and these are included within the range of the critical angle obtained from numerical simulations. An extensive study on square columns was done by Reyes et al. (2002). In the study, Reyes et al. substituting aluminium alloy to the columns and varying load angle, tube thickness, length, heat treatment and impact velocity. Results showed that collapse mode seemed to depend on both load angle and thickness. Another study by Reyes et al. (2003) on square aluminium tubes was done using computer simulation of LS-DYNA. Reyes et al. (2004) further the study by introducing aluminium foam-filled into the square column. Reyes et al. performed experimental study by varying load angle, heat treatment, and foam density and numerical study by using LS-DYNA. The study showed that high-density aluminium foam filler increased the energy absorption but the specific energy absorption was lower compared to the empty columns. Instead of study tapered tubes under axial loading. Nagel and Thambiratnam (2006) also studied tapered tubes response under oblique loading. They compared the energy absorption response of straight and tapered thin-walled rectangular tube by varying load angle, impact velocity, and tube dimensions. It was found that the mean load and energy absorption decreased significantly as the load angle increased. Study of foam-filled structure under this condition was done by Ismail (2008) and found out that energy absorption capability decreased as the load angle increased. There was good interaction between wall and foam by which observed for higher foam density resulted in higher energy absorption. Ahmad et al. (2010) investigated dynamic energy

absorption characteristics of foam-filled conical tubes which also done under axial crushing. For oblique loading, they studied the tube response by varying load angle and geometry parameters. The study showed that conical tube had ability to withstand oblique impact as effectively as axial impact and energy absorption capability of filled tube was better compared to empty tube.

2.7.3 Filler of Energy Absorber

2.7.3.1 Hexagon Honeycomb Filler

Metallic honeycomb is widely used as an energy absorption material structural application. This is because it has high energy absorption and high strength-to-weight ratio. The strength characteristics of metallic honeycomb applications depend upon the geometrical configuration. Wierzbicki (1983) developed a mathematical model of metallic hexagon honeycomb on energy dissipating and crush strength by quasi-static impact loading. The result showed that, the cell wall of honeycomb crushed progressively and buckling wavelength of $2H$. Yasui (2000) conducted an experiment on multi-layer honeycomb and found the honeycomb model was able to absorb more energy than the single-layer honeycomb. Eskandarian et al. (1997) studied on surrogate crash test on honeycomb when the vehicle crashed to roadside objects. Four different types of honeycomb were tested, multiple segments for each type able to undergo until maximum compaction. Then, Paik et al. (1999) carried out experimental and theoretical methods to study the compressive properties on honeycomb material with different parameters. Several core shapes and materials utilized the models. The result showed increased in thickness improved the performance. Meanwhile, core height, core cell thickness and panel aspect ratio were observed that the core height would be a crucial parameter affecting the sandwich panel ultimate compressive strength. Lastly, aluminium honeycomb core has excellent properties with regard to weight savings and fabrication costs. Aaron et al. (2003) developed experimental and finite element analysis to determine the crush strength of Formgrid honeycomb, found the parameters affecting the crush properties during sensitivity analysis. Then, a mathematical formulation is developed for determining the buckling stresses of the honeycomb.

Chou (1998) compared the properties honeycomb by several simulation software modelling. Chou found that an elastic–perfectly plastic model could give the

shear responses. Wu (1995) experimentally determined the plastic buckling mechanism of metallic honeycomb. The experiment showed that the half-wavelength was about 80 percent of the experimental values predicted by Wierzbicki (1983). On the other hand, Wu (1995) also found that the crush strength was reliable on the size of honeycomb cells but independent on the number of cell. Wu and Jiang (1997) had performed a study on the parameters affecting dynamic crush strength. The study showed that the width of the honeycomb cell played an important role in crush strength values.

Some researchers were developed to study with cell configuration of the structure. Different structure of geometry was explored such as hexagonal (Deqiang et al., 2010; Hong et al., 2008), circular (Hu et al., 2015), triangular (Liu & Zhang, 2009), square (Liang & Chen, 2006; Liu & Zhang, 2009), Nomex honeycomb core (Liu et al., 2015) and so on. Among these geometry structures, regular hexagon cells are the most popular. In terms of withstanding external crushing load for energy absorbing devices, the out-of-plane crushing properties have been found to compare favourably with the in-plane properties (Khan et al., 2012). Wierzbicki (1983) proposed and improved the solutions for out-of-plane plateau stress of hexagonal honeycombs. Found that, a simple and rational means of hexagonal cell structures. The hexagon honeycomb is excellent to design as energy absorbers in impact or impulsive loading situations. Furthermore, the enhancement of high strain rates crush strength under dynamic was discussed and studied experimentally (Xu et al., 2012). Extensive efforts (Deqiang et al., 2010; Xu et al., 2012) were devoted to identifying the relationships between crushing strength and other geometric details. These studies found that the influences of density of the material, edge length and cell wall thickness are the factors in the performance of honeycomb filler. Higher relative density material, smaller edge length and thicker cell wall thickness can increase crush strength, hence improve the crashworthiness of honeycomb structures. In addition, cell-wall angle (also frequently stated as expanding angle, central angle), and edge-length ratio can also affect the crush strength of honeycombs depending on whether the honeycomb is of uniform thickness or double thickness (Mozafari et al., 2016). In numerical studies it is common to adopt shell elements to simulate the behaviours of honeycomb walls.

Among several published works on hexagon honeycomb crushing behaviour, only a few contributed to the study of oblique impact loading. Some research studies

present that even when a 5° load angle is applied. the energy absorption drastically decreases, in comparison with the perfect axial crushing (Mohammadiha et al., 2015). Zarei and Kroger (2008) conducted an investigation of axial and oblique impact loading test on both empty and honeycomb filled aluminium square tubes. The honeycomb filled in the tube has improved the performance of energy absorption. Hence, they could access more efficient and lighter crash absorbers while achieving maximum energy absorption by adopting design optimisation techniques and response surface method (RSM). Mohammadiha et al. (2015) studied on square crash boxes filled with functionally graded honeycomb (FGH) subjected to oblique impact loading. The weighted average method, the geometrical average method, and multi-design objective optimisation technique were applied to optimized and utilise the square crash box by FGH. FGH was found the superiority compared to the uniform honeycomb filled box structures.

2.7.3.2 Circular Honeycomb Filler

Chung & Waas (2000) studied in-plane elastic properties of perfectly circular and elliptic cell honeycombs. Then, Chung and Waas developed an analytical solution on circular and eclipse honeycomb structural based on the result. The solution was expressed and derived elastic constants in terms of the material properties, cell wall thickness and parameter. Chung and Waas (2002a, 2002b) had done experiments and the numerical simulations on the response of the circular honeycombs under in-plane crushing and found that the non-uniform deformation within the honeycombs. Oruganti and Ghosh (2008) studied the creep deformation of the hexagonal and the circular honeycombs by the elastic-plastic finite element method. They found that the circular honeycombs were stronger than the hexagonal under the same relative density. Lin et al. (2012) studied the in-plane hexagonally packed circular honeycombs on Poisson's ratio, elastic modulus, plastic yielding strength and brittle crushing strength by using theoretical and numerical methods, and found that the in-plane mechanical properties of circular honeycombs were significantly affected by the ratio of cell wall thickness to the radius. An extensive study of concentrated filling inclusions circular honeycomb undergo in-plane test by three different loading mode carried out by He et al. (2018), which were quasi-static, transition and dynamic impact loading. This research found that the value of packing ratio and defect location may seriously influence localized

deformed band of transition mode and the plateau stress of the honeycomb relied on the defect location except for the packing ratio.

Numerous examinations as mentioned, the circular honeycombs are not much found on the out-of-plane crushing behaviours. However, honeycombs are typically utilized as the core of sandwich panels in terms of out-of-plane (Qin & Wang, 2009; Qin et al., 2009).

2.7.3.3 Multicell Filler

Thin-walled tube is an initial geometric structure studied as an energy absorber. Then, the multicell structure is an extensive study of thin-walled tube. Multicell thin-walled tube has been studied by many researchers because it has better performance compared to the conventional hollow thin-walled tube (Baroutaji et al., 2017; Chen & Wierzbicki, 2001; Qiu et al., 2015; Tabacu, 2016; Tran, 2017). This is due to the number of angular elements such as the corner configuration on a tube's cross-section which generally influences the crashing behaviours and energy absorption (Abramowicz & Wierzbicki, 1989; Wierzbicki & Abramowicz, 1983). Therefore, the internal column of a thin-walled tube is designed with divided or consisting of several compartments for achieving better energy absorbing performance.

Kim (2002) proposed a multicell tube with four square cells at every corner of the square tube (Figure 2.10b). The outcome demonstrated that this structure had a sensational improvement in EA compared to conventional square tube. Zhang et al. (2006) studied on both theoretical and numerical investigation of the tapered multicell tube (Figure 2.10c). From the result, an analytical solution of mean crushing force of multicell sections was derived which agreed well from the numerical results. Later, Nia and Sadeghi (2013) added the partitions at corners of 3×3 cellular tube, the energy absorption improved. Then, Nia and Parsapour (2013) also revised the formula of mean crushing load for multicell tubes with an unequally sized compartment from the study of Zhang et al. (2006). Some studies were aimed to enhance the performance in energy absorption and reduced the peak force. Hou et al. (2008) used Response Surface Method (RSM) to perform the design optimizations for 1 cell, 2 cells, 3 cells and 4 cells sectional columns by explicit dynamic impact test (Figure 2.10e). Tang et al. (2013) devised a circular multicell column and verified its superiority and more efficient

compared to the conventional square structure and square multicell structure. Zhang and Zhang (2013) studied on experimentally and analytically for multicell stub columns with different sectional configurations undergo quasi-static axial crushing (Figure 2.10h). Najafi and Rais-Rohani (2011) studied the square tubes with an inner square tube which connected with different acute or obtuse angle to compare the differences in energy absorption (Figure 2.10g). The angles affect the energy absorption, thus, the performance of multi-cell models is compared with that of a square tube of approximately similar energy absorption level with width at 80 mm and thickness at 40mm. Figure 2.10 showed the cross-sectional geometry design of multicell from previous studies.

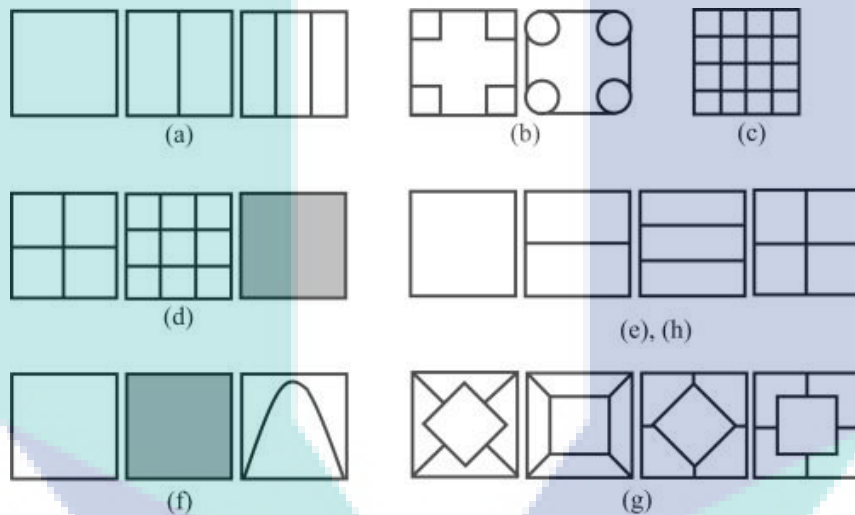


Figure 2.10 Cross-sectional geometry of multicell prismatic columns, (a) Chen & Wierzbicki (2001), (b) Kim (2002), (c) Zhang et al. (2006), (d) Zhang & Cheng (2007), (e) Hou et al. (2008), (f) Zhang et al. (2009), (g) Najafi & Rais-Rohani (2011), (h) Zhang & Zhang (2013).

Source: Jusuf et al. (2015)

Pirmohammad and Marzdashti (2016) compared the crush behaviours of multicell structures consisting of two straight columns with the same shape of cross-section connected together by several ribs. These models also studied on axial and oblique impact under static loading. The structure had lower performance when the angle of loading increased but multicell obtained better energy absorbers in order of the crashworthiness capability. Mahmoodi et al. (2016) investigated the crashworthiness behaviour of tapered multicell tubes theoretically and numerically. They found that the increased in the taper angle and the number of cells in the cross-section would improve

the crashworthiness of the structure. Song and Guo (2013) conducted a comparative study between windowed and multicelled square tube, both models had the same weight undergo axial and oblique impact loading. The result showed that multicell had higher mean crush force but higher peak crush force than the windowed tube. From those previous investigations above, the multicell structure has better energy absorption than single column thin-walled structure.

2.8 Finite Element Application in Crashworthiness

Today, using finite-element method (FEM) simulation has partially replaced the expensive full-scale physical experiment. This technology allows solving difficult problems on powerful workstations and clusters relatively quickly with high accuracy in short of time.

By using FEM simulation, that could designing a new state-of-art product with satisfy of reliability and safety criteria requirements. The most of the structures experienced operating loads that vary with time. Numerical method is an application method to design various structures by improving the quality and reliability of the process and products, and by opportunities to use new material are to be exposed. The effect of numerical engineering analysis technologies, Computer-Aided Engineering (CAE) is maximized during the designing process. By that, CAE helps the study saves a lot of time and cost, reduces the probability of malfunction, studies the behaviour by physical experiments with prototypes and evaluates the behaviour of the structure under different external influences.

2.8.1 Nonlinear Dynamic Explicit Analysis

Practically, most of the structures exhibit nonlinear behaviour that depends on the loading conditions. However, it is acceptable to assume linear behaviour with small displacements and strains. In other cases, the correct result cannot be accounting or nonlinear behaviour.

The explicit FE technique illuminates an arrangement of hyperbolic wave equations in the zone of impact of the wave front, and as needs be does not require coupling of a substantial number of equations. On the other hand, the unconditionally stable implicit solved provides a solution for all coupled equation of motion, which

requires assembly of a global stiffness matrix. A comparison of differences between explicit and implicit integration techniques shows in Table 2.3. For crash simulations involving extensive use of contact, multiple material models and a combination of non-traditional elements, it turned out that explicit solvers are more robust and computationally more efficient than implicit solvers.

Table 2.3 Comparison of explicit and implicit integration techniques

	Explicit	Implicit
Matrix	No matrix assembly and matrix inversion is not required	Require matrix assembly and inversion
Time Step	Small time step (conditional stable)	Large time step (unconditional stable)
Implementation	Easy and robust solution procedure even for high degree of nonlinearities	Solution procedure becomes complicated with increasing degree of nonlinearities

Source: Tho (2006)

2.8.2 Dynamic Effect on the Crash Resistance

Dynamic analysis consists of analysing the response of the structure to external influences that vary time. This analysis finds the structure's response, which manifests as displacements, velocities, accelerations, reactions forces, and stress as functions of time.

Dynamic loading involves many interacting effects that are not present in the static collapse. There are two most important factors identified in dynamic collapse under the impact velocity in the most of crash accidents where the strain rates are below 100 sec^{-1} . The first is the strain effect, which is a material property, whereby the yield or flow stress is raised. The second factor is the inertia effect developed within the structure by the rapid acceleration during the collapse.

While the inertia effects were shown to be responsible for peak magnitudes of the instantaneous resisting forces and therefore do not contribute the crash energy dissipation, many studies have been conducted on the strain rate empirically or analytically yielding simple equations relating the dynamic crash resistance and the static crush resistance. Ohkubo et al., (1974) suggested an empirical formula for

dynamic load factor in closed-hat axially compressed columns. By fitting experimental data, a ratio of dynamic to static crushing force was approximated linearly:

$$\frac{P_d}{P_s} = 1 + 0.0668V_0 \quad 2.24$$

where P_d is the dynamic crash force, P_s is the static crash force, and V_0 is the initial impact velocity. A different empirical formula was obtained by Wimmer for square mild steel columns:

$$\frac{P_d}{P_s} = 1 + 0.07V_0^{0.82} \quad 2.25$$

The Cowper & Symonds (1957) had widely been used to relate the dynamic flow stress, σ_0^d to the static flow stress, σ_0^s :

$$\frac{\sigma_0^d}{\sigma_0^s} = 1 + \left(\frac{\varepsilon}{C}\right)^{\frac{1}{p}} \quad 2.26$$

where ε is the strain rate, C and p are material constants to be determined from the dynamic tensile tests on the material.

Based on the strain rate sensitivity on the yield stress of material, Tani & Funahashi (1978) derived the following equation for mild steel structure by simply applying the Cowper-Symonds equation with one-dimensional uniform deformation assumption:

$$\frac{P_d}{P_s} = 1 + \left(\frac{V_0}{2.475 \times 10^{-4} L}\right)^{0.2} \quad 2.27$$

where L is the crushing distance.

Wierzbicki et al. (1977) derived the following equation with the consideration of complex folding mechanism of axially compressed mild steel box column:

$$\frac{P_d}{P_s} = 1 + 0.11V_0^{0.714} \quad 2.28$$

For impact velocities used in crash barrier tests, the dynamic correction factor is in the range $P_d/P_s = 1.2 \sim 1.4$ (Kim, 2001). This of course applies to utilized steel body structures. Aluminium alloy have no or very little strain rate sensitivity. All general application purposes, no dynamic correction factor needs to be introduced in all aluminium vehicle bodies. Wierzbicki et al. (1977) observed from the comparison of static and dynamic tests of crushing of thin-walled structures that the deformation patterns of sheet metal components differed little between static and dynamic loading conditions.

Modern techniques allow replacing field trials. The numerical modelling requires significant allocations of time and money by using state-of-art software for a broad spectrum of analyses. FE modelling allows the solution of many difficult dynamic problems without resorting to experimental methods. It has availability and constant improvement of computing system. In addition, dynamic analysis is allowed to determine the response of structures to dynamic effects such as impacts or random vibration.

2.9 Data Verification

To ascertain whether it is sufficiently accurate, FE model had been verified by the experimental and theoretical model in the works of literature (Robinson, 1997). In this study, there were two validation models been carried out. Both models made out of circular thin-walled aluminium empty tubes by Gameiro and Cirne (2007) and Zarei and Kröger (2006). Total energy absorption (EA) and mean crushing force (MCF) are the parameters for the performance indicators as following.

The first FE model was developed by the experimental specimen of Gameiro and Cirne (2007). The FE model was developed based on the numerical model with force-displacement response and total energy absorption is presented. The force-displacement response helps to better understand the crushing progress of the model during deformation. Gameiro and Cirne (2007) was comparing it with experimental axial dynamic tests on empty and cork-filled short circular aluminium tubes. However, only empty tube will be verified for the purpose of this study. The geometry details and material properties of aluminium are shown in Table 2.4 - Table 2.5.

The friction coefficient, μ is 0.2 and element size is 3mm with five integration points through thickness. Model undergo dynamic loading test. Both end sides of the circular tube are placed with rigid plate. The bottom rigid plate is fixed. The top rigid plate is impactor. The dynamic impact velocity applies as 10 m/s with a load impact of 500 kg.

Table 2.4 Geometry details and material properties for aluminum

Geometries	
Internal Diameter, D	76 mm
Tube wall thickness	1.52 mm
Tube length	300 mm
Material properties	
Initial yield stress	175 MPa
Young's modulus	69 GPa
Poisson's ratio	0.3
Density	2700 kg/m ³
D	6500 s ⁻¹
q	4

Table 2.5 True stress-strain data of the aluminum alloy

Plastic strain (%)	0.00000	0.00278	0.00778	0.01278	0.01778
Plastic stress (Mpa)	175.00	193.75	200.00	201.00	202.00

The second FE model is developed based on Zarei and Kröger (2006). There are three different models namely Z1, Z2 and Z3. These three models had a different diameter, thickness, velocity and angle of loading. The material is fixed, Aluminium alloy AA6060 T4 is used in this study. A 'node to surface' algorithm is modelled for the contact between the rigid impactor and the specimen. A single surface contact algorithm is used for the contact between the tube walls during deformation. The friction coefficient, μ is 0.25 and element size is found 3 mm. The material properties are initial stress, σ_0 was 80 MPa and ultimate stress, σ_{Ult} was 173 MPa. The variables of the model are shown in Table 2.6.

The walls of the circular tubes were modelled using four-node shell continuum elements with five integration points along with the element's thickness direction. 2 mm element size was chosen. The friction coefficient, μ is 0.2. Model undergo dynamic

loading test. Both end sides of the circular tube are placed with a rigid plate. The bottom rigid plate is fixed. The top rigid plate is impactor. The dynamic impact velocity applies as shown in Table 2.6. For material used was Aluminium Alloy 6060 T4 with material data as Table 2.7. This study also been carried out by Djameluddin, Abdullah, Ariffin, et al. (2015) as validation purpose.

Table 2.6 The details of the validation models

	Impactor		Geometry Parameter		
	Velocity, v (m/s)	Mass, m (kg)	Length, d (mm)	Diameter, D (mm)	Thickness, t (mm)
Z1	6.6	104.5	180	40	2
Z2	6.6	104.5	180	40	2.5
Z3	10.7	91	180	50	3

Source: Zarei and Kröger (2008)

Table 2.7 Strain hardening data for AA6060 T4

Plastic strain (%)	0.0	0.024	0.049	0.074	0.099	0.124	0.149	0.174
Plastic stress (Mpa)	80	115	139	150	158	167	171	173

Source: Santosa et al. (2000)

Table 2.8 showed result of comparison between simulation models to experiment specimen. There are three sets of simulation data which from Zarei and Kröger (2008), Djameluddin, Abdullah, Ariffin, et al., (2015) and the model been set up in this research. All simulation result were compared to experimental result Zarei and Kröger (2006). The result presented the performance of EA and MCF of the models then calculated the different percentage of every result. The software used for modeling and analysis result has been performed from both researchers were different. Zarei used UNIX server by explicit finite element code LS-DYNA. Thus, Djameluddin used ABAQUS–Explicit.

Table 2.8 FE simulation and experimental solution of empty circular tubes

Model	Zarei & Kröger (2008)						Djamaluddin et al., (2015)					
	Experiment		FE		Error		Experiment		FE		Error	
	EA (J)	MCF (kN)	EA (J)	MCF (kN)	EA (%)	MCF (%)	EA (J)	MCF (kN)	EA (J)	MCF (kN)	EA (%)	MCF (%)
Z1	2326	45.6	2266	45	2.65%	1.33%	-	-	2278	43.76	2.11%	4.20%
Z2	2260	42.3	2270	41.5	0.44%	1.93%	-	-	2176	41.68	3.86%	1.49%
Z3	5081	86	4987	83.9	1.88%	2.50%	-	-	4947	83.45	2.71%	3.06%

Source: Djamaluddin et al. (2015)

2.10 Summary

This chapter summarizes the previous study had done on crashworthiness of energy absorber. Included all relevant theoretical, experimental and simulation works existing in the literature in every mode impact conditions. As mentioned, the frontal impact was approximately 50 % of all accidents during high speed impact, which is the highest percentage among all directions. Therefore, axial and oblique loading under dynamic impact study is very important criteria to consider during determine the performance of energy absorber.

From previous works, a lot studies been done on the thin-walled tube as an energy absorber. The extensive study of the thin-walled tube was done to improve the capability of energy absorption by filling the empty thin walled tube. Filler is commonly used to improve the thin-walled tube such as honeycomb, foam or divide an empty column into multicell. However, hexagon honeycomb and multicell is the most popular design which that bring a superior performance compared to empty thin walled tube. Recently, circular honeycomb is found had stronger energy absorption capability compared to hexagon honeycomb under the same relative density. Meanwhile, there is not much work done on out-plane but on in-plane compressive test.

FEM simulation is the most saved time and costs in designing a new state-of-art product with satisfying reliability and safety criteria requirements compare to experimental work. This technology also solves the complicated problems with high accuracy and determined the behaviour of the structure under different external influences. The most important is simulation made most of the structures experienced operating loads that vary with time and save cost on those experiments consist of huge quantity sample test.

CHAPTER 3

RESEARCH METHODOLOGY

3.1 Introduction

This chapter focused on discussion of research flow and methodology for the study. The methods used to carry out the study were described. The proposed model of honeycomb filler with the design in geometries parameters and variations of angle loading were discussed. This will be elaborated with more details in the following separate sections.

3.2 Research Plan

In this research, there are four main ideas that will need to focus on. Description and details of all ideas were discussed. The entire outline of this research is shown in Figure 3.1 below.

The first part of this research is the literature review. The understanding of crashworthiness parameters, honeycomb filler and energy absorber under axial and oblique loading of the model will be described in this section. The second part of the research is to verify FE model setup before simulation process to be carried out. Preliminary study been carried out to ensure the model setup up by those setting with sufficient accuracy in result. The third part of research is to design the honeycomb filler. This research work comprises two major parts which are honeycomb filler influenced by geometrical and thickness subjected to four different angle of loading respectively. The numerical technique is adopted by utilizing FE model in this research work. The usage of this numerical technique for analysis has been proven to be cost effective and also time efficient. In the last part of this research, the results and conclusion on analysis of this research to be discuss.

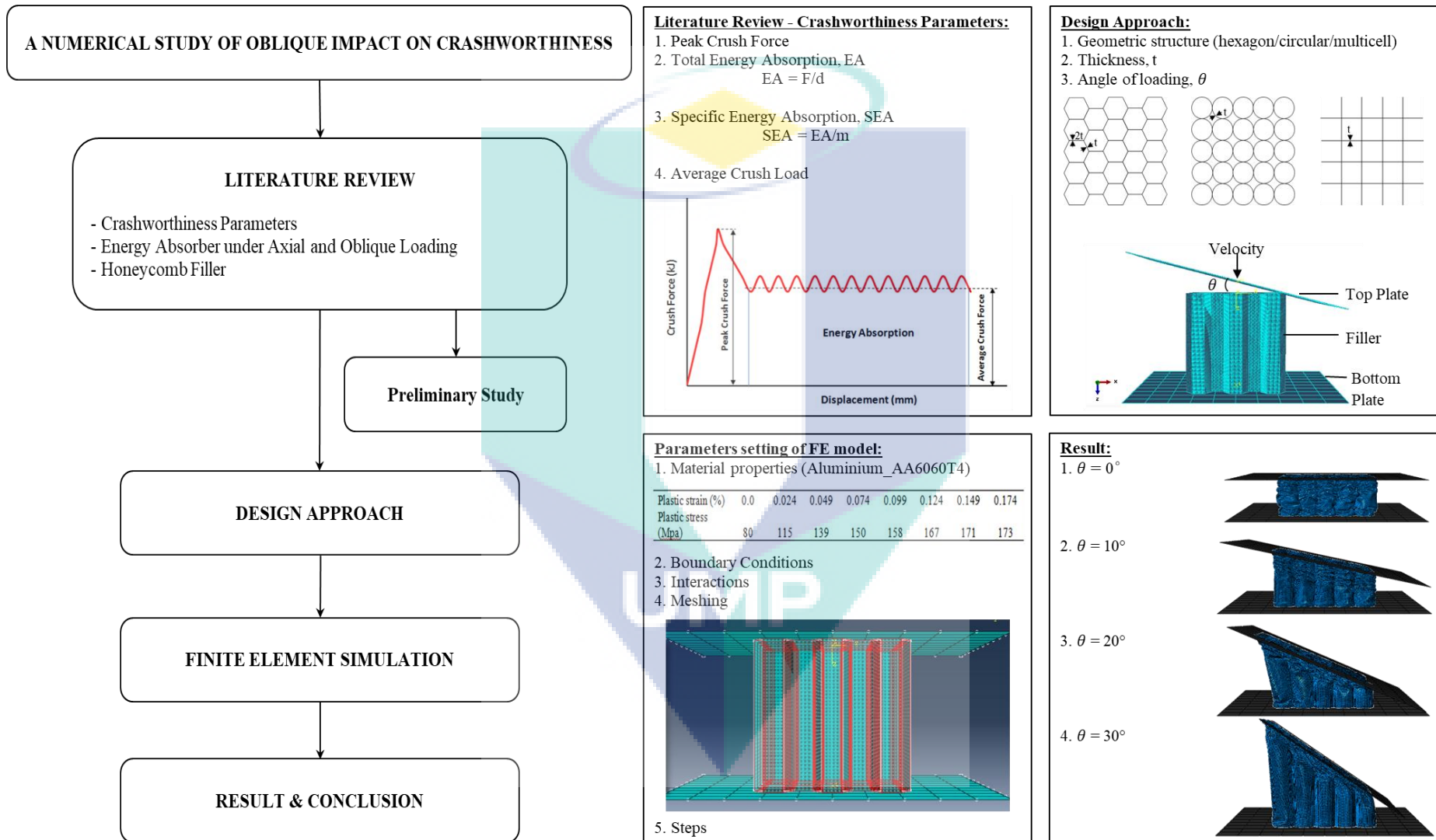


Figure 3.1 The adopted research methodology approached

3.3 Finite Element Model

In this research, the model that is carried out undergoes numerical test by ABAQUS software. The model will solve with nonlinear DYNAMIC/EXPLICIT solutions. The explicit dynamic analysis simulates high speed events like impact, drop test and crash. An explicit dynamic analysis is computationally effective for both of the analysis of expansive models with relatively short dynamic response times and for the analysis of great degree irregular occasions or processes. For an analysis with a definition of very general contact condition is allowed to run by explicit dynamic test. For time increment to be used is allowed either to be set as automatic or fixed by default. Abaqus/Explicit uses automatic time increment with the global time estimator (“Abaqus Analysis User’s Manual 6.10”, 2010). All setting to be discussed as following sub-chapters, these setting were verified during data verification in Chapter 2.8.2.

3.3.1 Preliminary Study

In this chapter, preliminary study carried out to verify the setting of FE model. All settings in preliminary study will be applied to this study as mentioned in Chapter 2.9. Based on the previous study, FE simulation has been conducted to verify the work of both Gameiro and Cirne (2007) and Zarei and Kröger (2006) work as shown in Table 2.8. For clarification, the results are indicated again as below.

The first FE model was developed by experimental specimen of Gameiro and Cirne (2007). Figure 3.2 and Figure 3.3 showed result of verified models compared to experiment specimen. The initial peak force rose up to 69 kN and drop immediately to about 20 kN after the impact occurred. For the peak load, it was slightly lower compared to Gameiro and Cirne’s model. After that, the load of crush progressive for both models was similarly oscillated at between 20 kN to 40 kN. The EA for the present FE model and validated model were 6.8 kJ and 6.5 kJ respectively. The variance between both models was 4.3 %.

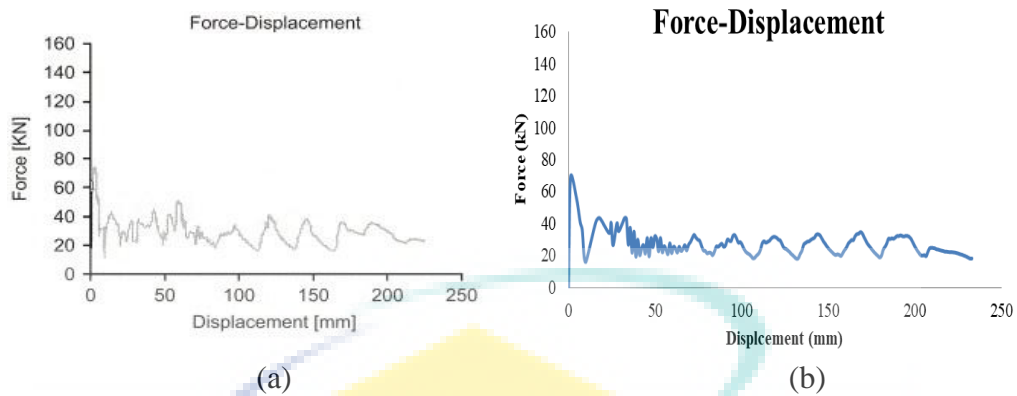


Figure 3.2 Force-Displacement response of FE model (a) Gameiro's model (b) preliminary study

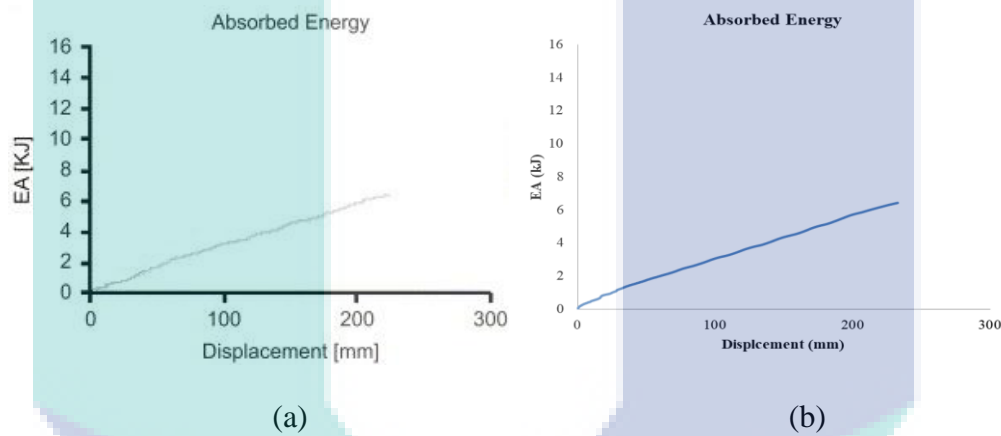


Figure 3.3 Absorbed energy response of FE model (a) Gameiro's model (b) preliminary study

Table 3.1 showed the result of second validation models compared to the experiment of Zarei and Kröger (2006). For model Z1, the EA and MCF were 2326J and 45.6kN respectively during experiment, while 2238J and 43.46kN respectively during simulation. The variances were 3.783% and 4.693% respectively. For model Z2, the EA and MCF were 2260J and 42.3kN respectively during experiment, while 2259J and 42.57kN respectively during simulation. The variances were 0.044% and 0.634% respectively. Lastly, the EA and MCF of Z3 were 5081J and 86kN respectively during experiment, while 5127J and 86.49kN respectively during simulation. The variances were 0.897% and 0.567% respectively. Based on the result showed, all validated models not more than 5% variance compared to experiment data.

Table 3.1 Comparison of FE simulation and experimental data of preliminary study

Model	Z1		Z2		Z3	
	EA (J)	MCF (kN)	EA (J)	MCF (kN)	EA (J)	MCF (kN)
Experimental (Zarei & Kröger, 2006)	2326	45.6	2260	42.3	5081	86
Preliminary Study	2238	43.46	2259	42.57	5127	86.49
Error	3.93%	4.92%	0.04%	0.63%	0.90%	0.57%

3.3.2 Design Approach

In this chapter, the designs of the model were discussed. Honeycomb filler was the main object to be studied in this research. The designation of the honeycomb filler structure was stated as below.

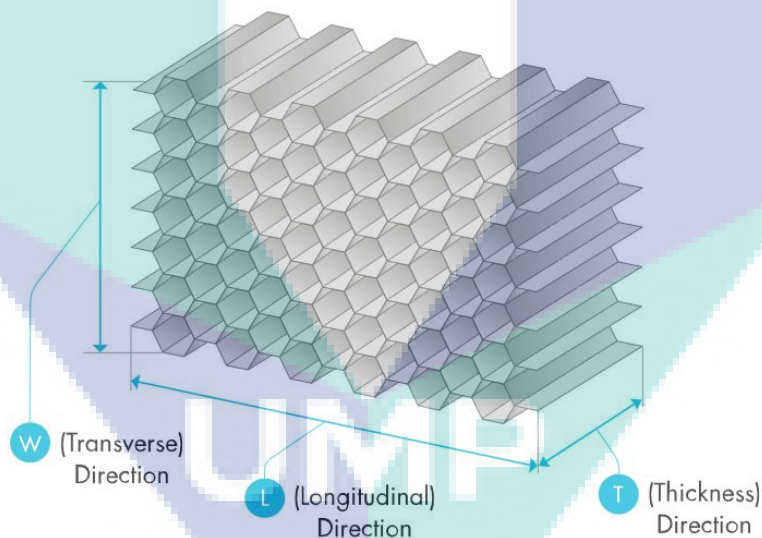


Figure 3.4 Honeycomb material direction

Source: Corex-Honeycomb (2018)

The strength of honeycomb was evaluated in three different axes: T-direction (thickness or cell depth), L-ribbon direction and W-transverse direction, as shown in Figure 3.4. In this study, the loading mass was applied on T-direction, which is the out-of-plane direction. This is due to out-of-plane direction is the particular strong direction for honeycombs. (Zhang & Ashby, 1992)

There are 3 types of honeycomb filler are studied. Figure (a) – (c) show the cross-sectional views of honeycomb fillers. For the first model (Figure a), it is regular hexagon honeycomb. Each edge side of the single cell is equally with 6mm length. The thickness of overlay panel between honeycomb cell can be considered as two single layers by omitting the thickness of epoxy (Yin, et al., 2011). For the second model (Figure b), it is circular-celled honeycomb (Hu et al., 2015). The radius, r of each single circular cell is 5.2 mm. For the third model (Figure c), it is multicell filler. Each side of the cells are equally to 10.4 mm. The dimensions of every single cell in second and third model are mainly modified from the first model. The edge size (10.4 mm) of every single cell is set according to the internal radius of the regular hexagon.

These honeycomb fillers are different in term of geometric. Meanwhile, the total size of width (W-direction) and length (L-direction) of all honeycomb fillers have been fixed. The quantity of cells on the out-of-plane has reported, not much effect on crushing load per cell (Mellquist & Waas, 2004). Hence the honeycomb fillers are 25 cells. Each block (5 x 5 cells) is numerically worked to verify the validity (Hu et al., 2015). Figure and Figure 3.6 show the geometry to be modelled along with some modelling parameters that need to be explored.

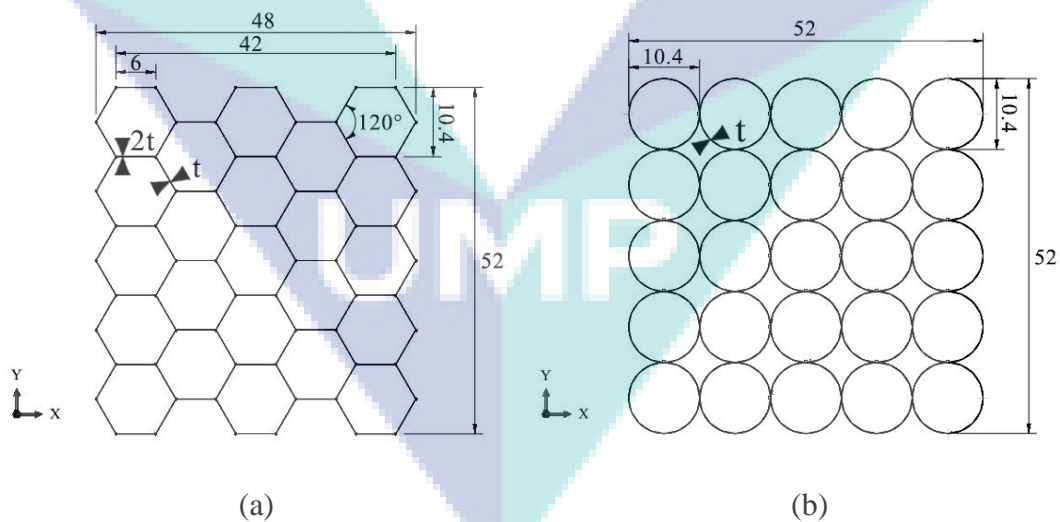


Figure 3.5 Cross-sectional view of the honeycomb fillers (mm) (a) hexagon honeycomb filler (b) circular honeycomb filler and (c) multicell filler

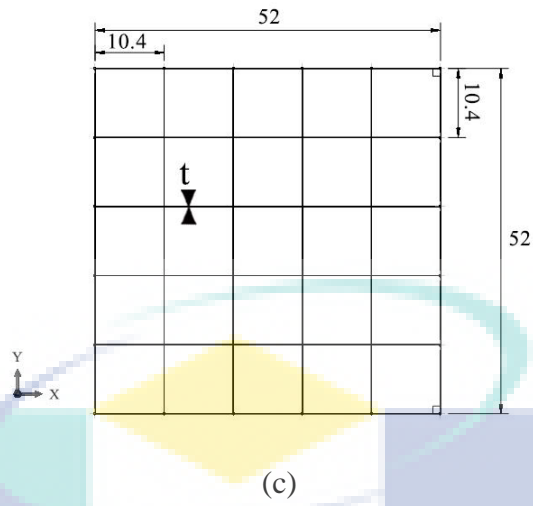


Figure 3.5 Continued

In this study, the honeycomb fillers are designed subjected to frontal dynamic impact loading. All models are tested under both axial and oblique loading. The variations of the angle loading, θ are 0° , 10° , 20° and 30° . The angle of loading, θ is the angle between top plate and model. Figure 3.6 shows a sample of FE model with the angle of impact loading, θ .

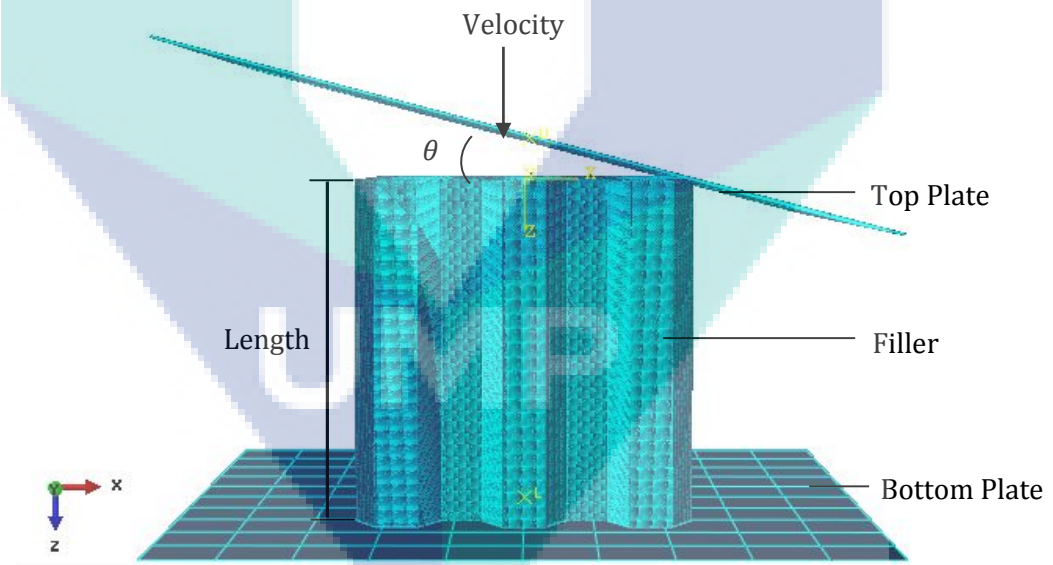


Figure 3.6 FE model of hexagon honeycomb filler with the angle of θ , 20°

3.3.3 Material Characteristic

The material used for honeycomb is aluminium alloy AA6060 T4. Aluminium alloy AA6060 T4 is insensitive to the strain rate, strain rate effects are of minor

importance. Negligible strain rate sensitivity is evident for 6xxx series aluminium alloy (Costas et al., 2016; Hu et al., 2008). The mechanical properties of AA6060 T4 for density $\rho = 2700 \text{ kg/m}^3$, the Young's Modulus $E = 68.2 \text{ GPa}$, the Poisson's ratio $\nu = 0.3$, initial yield stress $\sigma_0 = 80 \text{ MPa}$ and ultimate stress $\sigma_{\text{Ult}} = 173 \text{ MPa}$. The pair of the plastic strain and true stress were specified in Table 2.7 to accurately define the hardening characteristic in finite element models. Figure 3.7 showed the procedure to define AA6060 T4 material properties in ABAQUS software.

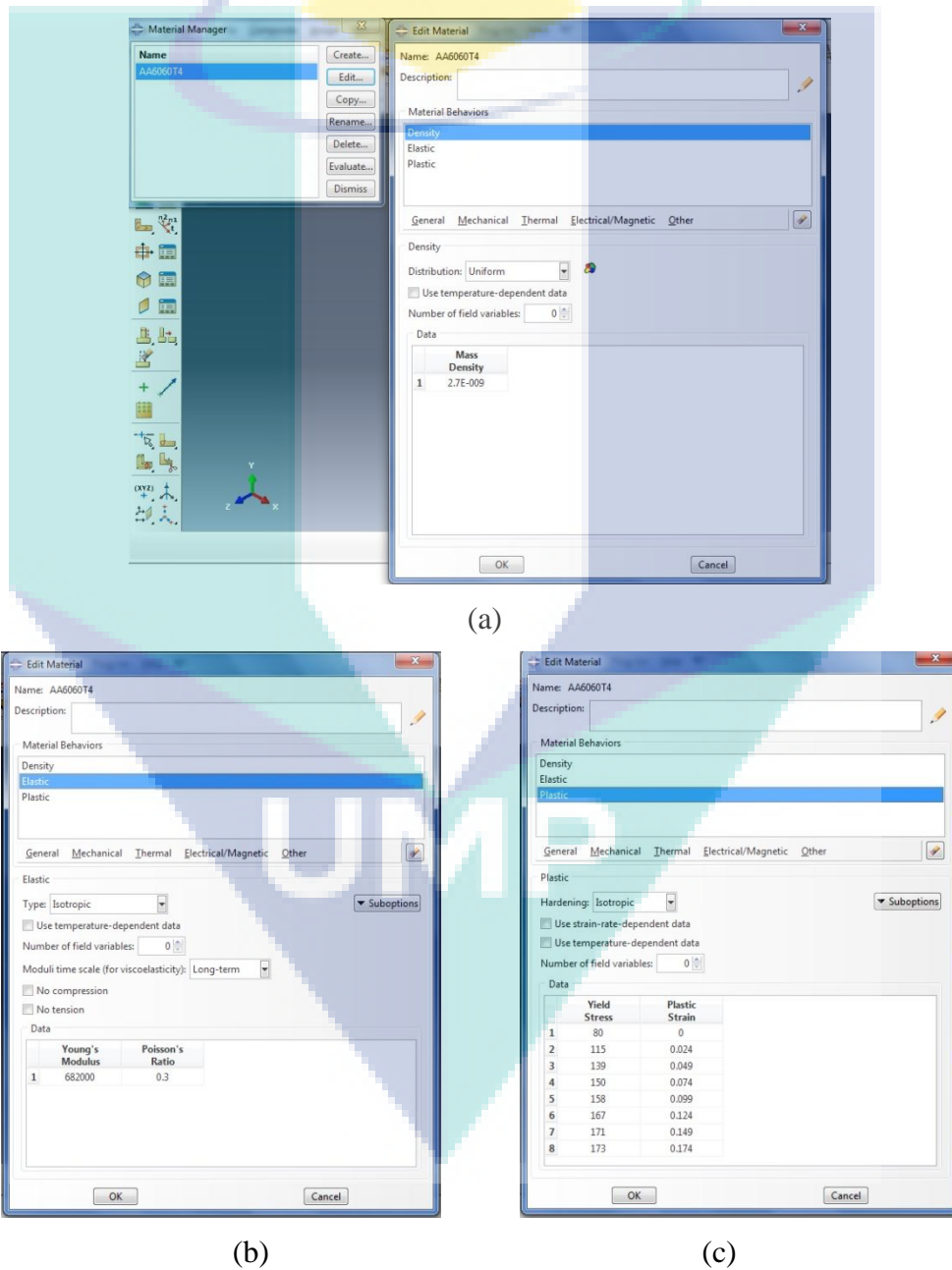


Figure 3.7 Setting of material properties with unit (a) density (tonne/mm^3) (b) young's modulus (N/mm^2) (c) yield stress (%) and plastic strain (MPa)

3.3.4 Boundary Condition

Boundary conditions can be used to specify the values of all essential arrangement factors (displacements, rotations, electrical potentials, temperatures, normalized concentrations, acoustic pressures, pore pressures, connector material flow, fluid pressures or warping amplitude,) at nodes. It can be given as “model” input data (within the initial step in Abaqus/CAE) to define zero-valued boundary conditions.

Dynamic test model contained of two rigid plates placed at both end of the model. The boundary condition for the bottom plate is set as ‘Encastre’ which fully constraint for all degree of freedom ($U1 = U2 = U3 = UR1 = UR2 = UR3 = 0$) as in Figure 3.8(a). The boundary condition for the top plate is set as ‘Displacement’ which fixed all direction in coordinate system (CSYS) except $U3$ (z-axis) direction. The $U3$ is the only direction which is allowed to move in the simulation environment as in Figure 3.8(b). All settings are shown in Figure 3.8.

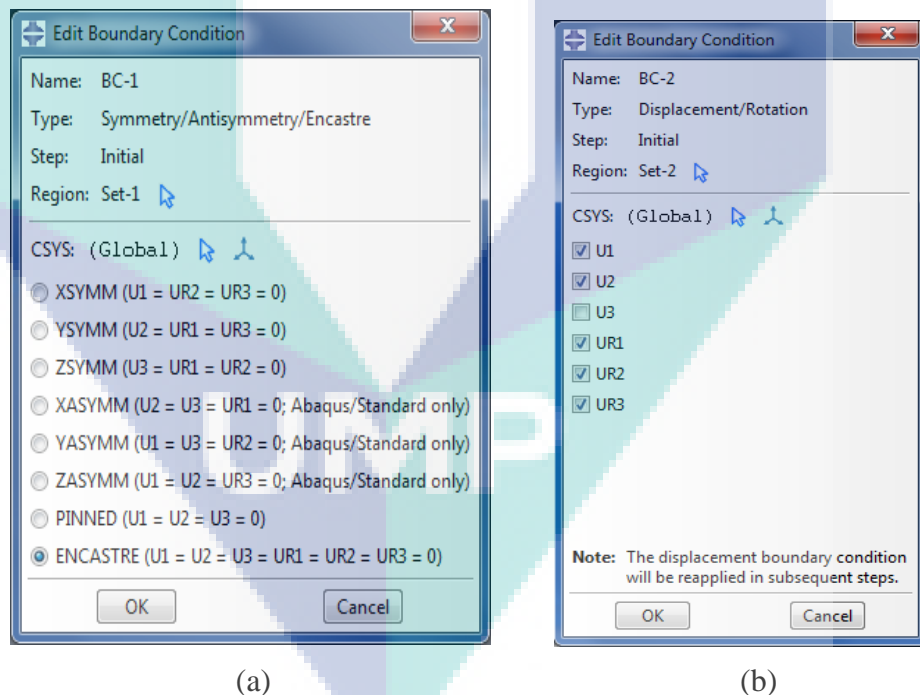


Figure 3.8 Boundary condition of (a) bottom plate (b) top plate

Figure 3.9 and Figure 3.10 showed the settings of the models for the impact velocity and load for top plate. This study was carried out on the dynamic impact test.

The dynamic impact velocity applied as 15 m/s. For the load impact, it was 400 kg (Sun et al., 2016).

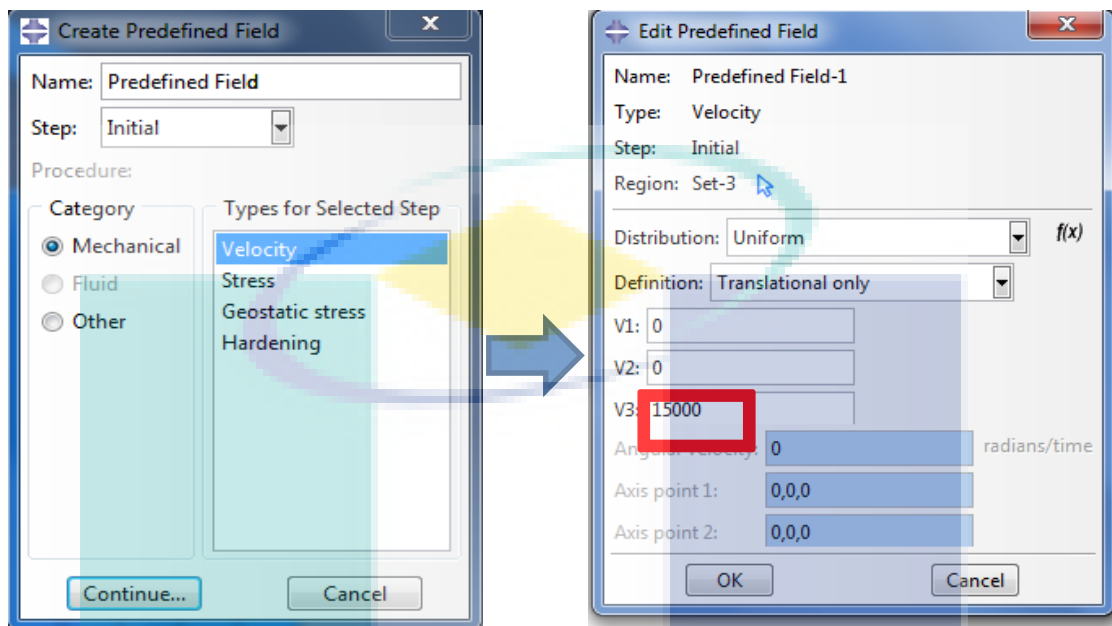


Figure 3.9 Setting of velocity for top plate (mm/s)

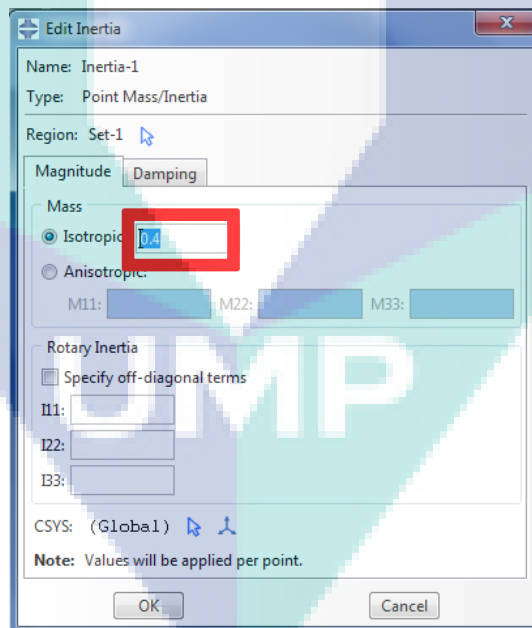


Figure 3.10 Setting of impact load for top plate (tonne)

3.3.5 Interaction

General contact is a contact interaction property that can define as tangential behaviour (friction and elastic slip) and normal behaviour (hard, soft, or damped contact

and separation). The FE simulations involve interaction between the honeycomb filler and bottom rigid plate and top plate. The contact interaction between all components is the general contact algorithm used to avoid interpenetration, which is less intense in terms of computational time. Meanwhile, the contact for the honeycomb is modelled as a finite sliding penalty based contact algorithm, with contact pairs and a hard contact. The kinetic friction coefficient of 0.2 is selected for the contact between the honeycomb filler, the top plate and the bottom plate for the dynamic cases (Olabi et al., 2008). The contact setting is shown in Figure 3.12.

In the other hand, a tie constraint is tied two regions together even though the meshes created on the surfaces of the regions may be dissimilar, so that there is no relative motion between them. When a contact pair contains two surfaces, the two surfaces are not allowed to include any of the same nodes. This constraint setting was applied to both top plate and bottom plate at the position which contact to honeycomb filler.

Since contact in ABAQUS depends upon the specification of primary and secondary surfaces and since analytically rigid surfaces are by default allowed being only primary contact surfaces (HKS, 2006). So, the internal surface of bottom plate as the master surface and the lower contact surface region of honeycomb as the slave surface. The interaction of the model setting is shown in Figure 3.11 – Figure 3.13.

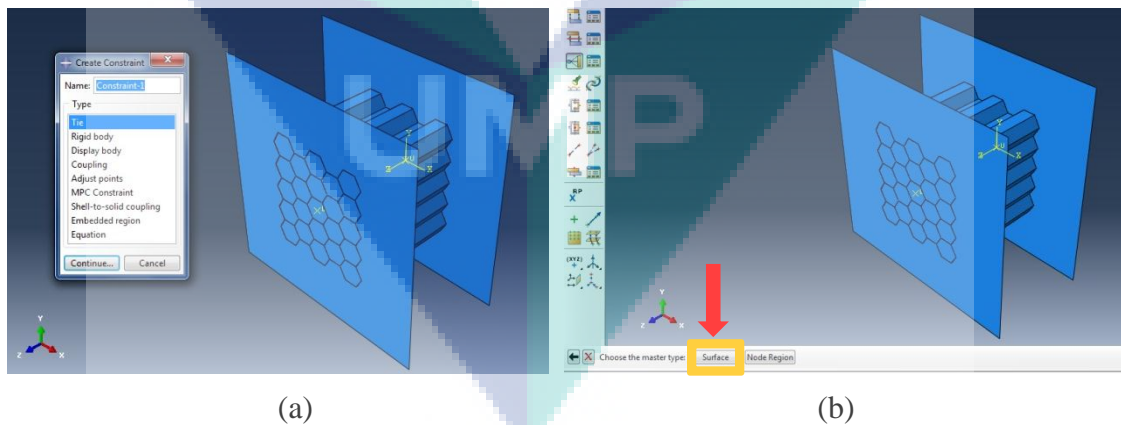


Figure 3.11 Interaction of honeycomb, top and bottom plate (a) constraint setting set as tie (b) surface contact of both top and bottom plate with honeycomb

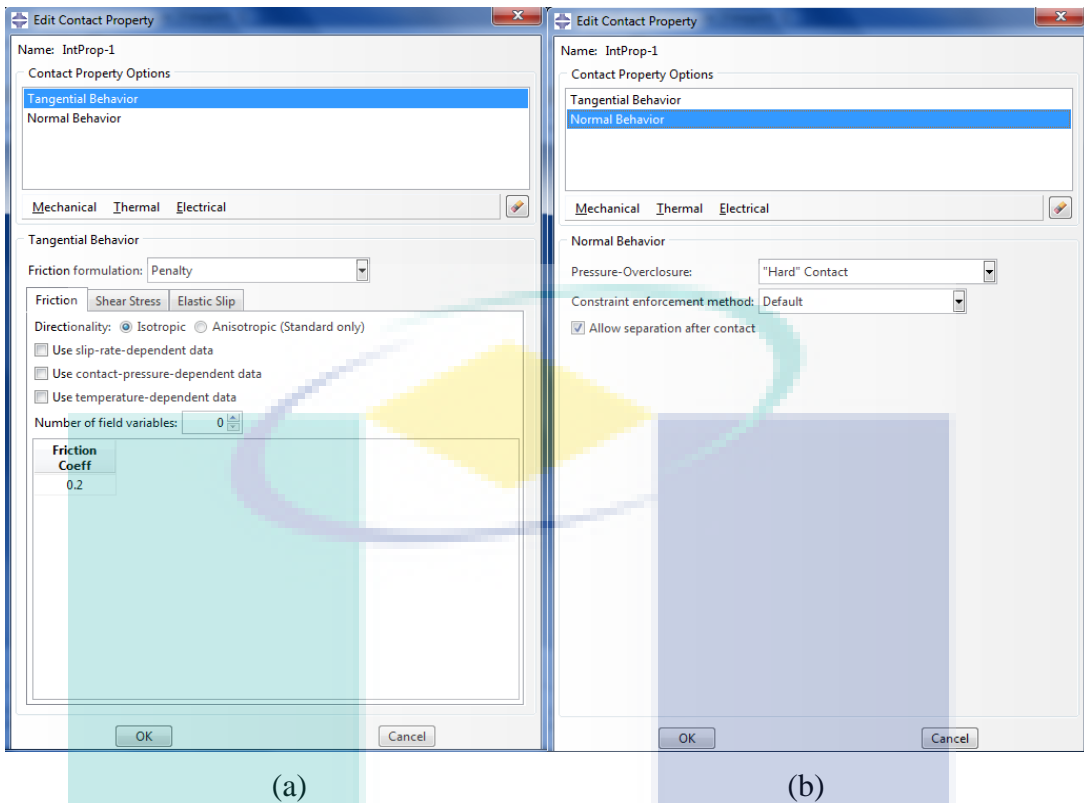


Figure 3.12 Contact property setting of (a) friction coefficient (b) hard contact

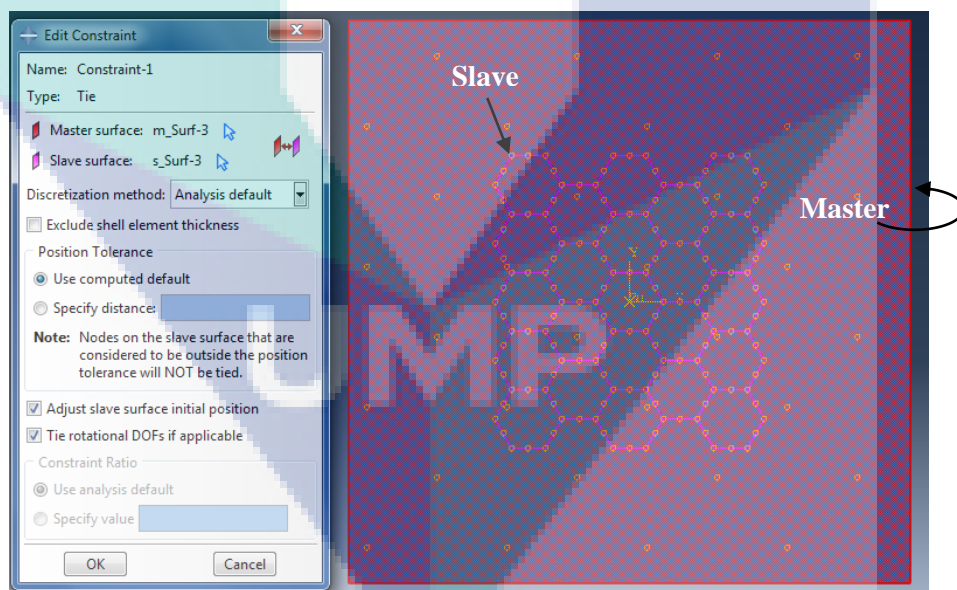


Figure 3.13 Surface contact between master and slave

3.3.6 Meshing

Meshing is a vital step in the FE simulation order to achieve a good trade-off between computational cost and accuracy. A smaller element size is desirable in order

to achieve solution with higher accuracy in result. In this research, the mesh size was chosen to achieve a good compromise between computational time and accuracy.

Figure 3.14 – Figure 3.16 show the mesh setting of the model in this study. In the preliminary stage of the design analysis (when approximate results are required for initial analysis) a large size element size is chosen in order to achieve faster solutions. In this analysis, the model is meshed with 4-node doubly curved thick shell elements with a reduced integration, active stiffness hourglass control (S4R). In order to determine the appropriate element size, a convergence study was performed among different element sizes. Based on Sun et al. (2016), the mesh size use for the model is 0.4mm. Meanwhile, the mesh surface control and algorithm are chosen as Quad and Medial Axis respectively. The default automatic mesher is used to generate the mesh based on a global element size, tolerance and local mesh control specifications.

Free meshing is meshing technique which used no pre-established mesh patterns. The pattern of the mesh was predicted based on the region topology. Free meshing allowed more flexibility due to unstructured technique. This meshing technique could mesh the topology of regions very complex. Quad, Quad-dominated and Tri element shape options for two-dimensional. Honeycomb structures in this study do not have complex region, therefore Quad was choice as element shape. This is due to Quad use exclusively quadrilateral elements. Meanwhile, Quad-dominated used primarily quadrilateral elements, but allow triangles in transition regions.

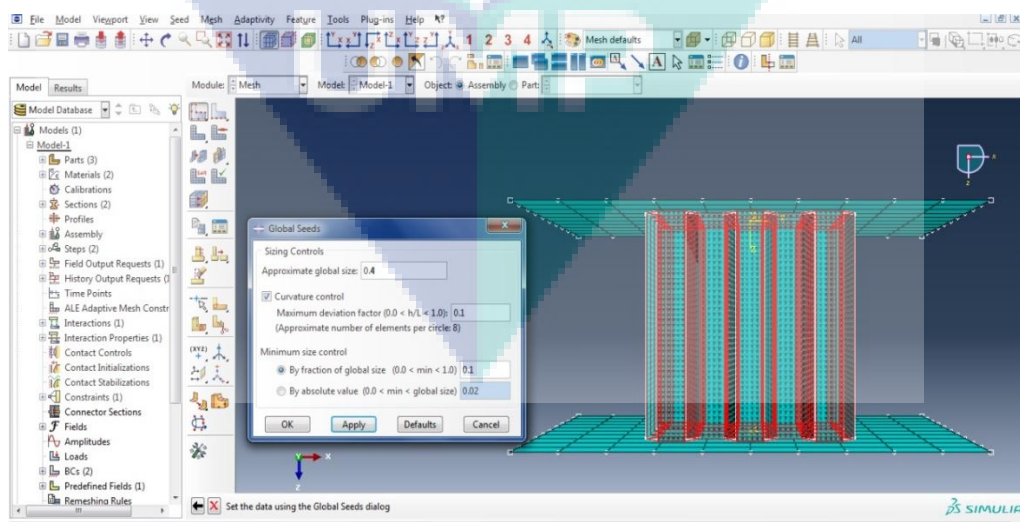


Figure 3.14 Setting of mesh size: 0.4 mm

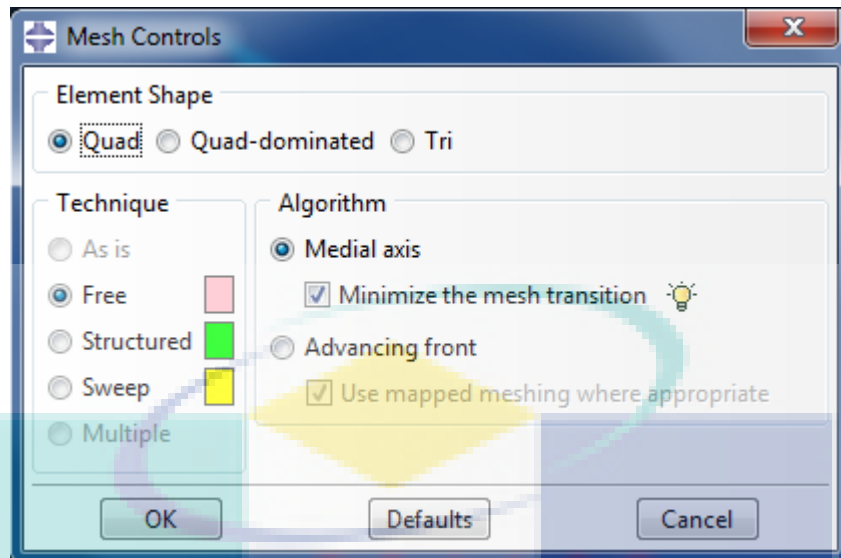


Figure 3.15 Setting of mesh type

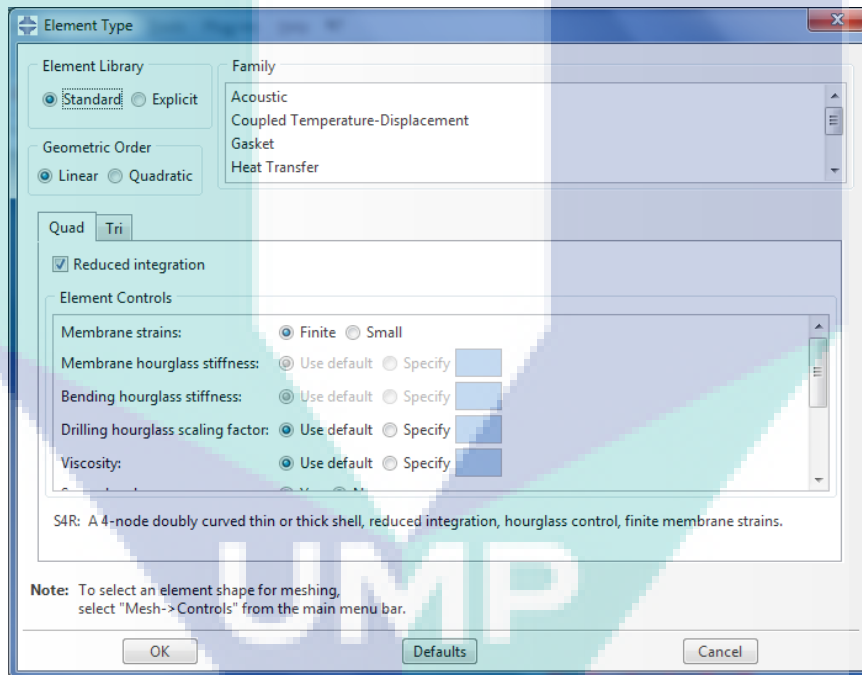


Figure 3.16 Setting of mesh element

3.3.7 Steps

An initial step is created at the beginning of the model's step sequence for FE model. General step is used for the FE simulation of all models. Figure 3.17 shows the setting of Step. It can be found in Predefined Field Manager. The type of procedure in this study is dynamic loading by Explicit. Meanwhile, the time period and increments of time frames are defined based on the model. In this study, there is only one step

required. A deformation of the honeycomb by dynamic impact loading subjected to different loading angle. A general type of Dynamic-Explicit is created. The time period of the model requires upon the length/mass/time is about 0.3. For the number of increments to be set is 100, this is for a better data interpretation.

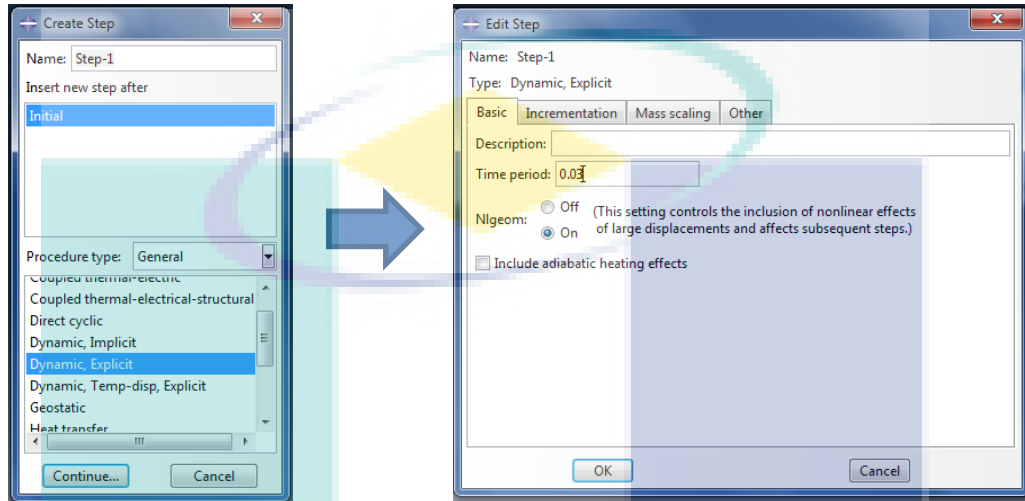


Figure 3.17 Setting of step

3.4 Honeycomb Thickness Design and Impact Angles

To study the performance of honeycomb subjected to the angle of loading, the variables and labelling are shown in Table 3.2. As mentioned in Chapter 2, the angle of loading affected the performance of the energy absorber. Each honeycomb filler will impact subjected to four types of loading angles. There are axial loading to represent 0° and oblique loading for 10°, 20° and 30° angle respectively. These angles of loading are investigated by the same condition of FE model setting.

Table 3.2 Design variable of parameter on angle of loading

Angle of Loading		Label
Axial Loading	0°	L0
	10°	L10
Oblique Loading	20°	L20
	30°	L30

In this study, the performances of honeycomb filler with three different thicknesses are investigated. The initial thickness of every honeycomb set as 0.06 mm. Then, thickness of honeycombs were increased and set as 0.12 mm and 0.18 mm. In

every model, 5 integration points through the cell wall thickness is fixed, as shown in Figure 3.18. Other parameters are kept constant which length at 50mm, the dimension of each cell in every models, the arrangement of single cells in every honeycomb block, and the number of single cells in a honeycomb block. Table 3.3 summarizes the variables of parameter in this study.

Table 3.3 Honeycomb thickness and labelling of models

Geometry	Thickness, mm	Label
Circular Honeycomb	0.06	C06
	0.12	C12
	0.18	C18
Hexagonal Honeycomb	0.06	H06
	0.12	H12
	0.18	H18
Multicell	0.06	M06
	0.12	M12
	0.18	M18

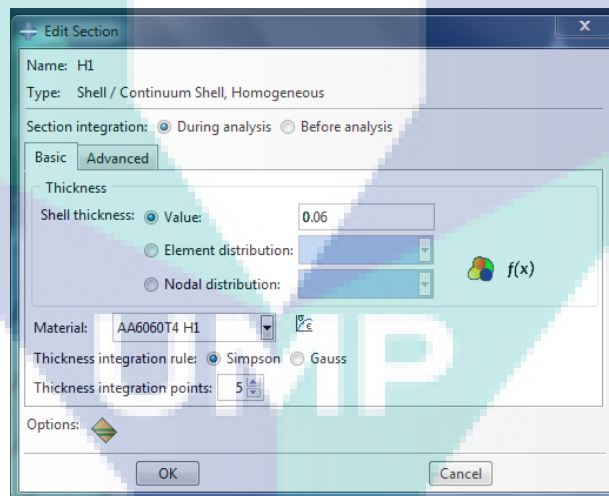


Figure 3.18 Setting of thickness and integration point (mm)

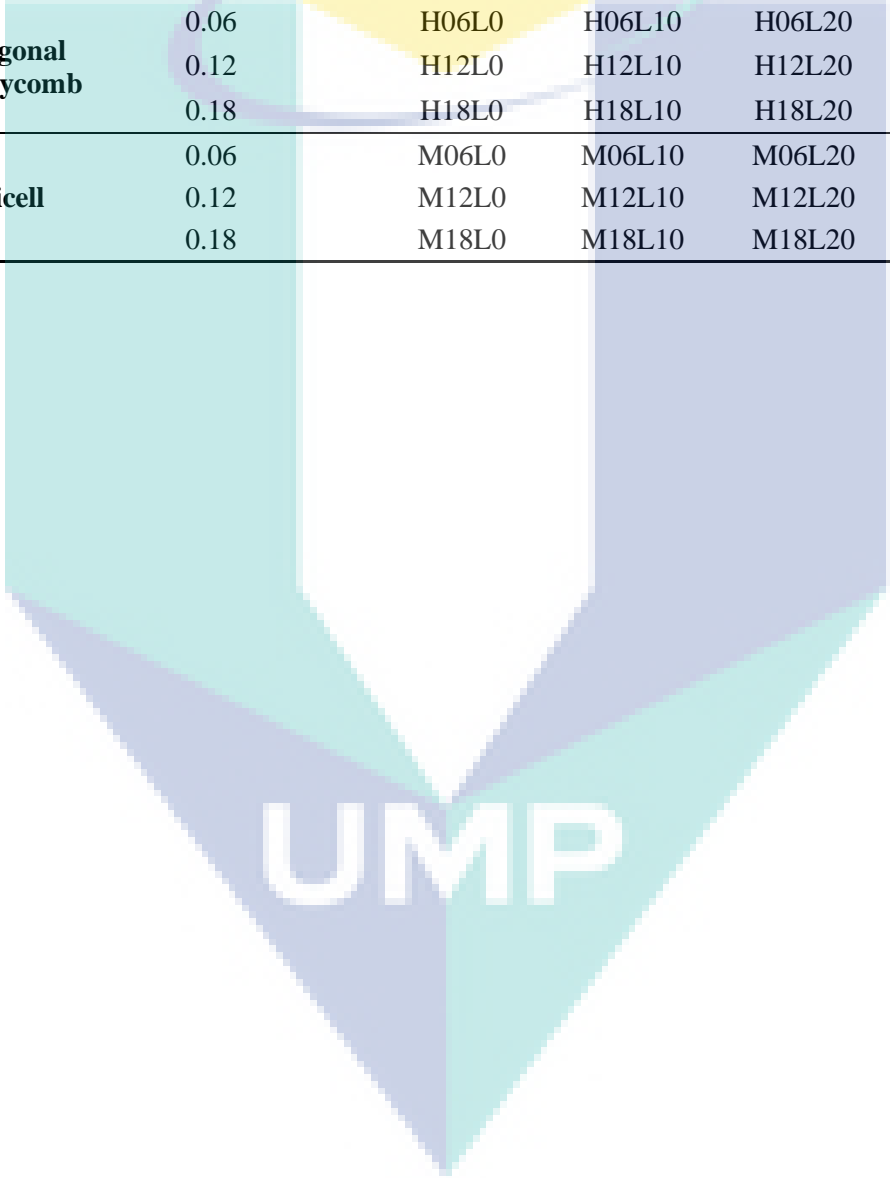
3.5 Summary

Research methodology adopted in this thesis work has been explained. There are two major parts. The first part of the study focused on comparison of different geometrical honeycomb fillers performance on different angle of loading. The second part of study focused on honeycomb fillers influenced by different thickness on

different angle of loading. Table 3.4 showed all models with different variables and labelling. The results obtained will be explained in the following chapter.

Table 3.4 Design variables and labelling of models subjected to angle of loading

Geometry	Thickness, mm	Angle of Loading			
		0°	10°	20°	30°
Circular Honeycomb	0.06	C06L0	C06L10	C06L20	C06L30
	0.12	C12L0	C12L10	C12L20	C12L30
	0.18	C18L0	C18L10	C18L20	C18L30
Hexagonal Honeycomb	0.06	H06L0	H06L10	H06L20	H06L30
	0.12	H12L0	H12L10	H12L20	H12L30
	0.18	H18L0	H18L10	H18L20	H18L30
Multicell	0.06	M06L0	M06L10	M06L20	M06L30
	0.12	M12L0	M12L10	M12L20	M12L30
	0.18	M18L0	M18L10	M18L20	M18L30



UMP

CHAPTER 4

RESULTS AND DISCUSSION

4.1 Introduction

The application of FE simulation study can significantly reduce the time and costs associated with the design and experiment test on crashworthiness of energy absorber. This may reduce the number of wastes during trial and error compared to conventional experiment. Based on the outcome of the FE simulation, deformation and energy absorption of models are shown in the result clearly. In this study, the variables of the models were mentioned in Chapter 3 and performance details of every model will then be discussed as follows. The efficiency is evaluated based on the crashworthiness criteria namely energy absorption (EA), specific energy absorption (SEA), peak crush force (PCF), mean crush force (MCF) and crush force efficiency (CFE) value. A

4.2 Effect of Geometry

The effect of geometrical on EA, SEA, PCF, MCF and CFE is analysed for circular honeycomb, hexagon honeycomb and multicell filler of thickness, $t = 0.06$ mm only. The mass of the models are 0.0051 kg, 0.0056 kg and 0.0066 kg for circular honeycomb, hexagon honeycomb and multicell filler respectively. All fillers versus geometrical are evaluated when the structure is subjected to frontal dynamic impact loading on different angles, $\theta = 0, 10, 20$ and 30 degrees.

4.2.1 0 Degree

The results of the crashworthiness criteria versus every geometric design were shown in Table 4.1. For Figure 4.1, the graph depicted the performance on force-displacement curves of every model. It obtained by the compressive test performance

and the deformation of the described honeycomb filler models. All models were tested by dynamic impact loading with the angle, $\theta = 0$ degrees, as known as axial loading.

Table 4.1 The result of honeycomb filler versus geometry at 0 degrees

	PCF (kN)	EA (kJ)	SEA (kJ/kg)	MCF (kN)	CFE
C06L0	3.994	0.118	17.833	1.667	41.7%
H06L0	3.517	0.133	23.662	2.288	65.0%
M06L0	3.310	0.054	10.645	0.880	26.6%

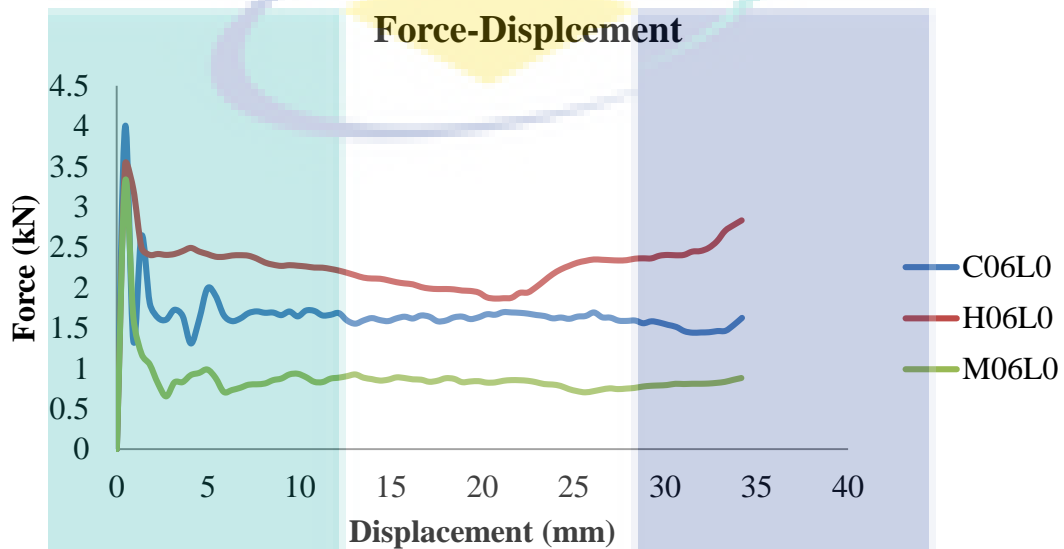


Figure 4.1 Force displacement of honeycomb filler at 0 degrees of impact loading

Circular honeycomb filler had the highest PCF among three models which was at 3.994 kN. The EA result showed 0.118 kJ while the result of SEA showed 17.833 kJ/kg. For the result of MCF, that showed 1.667 kN. Based on the ratio of MCF to PCF, the CFE showed 41.7 %. The graph showed that, the initial force rose steeply peaked at 4.0 kN. After that, the force dropped to 1.3 kN then the force rose up to 2.5 kN and was oscillating along with the displacement between 2 kN.

Hexagon honeycomb filler had the highest EA and highest SEA at 0.133 kJ and 23.662 kJ/kg. While, PCF of hexagon honeycomb filler is at 3.517 kN and the MCF is at 2.288 kN. For CFE, hexagon honeycomb is the highest among all models that found to be 65.0 %. The graph showed that, the peak force was reached to 3.5 kN then fall to 2.5 kN. Following, there was a gradual fall in force at 1.8 kN. During displacement 20 mm, the force rose erratically over the displacement.

The result of multicell filler for PCF, MCF, EA and SEA which were 3.310 kN, 0.880 kN, 0.054 kJ and 10.645 kJ/kg respectively. CFE was also found to be the lowest among all models which only 26.6 %. The graph showed that, multicell filler reached a high peak force at the beginning. The force peaked at 3.3 kN then fall to 0.8 kN. After that, the force rose and was oscillating along with the displacement between 0.8 kN.

4.2.2 10 Degrees

The results of crashworthiness criteria versus every geometric design were shown in Table 4.2. For Figure 4.2, the graph depicted the performance on force-displacement curves of every model. It obtained by the compressive test performance and the deformation of the described honeycomb filler models. All models were tested by frontal dynamic impact loading undergo oblique loading with the angle, $\theta = 10$ degrees.

Table 4.2 The result of honeycomb filler versus geometry at 10 degrees

	PCF (kN)	EA (kJ)	SEA (kJ/kg)	MCF (kN)	CFE
C06L10	1.851	0.080	12.146	1.432	77.4%
H06L10	2.114	0.092	16.388	1.808	85.5%
M06L10	1.527	0.037	7.309	0.747	48.9%

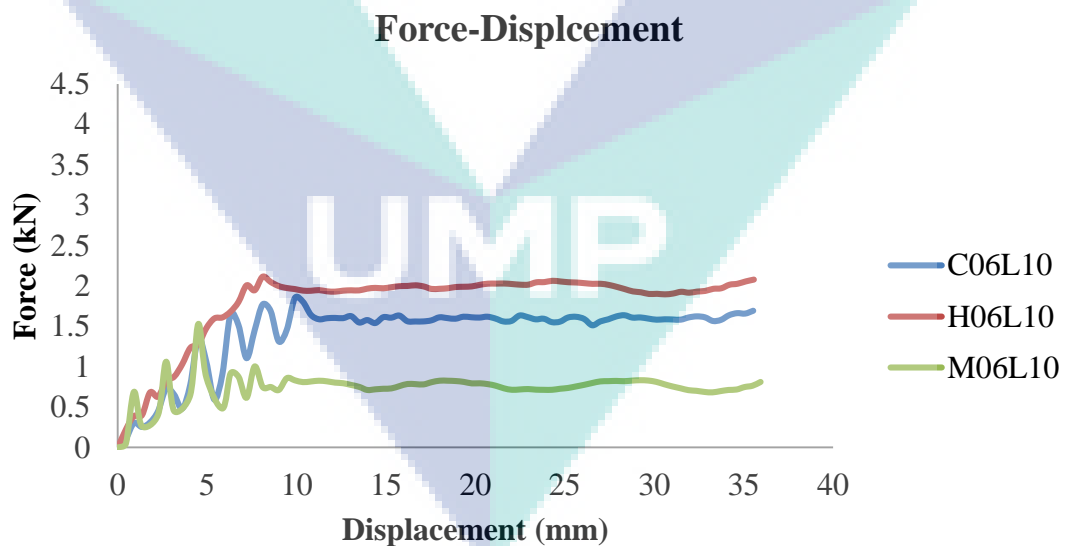


Figure 4.2 Force displacement of honeycomb filler at 10 degrees of impact loading

For circular honeycomb filler, the result of PCF and MCF were 1.851 kN and 1.432 kN respectively. Meanwhile, the EA and SEA were 0.080 kJ and 12.146 kJ/kg. For the result of CFE was 77.4 %. The result showed circular honeycomb filler is

second higher performance when loading angle, $\theta = 10$ degrees. The graph showed that, the force was increased unsteadily. A fluctuated at beginning along with the displacement to 10 mm. After reached the maximum point of force at 1.85 kN, the force fall to 1.58 kN. Then, the performance of force was almost remained constant at 1.6 kN.

For hexagon honeycomb filler, the result of PCF and MCF were 2.114 kN and 1.808 kN respectively. Meanwhile, the EA and SEA were 0.093 kJ and 16.388 kJ/kg. For the CFE was 85.5 %. The graph showed that, there was a steep rise in force. Force increased to first peak at 1.98 kN, then fall and rose to second peak at 2.11 kN. Lastly, the force was levelled off at 2.0 kN. Hexagon honeycomb filler was the best performance in the result.

Lastly, multicell filler showed the lowest performance among three models. The overall result of EA, SEA and MCF were just achieved half of circular honeycomb filler. In result, PCF were 1.527 kN and MCF were 0.747 kN. For EA and SEA, there were only 0.037 kJ and 7.309 kJ/kg. Meanwhile, CFE was found only 48.9 %. The graph showed that, a serious undulated in force at the beginning. The maximum force rose up to 1.5kN at 5mm. Generally, it showed an increase trend along with the displacement to 10mm. After that, the force was remained constant less than 1kN.

4.2.3 20 Degrees

The results of crashworthiness criteria versus every geometric design were shown in Table 4.3. For Figure 4.3, the graph depicted the performance on force-displacement curves of every model. It obtained by the compressive test performance and the deformation of the described honeycomb filler models. All models were tested by frontal dynamic impact loading undergo oblique loading with the angle, $\theta = 20$ degrees.

Table 4.3 The result of honeycomb filler versus geometry at 20 degrees

	PCF (kN)	EA (kJ)	SEA (kJ/kg)	MCF (kN)	CFE
C06L20	1.532	0.045	6.871	1.116	72.8%
H06L20	1.744	0.054	9.528	1.322	75.8%
M06L20	0.798	0.022	4.358	0.549	68.8%

Force-Displacement

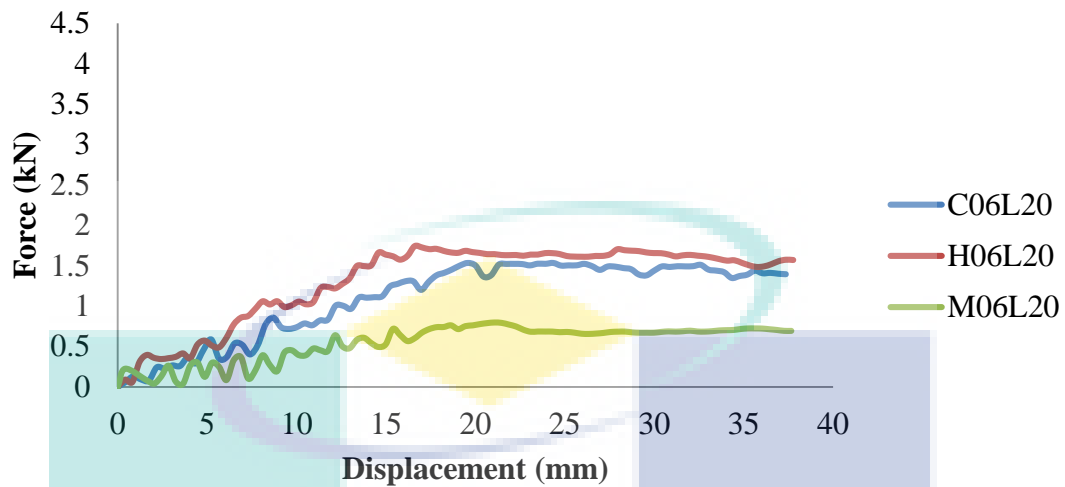


Figure 4.3 Force displacement of honeycomb filler at 20 degrees of impact loading

For circular honeycomb filler, the result of PCF and MCF were 1.532 kN and 1.116 kN respectively. Meanwhile, the EA and SEA were 0.045 kJ and 6.871 kJ/kg. For the result of CFE was 72.8 %. The graph showed that, an increase trend along with the displacement till 20 mm. The force rose up to 1.5 kN. After that, the force was remained at below 1.5 kN. Generally, it showed a fluctuation along with the displacement.

For hexagon honeycomb filler, the result of PCF and MCF were 1.744 kN and 1.322 kN respectively. Meanwhile, the EA and SEA were 0.054 kJ and 9.528 kJ/kg. For the CFE, hexagon honeycomb filler was achieved 75.8 % which was 3 % higher than circular honeycomb filler. The graph showed that, an increased trend of force at the beginning of displacement along with 16 mm. Force peaked at 1.7 kN, then remained at 1.6 kN. Found that, the steady force was slightly higher than circular honeycomb filler. Lastly, the force was slightly slipped to 1.5 kN. Hexagon honeycomb filler had the best performance in the result in terms of MCF, EA, SEA and CFE.

Lastly, multicell filler also showed the lowest performance among three models. The overall results were just achieved half of circular honeycomb filler and one third of hexagon honeycomb filler. In result, PCF were 0.798 kN and MCF were 0.549 kN. For EA and SEA, there were only 0.022 kJ and 4.358 kJ/kg. However, CFE was found to be 68.8 % which was considered close to other two fillers. The graph showed that, force fluctuated at the beginning. The force oscillating between 0.03 kN to 0.4 kN at initial 10

mm. On next 10 mm, the force rose up to maximum point at 1.8 kN. Generally, it showed an increase trend along with the displacement to 20mm. After that, the force was remained constant at 0.7 kN.

4.2.4 30 Degrees

The results of crashworthiness criteria versus every geometric design were shown in Table 4.4. For Figure 4.4, the graph depicted the performance on force-displacement curves of every model. It obtained by the compressive test performance and the deformation of the described honeycomb filler models. All models were tested by frontal dynamic impact loading undergo oblique loading with the angle, $\theta = 30$ degrees.

Table 4.4 The result of honeycomb filler versus geometry at 30 degrees

	PCF (kN)	EA (kJ)	SEA (kJ/kg)	MCF (kN)	CFE
C06L30	1.235	0.030	4.602	0.709	57.4%
H06L30	1.366	0.032	5.618	0.861	63.0%
M06L30	0.607	0.014	2.718	0.376	61.9%

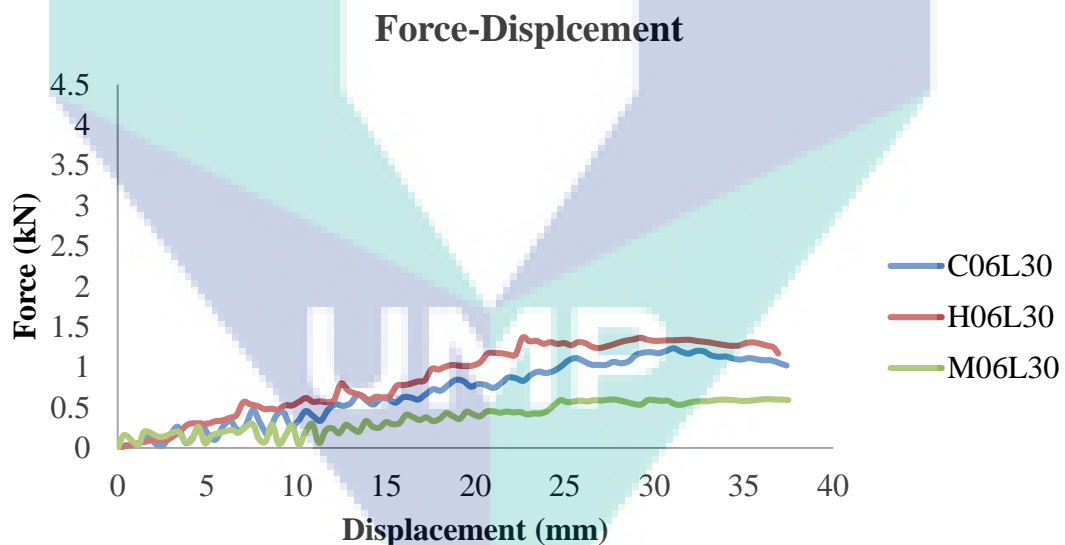


Figure 4.4 Force displacement of honeycomb filler at 30 degrees of impact loading

For circular honeycomb filler, the result of PCF and MCF were 1.235 kN and 0.709 kN respectively. The result of EA and SEA were 0.030 kJ and 4.602 kJ/kg. Thus, there was little different when angle at 20 degrees and below. Found that, the result of CFE was lowest among three models which at 57.4 %. The graph showed that, force

increased to 1.2 kN at beginning displacement until 30 mm. Then, the force was slightly decreased to 1.0 kN along with displacement. The trend of graph was fluctuated.

For hexagon honeycomb filler, the result of PCF and MCF were 1.366 kN and 0.861 kN respectively. The result of EA and SEA were 0.032 kJ and 5.618 kJ/kg. For the CFE, hexagon honeycomb filler was achieved 63.0 %. The graph showed that, force increased to the highest point at 1.4 kN. The peak force when displacement was 23 mm. After that, the force was steady and constant at 1.3 kN. Although the result was slightly higher than circular honeycomb filler, hexagon honeycomb filler remained the best performance in overall result.

Lastly, multicell filler still showed the lowest performance on every angle of loading among geometry. Although multicell filler had low PCF and MCF with high CFE, but, the performance of the EA and SEA were the lowest. The PCF and MCF of multicell filler were 0.607 kN and 0.376 kN respectively. The result of EA and SEA were 0.014 kJ and 2.718 kJ/kg. The overall result was found around 50 % lower than the another two models. The graph showed that, force fluctuated at initial 25 mm. Then, the force was increased to peak at 0.6 kN. Along with the displacement, the force was remained constant at 0.6 kN.

4.2.5 Overall Result

In this section, the evaluation of energy absorber of honeycomb filler versus geometric and structure subjected by the different angle of loading was concluded. Firstly, based on the total weight of honeycomb filler, multicell filler was the lightest weight model, then, followed by hexagon honeycomb filler and circular honeycomb filler.

Secondly, the results of PFC, MCF and CFE were compared among the three models. Hexagon had the highest PCF and MCF. Thus, due to the difference between both values was the smallest, so, it had the highest performance in CFE which at 70 %. However, multicell filler had high PCF but low MCF. So, it was a very low CFE performance at around 50 %.

Next, for the result of EA & SEA, hexagon honeycomb filler found as the highest. Followed by circular honeycomb filler, which was slightly lower than hexagon

honeycomb filler. Thus, multicell is the worst performance, the performance is not more than 50% of hexagon honeycomb filler. The performance of both EA and SEA were a 40% lower than the others model. It consisted of high peak load but low mean crush force, therefore, the CFE value very low.

Lastly, when the angle of loading increased, the performance of EA, SEA and CFE were decreased. There was a 40% decline of performance in every 10 degrees of angle inclined. For example, when θ is 0 degrees and performance as 100%, during 10 degrees of angle inclined, found 40% dropped off result which is 60 % at the stage. Respectively, when θ is at 10° and EA and SEA at 60 %, a 10° increase in θ to 20° will result in a 40 % drop of EA and SEA which is 36 % at the stage. Followed by 30°, and resulting 21.4 % of EA and SEA. Figure 4.5 shows the overall performance of honeycomb filler when angle of loading.

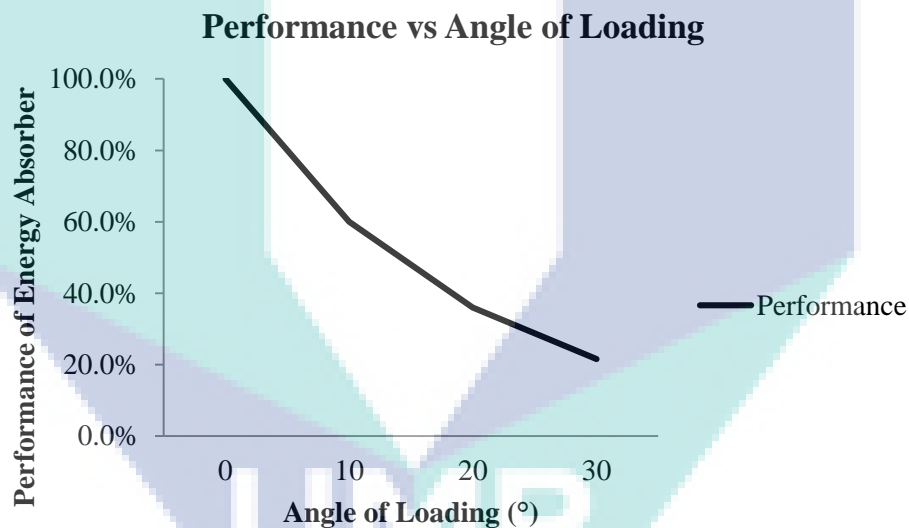


Figure 4.5 Overall performance of honeycomb filler when angle of loading

From the overall result, hexagon honeycomb filler performed as the best geometric design. This model had the highest performance on the result of crashworthiness criteria. Hexagon honeycomb filler had the low PCF but high MCF with a stable performance. Based on the result, hexagon honeycomb filler was the most effective energy absorber of honeycomb filler geometrical when structure subjected by dynamic impact loading of different angles. Hexagon was found to have better performance than circular from previous study (Usta & Turkmen, 2017; Yin et al.,

2011). Following table summarize the details of result for honeycomb filler versus geometric and structure subjected by the different angle of loading as in Table 4.5.

Table 4.5 Summary of honeycomb filler versus geometric and structure subjected by different angle of loading

Angle of Loading	Performance	EA	SEA	MCF	CFE
0 degrees	Highest value	Hexagon	Hexagon	Hexagon	Hexagon
	Best Structure	Hexagon	Hexagon	Hexagon	Hexagon
10 degrees	Highest value	Hexagon	Hexagon	Hexagon	Hexagon
	Best Structure	Hexagon	Hexagon	Hexagon	Hexagon
20 degrees	Highest value	Hexagon	Hexagon	Hexagon	Hexagon
	Best Structure	Hexagon	Hexagon	Hexagon	Hexagon
30 degrees	Highest value	Hexagon	Hexagon	Hexagon	Hexagon
	Best Structure	Hexagon	Hexagon	Hexagon	Hexagon

4.3 Effect of Thickness

The influence of different thickness on EA, SEA, PCF, MCF and CFE is analysed for circular honeycomb, hexagon honeycomb and multicell filler. Three thicknesses were set to each model and compared. The thickness were increased from, $t = 0.06$ mm to $t = 0.12$ mm and 0.18 mm. For circular honeycomb, the mass are recorded as 0.0066 kg, 0.0132 kg and 0.0198 kg when thickness, $t = 0.06$ mm, 0.12 mm and 0.18 mm respectively. For hexagon honeycomb, the mass are recorded as 0.0056 kg, 0.0113 kg and 0.0169 kg when thickness, $t = 0.06$ mm, 0.12 mm and 0.18 mm respectively. For multicell filler, the mass are recorded as 0.0051 kg, 0.0101 kg and 0.0152 kg when thickness, $t = 0.06$ mm, 0.12 mm and 0.18 mm respectively. All filler versus thickness are evaluated when structure is subjected to frontal dynamic impact loading on different angles, $\theta = 0, 10, 20$ and 30 degrees.

4.3.1 0 Degrees

The result for crashworthiness criteria versus thickness of every geometric design was shown in Table 4.6. For Figure 4.6 to Figure 4.8, the graph depicted performance trend of every model when thickness increased. The thickness of honeycomb filler were increased from $t = 0.06$ mm to 0.12 mm and 0.18 mm. All models were tested by same variable and setting. This part discussed on performance of

honeycomb filler based on the influence of different thickness when axial loading, $\theta = 0$ degrees.

Table 4.6 Result of honeycomb filler versus thickness at 0 degrees impact loading

Thickness	PCF (kN)	EA (kJ)	SEA (kJ/kg)	MCF (kN)	CFE
C06L0	3.994	0.118	17.833	1.667	41.7%
C12L0	10.201	0.379	28.744	5.479	53.7%
C18L0	17.345	0.643	32.464	9.746	56.2%
H06L0	3.517	0.133	23.662	2.288	65.0%
H12L0	8.905	0.395	34.996	6.663	74.8%
H18L0	15.307	0.546	32.336	12.446	81.3%
M06L0	3.310	0.054	10.645	0.880	26.6%
M12L0	6.733	0.158	15.605	2.443	36.3%
M18L0	11.244	0.186	12.221	4.550	40.5%

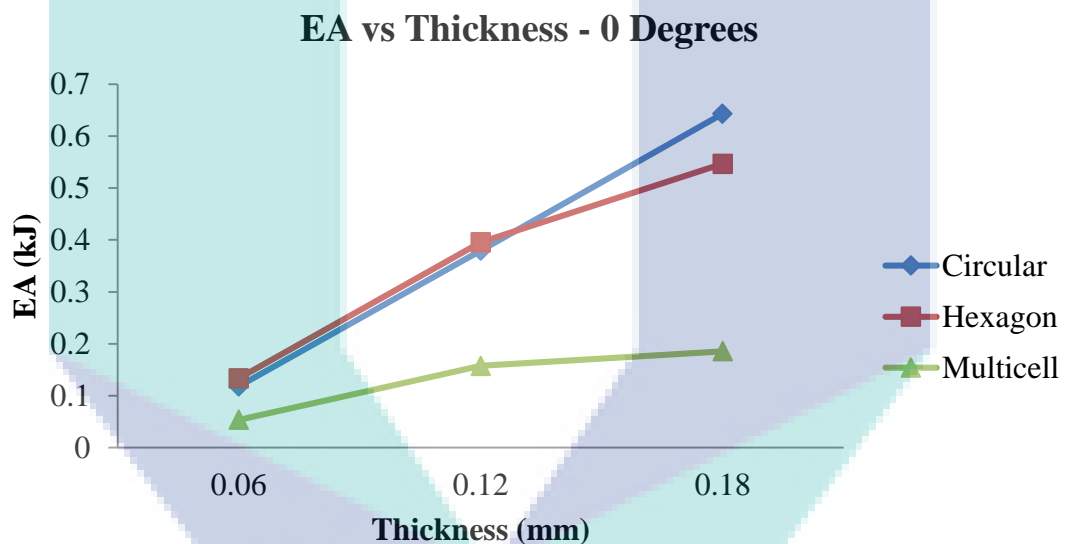


Figure 4.6 Effect of thickness on EA across geometric design when $\theta = 0$ degrees

Figure 4.6 showed the effect of EA when thickness increased during axial loading. By increased cell wall thickness of fillers to 0.12 mm, EA of circular and hexagon honeycomb filler increased approximately by the same amounts. That was found an increase of approximately by 0.26 kJ. The EA of circular honeycomb was increased from 0.118 kJ to 0.379 kJ. Likewise, EA of hexagon honeycomb was increased from 0.133 kJ to 0.395 kJ. However, the lowest increase was in multicell filler, where the EA had increased by 0.054 kJ to 0.158 kJ. The EA was only increased 0.1 kJ. The overall result showed increased approximately by 200 % when thickness increased in every geometric design.

When cell wall thickness of fillers increased to 0.18 mm, circular honeycomb filler was the only model that performed linearly increased. Meanwhile, EA of hexagon honeycomb and multicell filler increased not much compared to circular honeycomb filler. Circular honeycomb filler was increased approximately by 0.26 kJ in every 0.06 mm thickness increased. For hexagon honeycomb filler, EA was increased from 0.395 kJ to 0.546 kJ, which increased 38 %. For multicell filler, found the total EA increased versus thickness were the lowest. EA was increased from 0.186 kJ to 0.158 kJ, which increased 18 %.

By increased thickness of fillers from 0.06 mm to 0.18 mm, found that, circular honeycomb filler had the highest improvement, and then followed by hexagon honeycomb filler and multicell filler. The total EA of fillers was increased approximately by 450 %, 310 % and 250% respectively. However, when thickness of filler increased from 0.06 mm to 0.12 mm, EA of hexagon honeycomb filler was slightly higher than circular honeycomb filler. Thus, the performance of hexagon honeycomb filler was significantly lower than circular honeycomb. So, circular honeycomb was the most stable geometric design when thickness increased during axial loading.

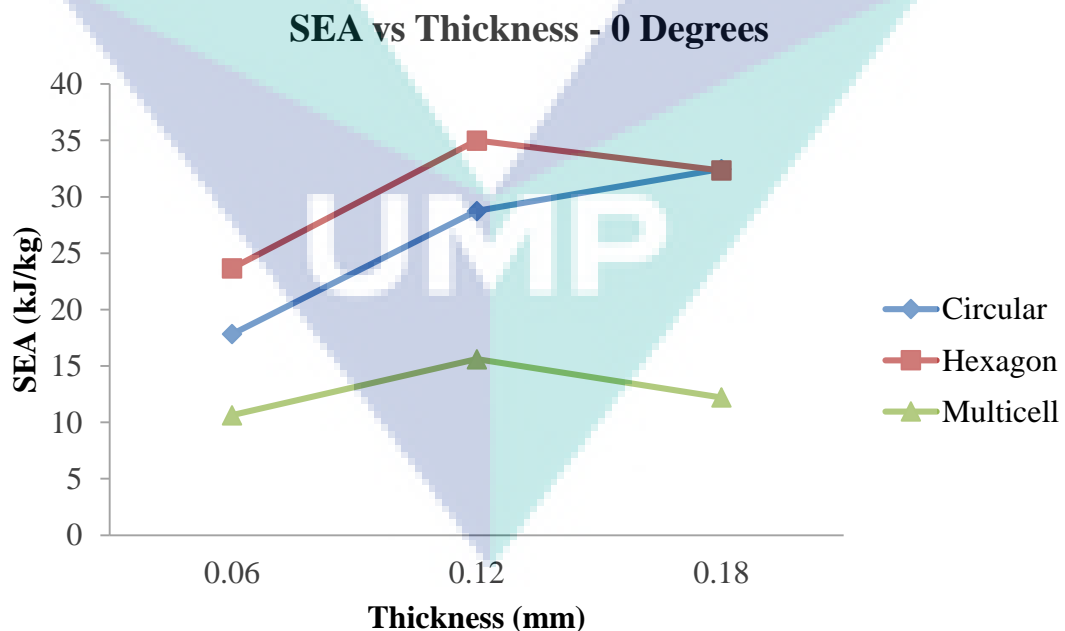


Figure 4.7 Effect of thickness on SEA across geometric design when $\theta = 0$ degrees

Figure 4.7 showed the effect of SEA when thickness increased during axial loading. By increased cell wall thickness of fillers from 0.06 mm to 0.12 mm, the result of SEA for all models showed an increase trend. However, when thickness increased from 0.12 mm to 0.18mm, the SEA performance of all models was decreased except circular honeycomb filler. SEA result of circular honeycomb filler were kept increased when thickness increased.

When thickness increased from 0.06 mm to 0.12 mm, both circular and hexagon honeycomb filler were increased approximately by 11 kJ/kg. For circular honeycomb filler, SEA increased from 17.833 kJ/kg to 28.744 kJ/kg, which was increased by 61 %. For hexagon honeycomb filler, SEA increased from 23.662 kJ/kg to 34.996 kJ/kg, which was increased by 48 %. For multicell filler, SEA was increased by 4.959 kJ/kg, from 10.645 kJ/kg to 15.605 kJ/kg, which was increased 48 %.

When thickness increased from 0.12 mm to 0.18 mm, SEA of circular honeycomb filler was the only geometric design which showed an increasing trend. SEA was increased by 3.720 kJ/kg, which was 13 %. Meanwhile, SEA of hexagon honeycomb and multicell filler were decreased, both models were decreased 8 % and 22 % respectively.

From the overall result, hexagon honeycomb filler was the highest SEA along with the increased thickness. Although SEA trend of hexagon honeycomb filler was decreased when thickness increased to 0.18 mm, however, the SEA of both circular and hexagon honeycomb filler was found 32 kJ/kg when thickness at 0.18 mm. Circular honeycomb filler was second best geometric design after hexagon honeycomb filler. Lastly, multicell filler was the lowest performance among all geometric. Multicell filler showed the lowest result, at the same time, SEA decreased when the thickness increased from 0.12 mm to 0.18 mm.

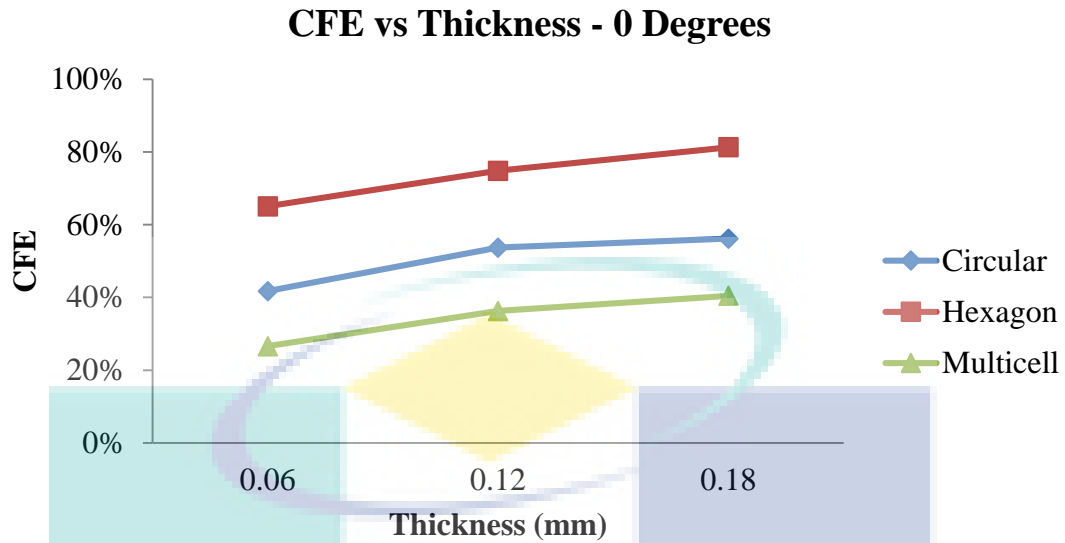


Figure 4.8 Effect of thickness on CFE across geometric design when $\theta = 0$ degrees

Figure 4.8 showed the effect of CFE when thickness increased during axial loading. The graph showed all models had an increase trend of CFE result when thickness increased. For circular honeycomb filler, CFE were increased 28.7 % at 0.12 mm and 34.6 % at 0.18 mm while compared to 0.06 mm. Both hexagon honeycomb and multicell filler were increased approximately by 9.7 % when 0.12 mm. For hexagon honeycomb filler, CFE was increased 15.0 % and 25.0 % when thickness increased from 0.06 mm to 0.12 mm and 0.18 mm respectively. Meanwhile, this geometric was the only model which increased in a linear trend. Lastly, multicell filler was the lowest CFE performance. However, the result showed multicell had highest improvement of CFE versus thickness. Found that, CFE was increased by 36.5 % and 52.2 % when thickness increased from 0.06 mm to 0.12 mm and 0.18 mm respectively. Overall, hexagon honeycomb filler had the highest performance of CFE, thus, multicell filler had the highest improvement versus thickness.

4.3.2 10 Degrees

The result for crashworthiness criteria versus thickness of every geometric design were shown in Table 4.7. For Figure 4.9, Figure 4.10 and Figure 4.11, the graph depicted performance trend of every model when thickness increased. The thickness of honeycomb filler were increased from $t = 0.06$ mm to 0.12 mm and 0.18 mm. All models were tested by same variable and setting. This part discussed on performance of

honeycomb filler based on the influence of different thickness when oblique loading, $\theta = 10$ degrees.

Table 4.7 Result of honeycomb filler versus thickness at 10 degrees impact loading

Thickness	PCF (kN)	EA (kJ)	SEA (kJ/kg)	MCF (kN)	CFE
C06L10	1.851	0.080	12.146	1.432	77.4%
C12L10	5.093	0.226	17.118	4.136	81.2%
C18L10	9.204	0.350	17.674	7.868	85.5%
H06L10	2.114	0.092	16.388	1.808	85.5%
H12L10	6.185	0.257	22.747	5.283	85.4%
H18L10	12.285	0.444	26.292	10.111	82.3%
M06L10	1.527	0.037	7.309	0.747	48.9%
M12L10	3.363	0.105	10.405	2.146	63.8%
M18L10	6.710	0.192	12.617	3.811	56.8%

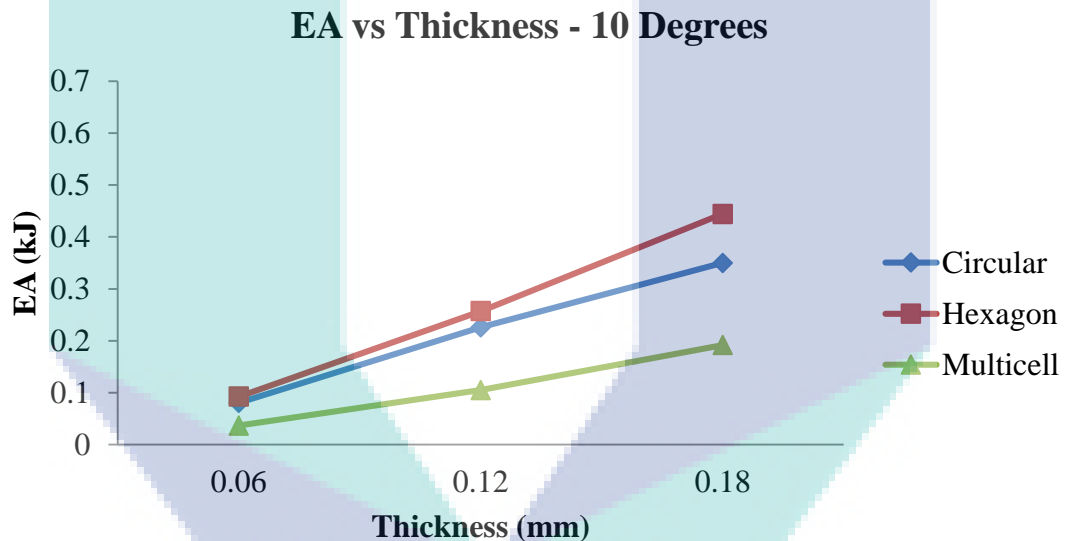


Figure 4.9 Effect of thickness on EA across geometric design when $\theta = 10$ degrees

Figure 4.9 showed the effect of EA when thickness increased during oblique loading at 10 degrees. The result showed all models were increased linearly along with the thickness.

For circular honeycomb filler, EA was increased from 0.080 kJ to 0.226 kJ and 0.350 kJ at 0.12 mm and 0.18 mm respectively. There was an increase of 0.146 kJ from 0.06 mm to 0.12 mm and 0.124 kJ from 0.12 mm to 0.18 mm. For hexagon honeycomb filler, EA was increased from 0.092 kJ to 0.257 kJ and 0.444 kJ at 0.12 mm to 0.18 mm respectively. There was an increase of 0.165 kJ from 0.06 mm to 0.12 mm and 0.187 kJ from 0.12 mm to 0.18 mm. For multicell filler, EA was increased from 0.037 kJ to

0.105 kJ and 0.192 kJ at 0.12 mm and 0.18 mm respectively. There was an increase of 0.068 kJ from 0.06 mm to 0.12 mm and 0.087 kJ from 0.12 mm to 0.18 mm.

When thickness increased from 0.06 mm to 0.12 mm, all models improved approximately by 180 %. When thickness of fillers from .06 mm to 0.18 mm, found that multicell filler was the highest percentage of improvement which was at approximately by 420 %, although the improvement of different value of EA was the least. While, the EA performance of hexagon and circular honeycomb filler was improved approximately by 380 % and 340 %. From the result above, hexagon honeycomb filler had the highest EA thus multicell had the highest improvement versus thickness.

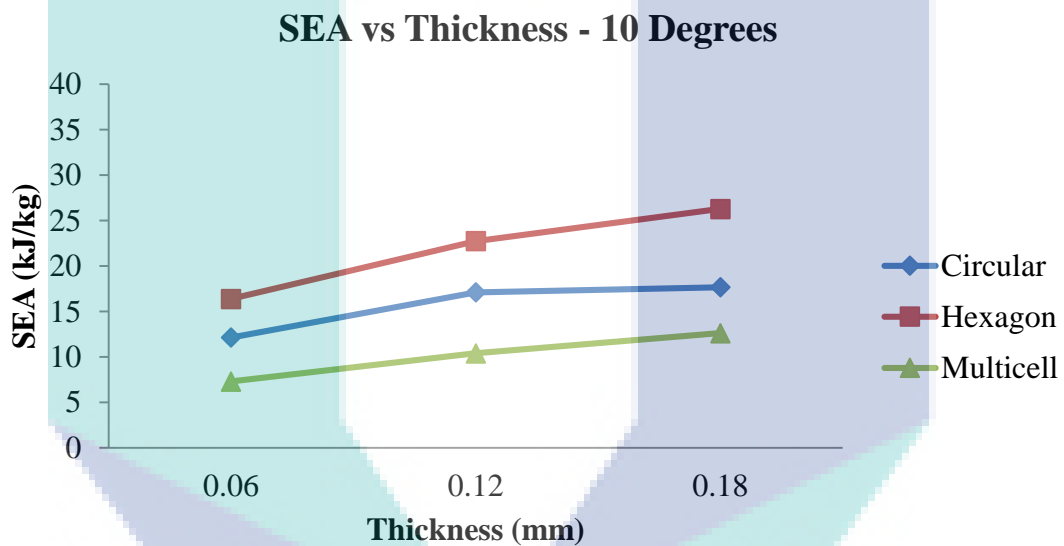


Figure 4.10 Effect of thickness on SEA across geometric design when $\theta = 10$ degrees

Figure 4.10 showed the effect of SEA when thickness increased during oblique loading at 10 degrees. By increased cell wall thickness of fillers from 0.06 mm to 0.12 mm, all models were increased approximately by 40 %. When thickness of fillers increased from 0.06 mm to 0.18 mm, the overall performance of SEA was increased proportional except circular honeycomb filler.

For circular honeycomb filler, SEA was an increased 4.972 kJ/kg when thickness increased from 0.06 mm to 0.12 mm. However, when thickness increased from 0.12 mm to 0.18 mm, the SEA was remained constant at 17 kJ/kg. This might due to the circular honeycomb filler reached an optimized thickness in structure when thickness at 0.12 mm.

For hexagon honeycomb filler, SEA was increased from 16.388 kJ/kg to 22.747 kJ/kg and 26.292 kJ/kg when thickness at 0.06 mm, 0.12 mm and 0.18 mm respectively. There was an increase of 6.538 kJ/kg from 0.06 mm to 0.12 mm and 3.545 kJ/kg from 0.12 mm to 0.18 mm. That was increased 39 % and 60 % when thickness at 0.12 mm and 0.18 mm compared to original thickness.

For multicell filler, SEA was increased from 7.309 kJ/kg to 10.405 kJ/kg and 12.617 kJ/kg when thickness at 0.06 mm, 0.12 mm and 0.18 mm respectively. There was an increase of 3.096 kJ/kg from 0.06 mm to 0.12 mm and 2.212 kJ/kg from 0.12 mm to 0.18 mm. That was increased 42 % and 73 % when thickness at 0.12 mm and 0.18 mm compared to original thickness.

From the overall result showed hexagon honeycomb filler had the highest improvement of SEA in terms of value. Thus, multicell had the highest improvement of SEA in terms of percentage. For circular honeycomb filler, the performance of SEA get stable after thickness increased to 0.12 mm.

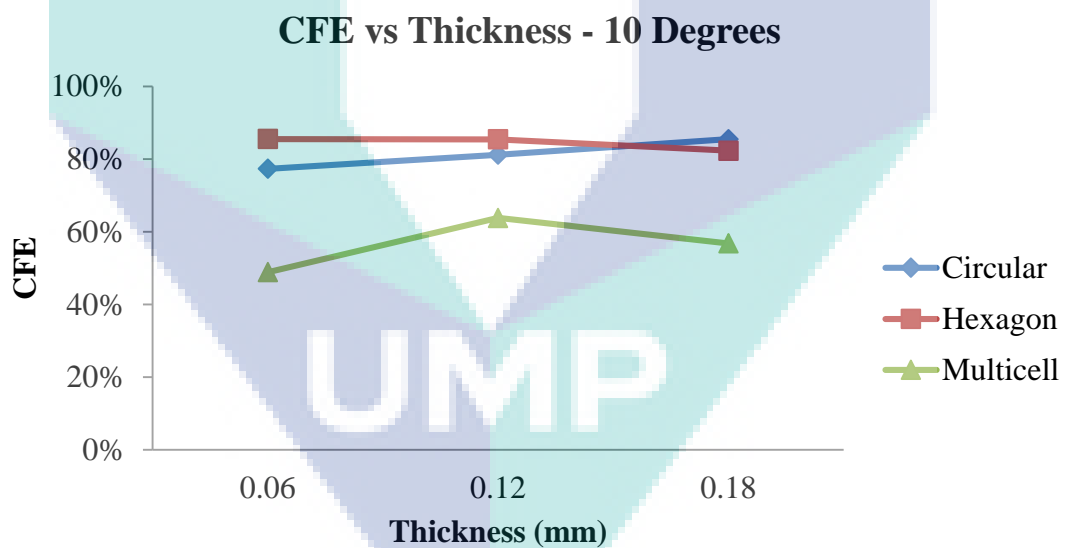


Figure 4.11 Effect of thickness on CFE across geometric design when $\theta = 10$ degrees

Figure 4.11 showed the effect of CFE when thickness increased during oblique loading at 10 degrees. For circular honeycomb filler, the result showed CFE was increased gradually versus thickness. CFE was increased 5 % every 0.06 mm of thickness increased. The CFE was increased from 77.4 % to 81.2 % and 85.5 % at 0.12 mm and 0.18mm. For hexagon honeycomb filler, CFE were decreased 0.1 % at

approximately 85 %. When the thickness increased to 0.18 mm, the CFE was decreased. That was decreased by 4 % to 82.3 %. For multicell filler, CFE was increased initially from 48.9 % to 63.8 % then decreased by 11 % to 56.8 %. By compared the CFE versus thickness, circular honeycomb filler had the highest CFE when thickness increased to 0.18mm. Then followed by hexagon honeycomb filler, even though the result showed decreasing trend when thickness increased. Thus hexagon honeycomb had the highest CFE when thickness was 0.06 mm. Lastly, the best thickness for multicell filler in CFE was when thickness increased to 0.12 mm.

4.3.3 20 Degrees

The result for crashworthiness criteria versus thickness of every geometric design were shown in Table 4.8. For Figure 4.12 to Figure 4.14, the graph depicted performance trend of every model when thickness increased. The thickness of honeycomb filler were increased from $t = 0.06$ mm to 0.12 mm and 0.18 mm. All models were tested by same variable and setting. This part discussed on performance of honeycomb filler based on the influence of different thickness when oblique loading, $\theta = 20$ degrees.

Table 4.8 Result of honeycomb filler versus thickness at 20 degrees impact loading

Thickness	PCF (kN)	EA (kJ)	SEA (kJ/kg)	MCF (kN)	CFE
C06L20	1.532	0.045	6.871	1.116	72.8%
C12L20	4.422	0.133	10.098	3.252	73.5%
C18L20	8.217	0.251	12.668	6.054	73.7%
H06L20	1.744	0.054	9.528	1.322	75.8%
H12L20	5.290	0.148	13.082	3.704	70.0%
H18L20	9.703	0.287	16.985	7.079	73.0%
M06L20	0.798	0.022	4.358	0.549	68.8%
M12L20	2.630	0.065	6.390	1.597	60.7%
M18L20	4.647	0.120	7.902	2.968	63.9%

EA vs Thickness - 20 Degrees

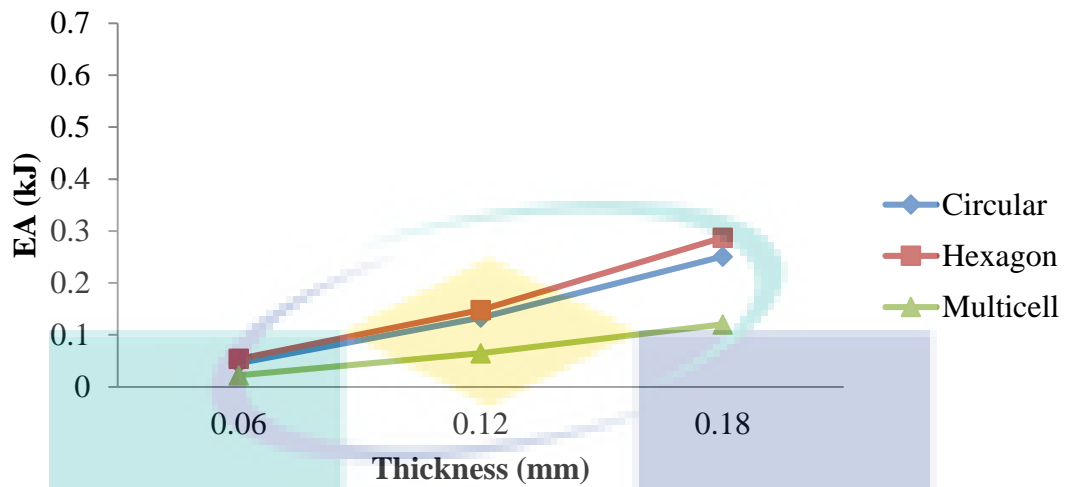


Figure 4.12 Effect of thickness on EA across geometric design when $\theta = 20$ degrees

Figure 4.12 showed the effect of EA when thickness increased during oblique loading at 20 degrees. The result of EA showed all models were increased along with the thickness.

For circular honeycomb filler, EA was increased from 0.045 kJ to 0.133 kJ and 0.251 kJ at 0.12 mm and 0.18 mm respectively. There was an increase of 0.088 kJ from 0.06 mm to 0.12 mm and 0.118 kJ from 0.12 mm to 0.18 mm. For hexagon honeycomb filler, EA was increased from 0.054 kJ to 0.148 kJ and 0.287 kJ at 0.12 mm to 0.18 mm respectively. There was an increase of 0.094 kJ from .06 mm to 0.12 mm and 0.118 kJ from 0.12 mm to 0.18 mm. For multicell filler, EA was increased from 0.022 kJ to 0.065 kJ and 0.120 kJ at 0.12 mm and 0.18 mm respectively. There was an increase of 0.043 kJ from 0.06 mm to 0.12 mm and 0.056 kJ from 0.12 mm to 0.18 mm.

When thickness increased from 0.06 mm to 0.12 mm, circular honeycomb and multicell filler were improved 193 % then there was just 175 % for hexagon honeycomb filler. When thickness of fillers increased from 0.06 mm to 0.18 mm, found that EA were increased 451 %, 434 % and 446 % for circular honeycomb, hexagon honeycomb and multicell filler respectively. From the result above, circular honeycomb and multicell filler had similar percentage of improvement versus thickness. For hexagon honeycomb filler, showed the highest EA among three models.

SEA vs Thickness - 20 Degrees

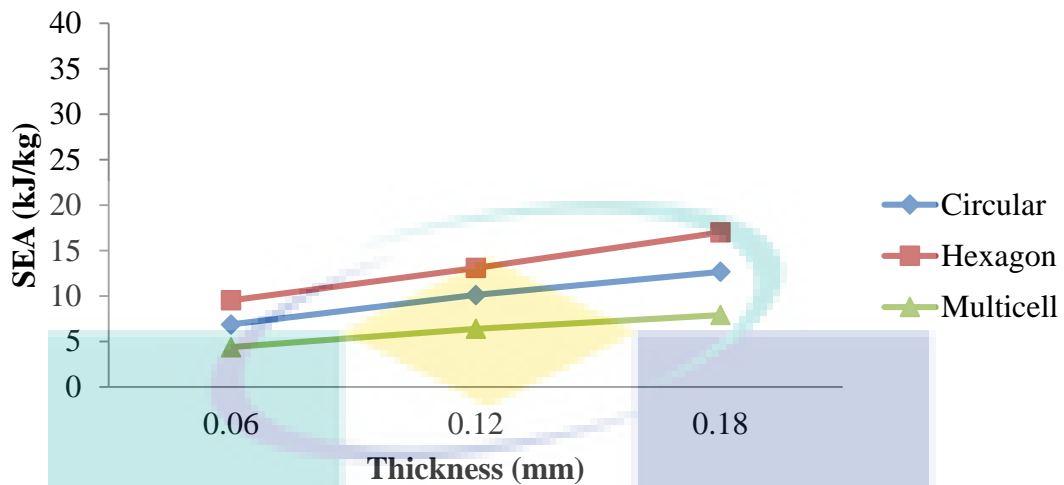


Figure 4.13 Effect of thickness on SEA across geometric design when $\theta = 20$ degrees

Figure 4.13 showed the effect of SEA when thickness increased during oblique loading at 20 degrees. The result of SEA showed all models were increased proportional along with the thickness.

For circular honeycomb filler, SEA was increased from 6.871 kJ/kg to 10.098 kJ/kg and 12.668 kJ/kg at 0.12 mm and 0.18 mm respectively. There was an increase of 3.226 kJ/kg from 0.06 mm to 0.12 mm and 2.570 kJ/kg from 0.12 mm to 0.18 mm. For hexagon honeycomb filler, SEA was increased from 9.528 kJ/kg to 13.082 kJ/kg and 16.985 kJ/kg at 0.12 mm to 0.18 mm respectively. There was an increase of 3.554 kJ/kg from 0.06 mm to 0.12 mm and 3.902 kJ/kg from 0.12 mm to 0.18 mm. For multicell filler, SEA was increased from 4.358 kJ/kg to 6.390 kJ/kg and 7.902 kJ/kg at 0.12 mm and 0.18 mm respectively. There was an increase of 2.032 kJ/kg from 0.06 mm to 0.12 mm and 1.512 kJ/kg from 0.12 mm to 0.18 mm.

When thickness increased from 0.06 mm to 0.12 mm, circular honeycomb and multicell filler were improved 47 % then there was just 37 % for hexagon honeycomb filler. When thickness of fillers increased from 0.06 mm to 0.18 mm, found that SEA were increased 84 %, 78 % and 81 % for circular honeycomb, hexagon honeycomb and multicell filler respectively. From the result above, circular honeycomb and multicell filler had similar percentage of improvement versus thickness. For hexagon honeycomb filler, showed the highest SEA among three models.

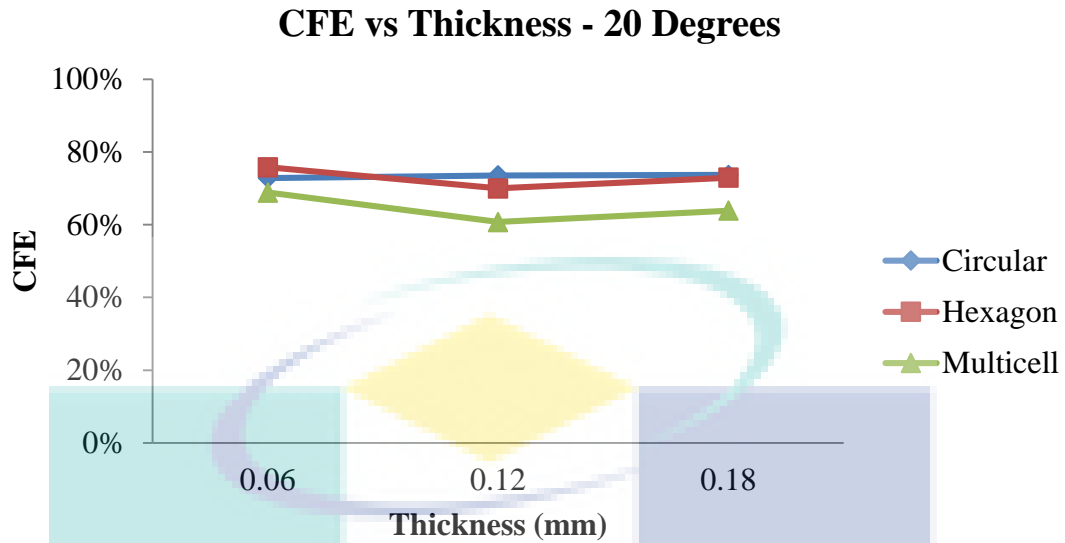


Figure 4.14 Effect of thickness on CFE across geometric design when $\theta = 20$ degrees

Figure 4.14 showed the effect of CFE when thickness increased during oblique loading at 20 degrees. For circular honeycomb filler, the result showed CFE was remained constant versus thickness. CFE was slightly increased 0.7 % when thickness increased from 0.06 mm to 0.12 mm. Then, CFE was remained at 73 %. Meanwhile, hexagon honeycomb and multicell filler, both CFE result showed decreased of performance when increased of thickness. For hexagon honeycomb filler, CFE was decreased 5.8% from 0.06 mm to 0.12 mm then rose up 2.9% from 0.12 mm to 0.18 mm. For multicell filler, CFE was decreased 8.1% from 0.06 mm to 0.12 mm then rose up 3.1% from 0.12 mm to 0.18 mm.

From the result above, circular honeycomb filler was the only model showed improvement versus thickness. When thickness increased to 0.18 mm, circular honeycomb filler was the highest CFE among all models although CFE was not the highest during initial thickness. Hexagon honeycomb and multicell filler showed the best thickness on CFE performance when thickness was 0.06 mm. The performance of CFE did not improved along with the thickness increased.

4.3.4 30 Degrees

The result for crashworthiness criteria versus thickness of every geometric design were shown in Table 4.9. For Figure 4.15 to Figure 4.17, the graph depicted performance trend of every model when thickness increased. The thickness of

honeycomb filler were increased from $t = 0.06$ mm to 0.12 mm and 0.18 mm. All models were tested by same variable and setting. This part discussed on performance of honeycomb filler based on the influence of different thickness when oblique loading, $\theta = 30$ degrees.

Table 4.9 Result of honeycomb filler versus thickness at 30 degrees impact loading

Thickness	PCF (kN)	EA (kJ)	SEA (kJ/kg)	MCF (kN)	CFE
C06L30	1.235	0.030	4.602	0.709	57.4%
C12L30	3.359	0.087	6.566	2.004	59.6%
C18L30	6.469	0.163	8.209	3.791	58.6%
H06L30	1.366	0.032	5.618	0.861	63.0%
H12L30	4.145	0.103	9.095	2.776	67.0%
H18L30	7.574	0.179	10.604	4.880	64.4%
M06L30	0.607	0.014	2.718	0.376	61.9%
M12L30	1.878	0.039	3.877	1.044	55.6%
M18L30	3.832	0.077	5.065	2.074	54.1%

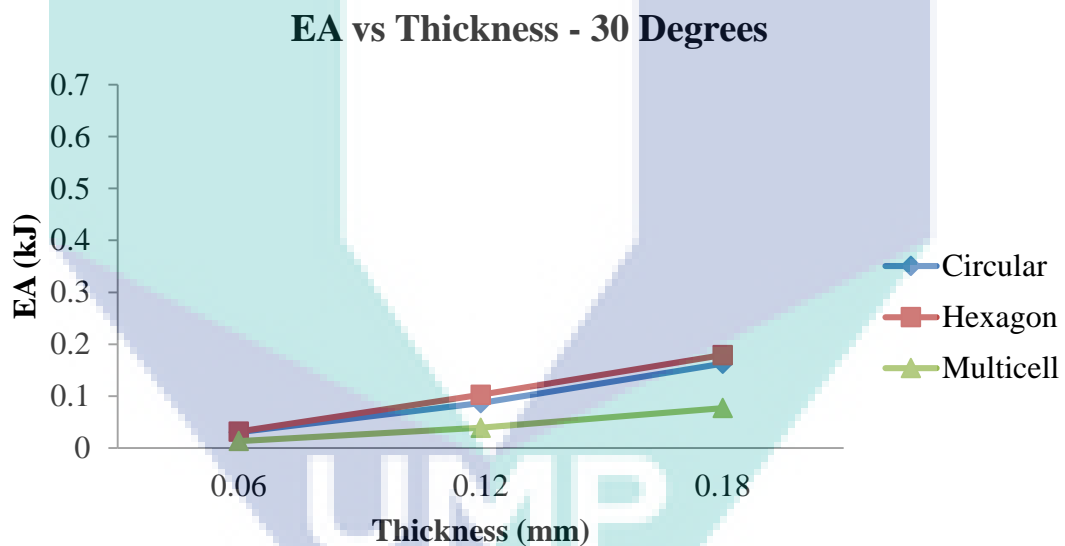


Figure 4.15 Effect of thickness on EA across geometric design when $\theta = 30$ degrees

Figure 4.15 showed the effect of EA when thickness increased during oblique loading at 30 degree. The result of EA showed all models were increased along with the thickness.

For circular honeycomb filler, EA was increased from 0.030 kJ to 0.087 kJ and 0.163 kJ at 0.12 mm and 0.18 mm respectively. There was an increase of 0.056 kJ from 0.06 mm to 0.12 mm and 0.76 kJ from 0.12 mm to 0.18 mm. For hexagon honeycomb filler, EA was increased from 0.032 kJ to 0.103 kJ and 0.179 kJ at 0.12 mm to 0.18 mm

respectively. There was an increase of 0.071 kJ from .06 mm to 0.12 mm and 0.76 kJ from 0.12 mm to 0.18 mm. For multicell filler, EA was increased from 0.014 kJ to 0.039 kJ and 0.077 kJ at 0.12 mm and 0.18 mm respectively. There was an increase of 0.025 kJ from 0.06 mm to 0.12 mm and 0.038 kJ from 0.12 mm to 0.18 mm.

When thickness increased from 0.06 mm to 0.12 mm, circular honeycomb and multicell filler were improved 185 %. Hexagon honeycomb filler was increased a lot compared to another two models which rose 224 %. When thickness of fillers increased from 0.06 mm to 0.18 mm, found that EA were increased 434 %, 466 % and 461 % for circular honeycomb, hexagon honeycomb and multicell filler respectively. From the result above, circular and hexagon honeycomb filler had similar improvement of EA versus thickness. For hexagon honeycomb filler, showed the highest EA in terms of value and percentage of improvement along with the thickness among three models.

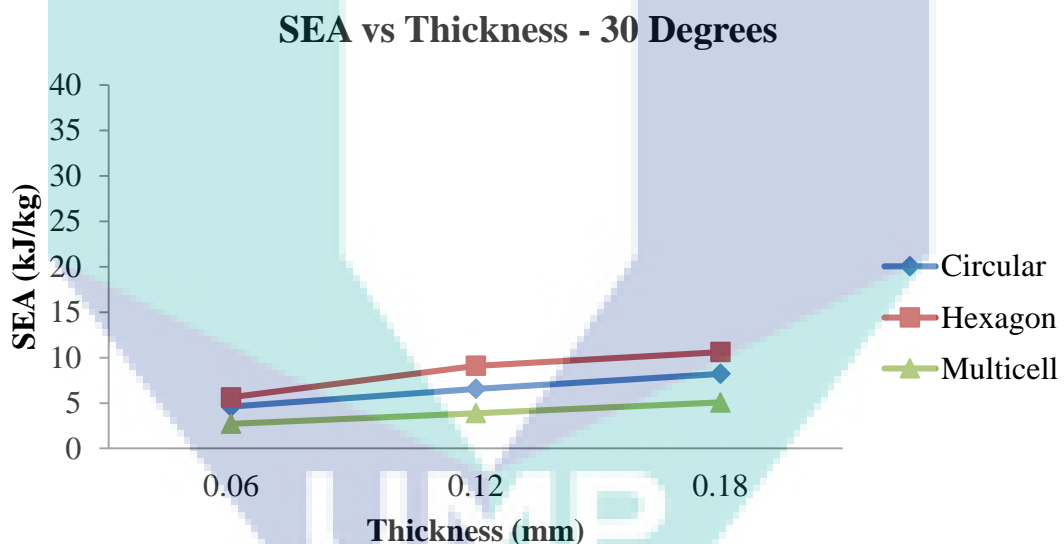


Figure 4.16 Effect of thickness on SEA across geometric design when $\theta = 30$ degrees

Figure 4.16 showed the effect of SEA when thickness increased during oblique loading at 30 degrees. The result of SEA showed all models were increased proportional along with the thickness.

For circular honeycomb filler, SEA was increased from 4.602 kJ/kg to 6.566 kJ/kg and 8.209 kJ/kg at 0.12 mm and 0.18 mm respectively. There was an increase of 1.964 kJ/kg from 0.06 mm to 0.12 mm and 1.643 kJ/kg from 0.12 mm to 0.18 mm. For hexagon honeycomb filler, SEA was increased from 5.618 kJ/kg to 9.095 kJ/kg and

10.604 kJ/kg at 0.12 mm to 0.18 mm respectively. There was an increase of 3.477 kJ/kg from 0.06 mm to 0.12 mm and 1.509 kJ/kg from 0.12 mm to 0.18 mm. For multicell filler, SEA was increased from 2.718 kJ/kg to 3.877 kJ/kg and 5.065 kJ/kg at 0.12 mm and 0.18 mm respectively. There was an increase of 0.376 kJ/kg from 0.06 mm to 0.12 mm and 1.044 kJ/kg from 0.12 mm to 0.18 mm.

When thickness increased from 0.06 mm to 0.12 mm, circular honeycomb and multicell filler were improved 43 %. Hexagon honeycomb filler was increased a lot compared to another two models which rose 62 %. When thickness of fillers increased from 0.06 mm to 0.18 mm, found that SEA were increased 78 %, 89 % and 86 % for circular honeycomb, hexagon honeycomb and multicell filler respectively. From the result above, circular and hexagon honeycomb filler had similar percentage of improvement versus thickness. For hexagon honeycomb filler, showed the highest SEA in terms of value and percentage of improvement along with the thickness among three models.

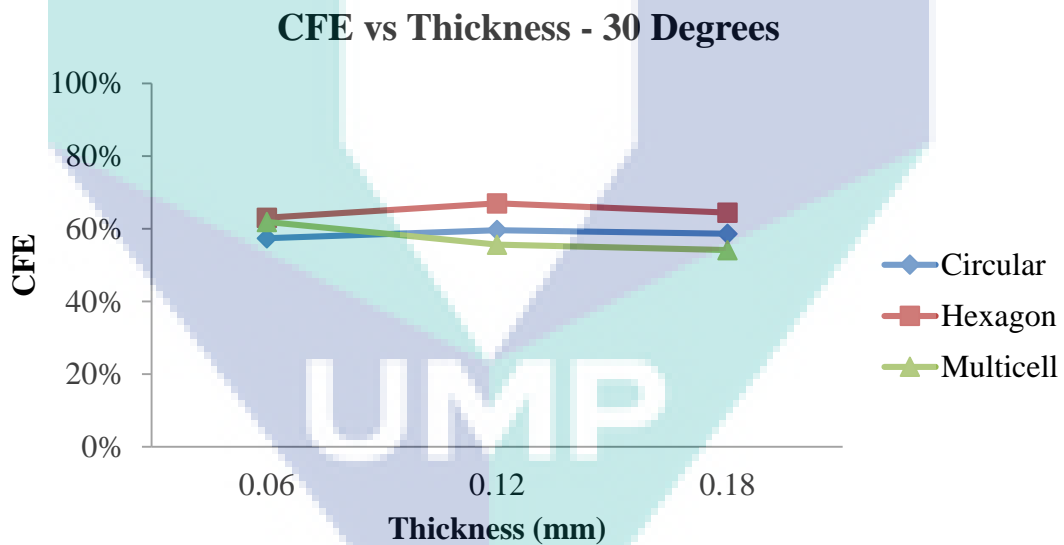


Figure 4.17 Effect of thickness on CFE across geometric design when $\theta = 30$ degrees

Figure 4.17 showed the effect of CFE when thickness increased during oblique loading at 30 degrees. The CFE result of circular and hexagon honeycomb filler was improved versus thickness. For circular honeycomb filler, CFE was increased 2.2% when thickness increased from 0.06 mm to 0.12 mm then decreased 1 % from 0.12 mm to 0.18 mm. For hexagon honeycomb filler, CFE was increased 4 % from 0.06 mm to 0.12 mm then decreased 2.5 % from 0.12 mm to 0.18 mm. For multicell filler, CFE was

decreased along with the thickness. CFE was decreased from 61.9 % to 55.6 % and 54.1 % at 0.12 mm and 0.18 mm respectively.

From the result above, hexagon honeycomb filler was the highest CFE among all models. For circular and hexagon honeycomb, the best thickness on CFE performance was when thickness at 0.12 mm. Multicell filler was the only model showed decreased trend. However, CFE of multicell was higher than circular honeycomb filler when thickness at 0.06 mm.

4.3.5 Overall Result

In this section, the determination on energy absorber of honeycomb filler versus thickness and structure subjected by the different angle of loading were concluded. From the overall, the result showed the performance of honeycomb fillers improved when the thickness increased. Meanwhile, the performance of CFE was not as improved as EA and SEA when thickness increased. This happened during oblique impact loading.

Table 4.10 Summary of result for honeycomb filler influenced by thickness versus angle of loading

Angle of Loading	Performance	EA	SEA	CFE
0 degrees	Highest value	Circular	Hexagon	Hexagon
	Highest improvement	Circular	Circular	Multicell
	Best Structure	Circular	Hexagon	Hexagon
	Best thickness	0.18 mm	0.12 mm	0.18 mm
10 degrees	Highest value	Hexagon	Hexagon	Hexagon
	Highest improvement	Multicell	Multicell	Multicell
	Best Structure	Hexagon	Hexagon	Hexagon
	Best thickness	0.18 mm	0.18 mm	0.06 mm
20 degrees	Highest value	Hexagon	Hexagon	Hexagon
	Highest improvement	Multicell	Circular	Circular
	Best Structure	Hexagon	Hexagon	Hexagon
	Best thickness	0.18 mm	0.18 mm	0.06 mm
30 degrees	Highest value	Hexagon	Hexagon	Hexagon
	Highest improvement	Hexagon	Hexagon	Hexagon
	Best Structure	Hexagon	Hexagon	Hexagon
	Best thickness	0.18 mm	0.18 mm	0.12 mm

The details were summarized in Table 4.10. During axial loading, circular honeycomb filler showed the best result when thickness increased in EA. Even though circular honeycomb filler performed as the best structure in EA, thus, hexagon honeycomb filler was better than circular honeycomb filler in SEA. This is due to the total weight of structure affected the hexagon honeycomb became better than circular honeycomb filler although lower EA.

During oblique loading, hexagon honeycomb showed the best result among all models. Although hexagon honeycomb filler was not the highest improvement in result when thickness increased. For EA and SEA, hexagon honeycomb filler showed the highest value when thickness at 0.18 mm. Meanwhile, the best thickness of hexagon honeycomb filler for CFE was thickness at 0.06 mm during 10 degrees and 20 degrees of angle loading then thickness at 0.12 mm during 30 degrees of angle loading.

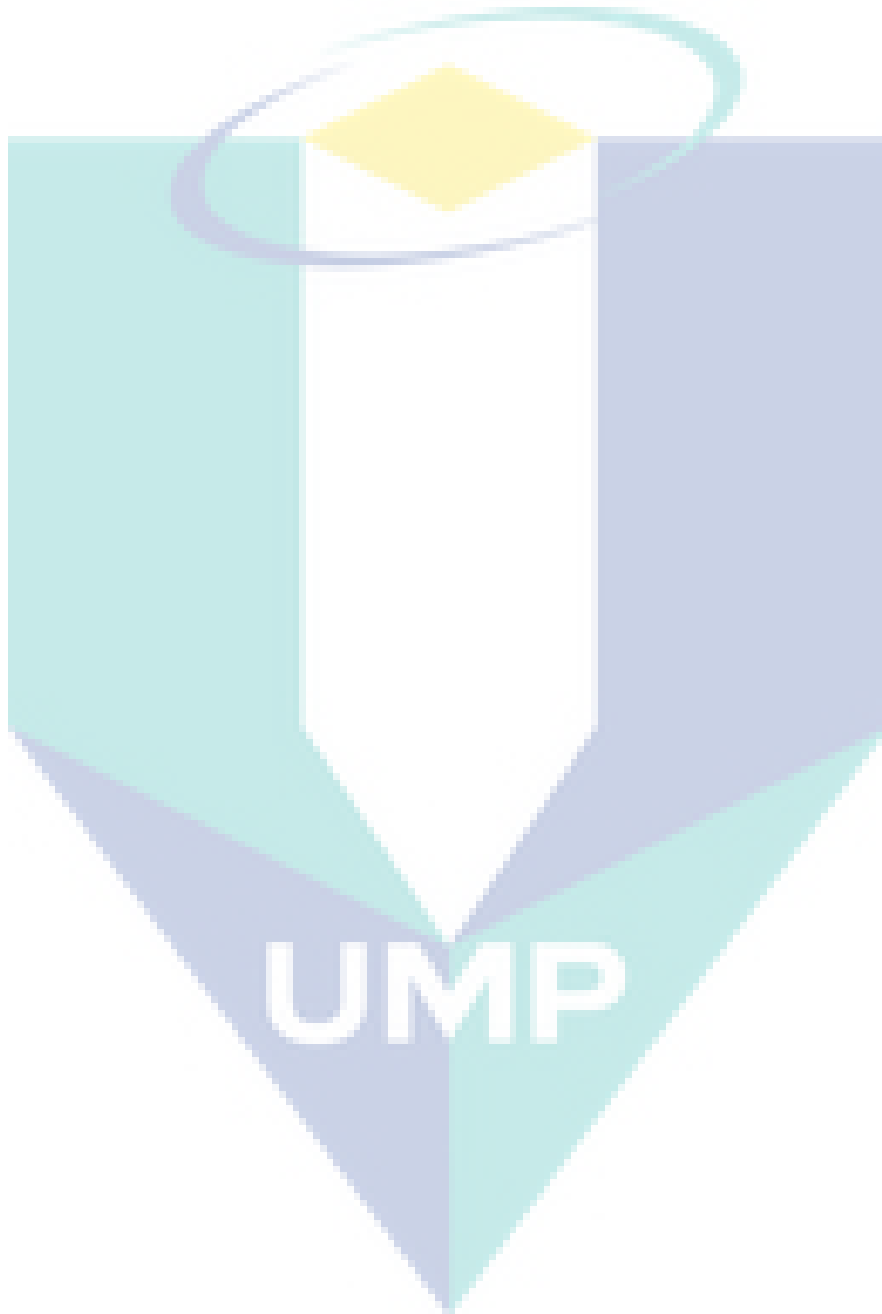
From the result of multicell filler, it showed the lowest value result among all models. It is detrimental due to consist of very high peak force under axial loading. When the oblique loads were taken into account, the models undergo an inefficient deformation mode namely global bending mode. This was also found similar result from the study of Fang et al. (2015).

From the overall result, hexagon honeycomb filler performed as the best geometric design by influenced of thickness. This model had the highest performance on the result of crashworthiness criteria. As the thickness increased, hexagon honeycomb filler showed good improvement in performance of EA, SEA and CFE. Based on the result, hexagon honeycomb filler was the most effective energy absorber of honeycomb filler geometrical when the structure is subjected by dynamic impact loading of different angles.

4.4 Summary

In this chapter, the evaluation and determination of efficiency performance of honeycomb filler as energy absorber on axial and oblique dynamic impact were presented. Firstly, the results of the honeycomb filler were compared to each other in Section 4.2. Found that, hexagon honeycomb filler performed as the best structure when thickness as 0.06 mm during every angle of loading. Secondly, as discussed in Section 4.3, the influence of thickness increased was found improvement of performance.

During axial loading, circular honeycomb filler was the best structure when thickness increased. However, hexagon honeycomb filler was found performed better during angle of loading was increased. Therefore, hexagon honeycomb filler showed as the best structural design.



CHAPTER 5

CONCLUSION

5.1 Introduction

In this thesis, the crash response of the honeycomb filler was analysed with dynamic impact loading. Numerical study was carried out on every identical design models by using ABAQUS. These FE models were made up from different geometry and thickness that applied with several angle of loading. The conclusions drawn based on findings of this research are presented on this chapter. In addition, a few recommendations are made in order to extend the current knowledge concerning crash response of honeycomb filler.

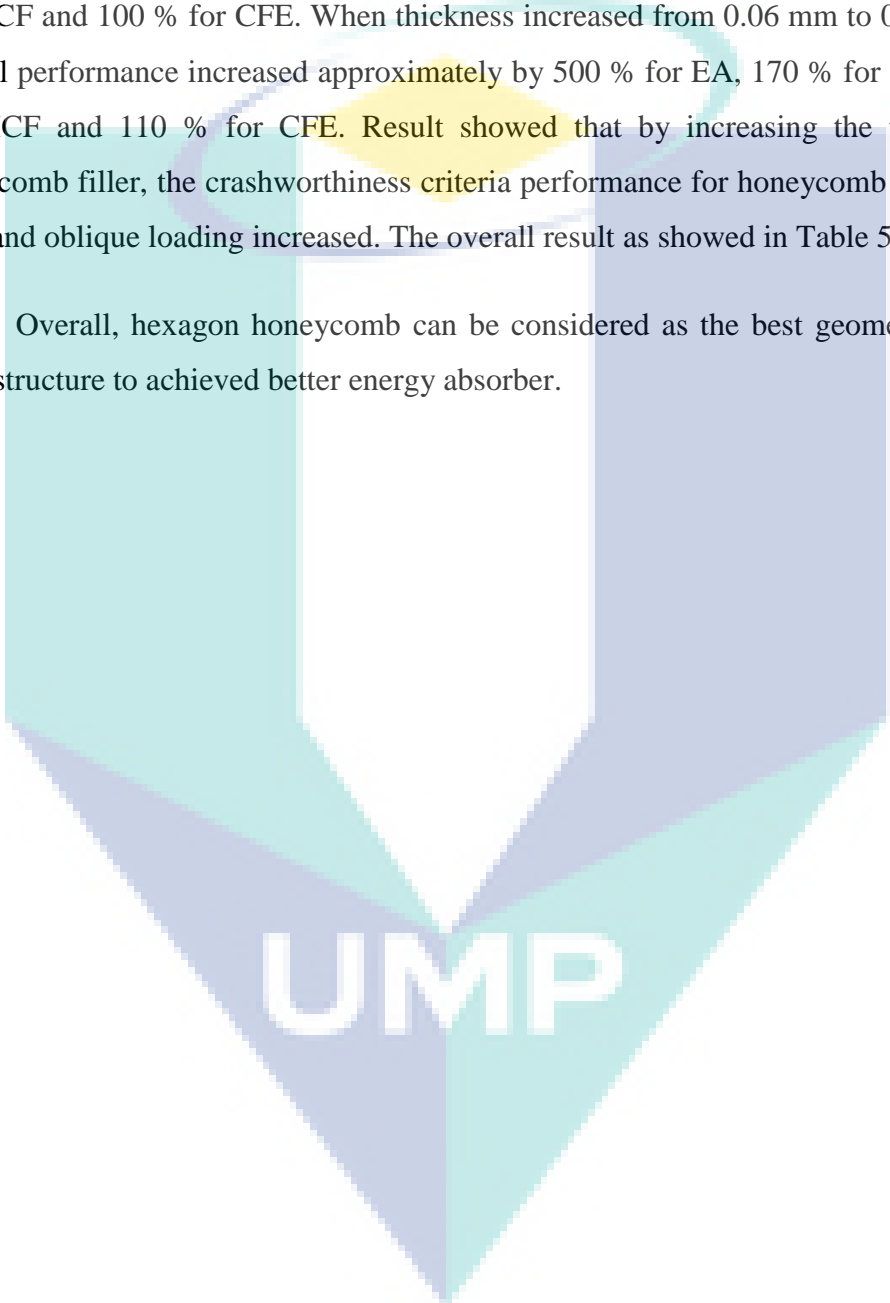
5.2 Conclusion

Conclusions have been drawn thought out the research. The extensive knowledge in the numerical study of crash response of honeycomb filler was analysed with frontal dynamic impact loading has concluded as following:

Conclusion 1: Among all designs of the honeycomb filler, hexagon honeycomb is the best design. In terms of weight, it is slightly heavier than the lightest model, which is 10 % heavier than multicell filler. However, its performance of EA, SEA and CFE is the highest compared to circular and multicell filler. The result showed hexagon honeycomb is 230 % higher than multicell filler and 120 % higher than circular honeycomb. Hexagon honeycomb had the highest performance result in terms of EA, SEA and CFE compared to circular honeycomb and multicell filler during axial and oblique loading.

Conclusion 2: The thickness of the models, $t=0.06$ mm, 0.12 mm and 0.18 mm were investigated. When thickness increased from 0.06 mm to 0.12 mm, the overall performance increased approximately by 290 % for EA, 150 % for SEA, 290 % for MCF and 110 % for CFE. When the thickness increased from 0.12 mm to 0.18 mm, the overall performance increased approximately by 170 % for EA, 120 % for SEA, 190 % for MCF and 100 % for CFE. When thickness increased from 0.06 mm to 0.18 mm, the overall performance increased approximately by 500 % for EA, 170 % for SEA, 550 % for MCF and 110 % for CFE. Result showed that by increasing the thickness of honeycomb filler, the crashworthiness criteria performance for honeycomb filler during axial and oblique loading increased. The overall result as showed in Table 5.1

Overall, hexagon honeycomb can be considered as the best geometrical shape of car structure to achieved better energy absorber.

The logo for UIMP (Universiti Malaysia Perlis) is a large, downward-pointing arrow shape. It is composed of four triangular sections meeting at a central point. The top-left and bottom-right sections are light blue, while the top-right and bottom-left sections are a slightly darker shade of blue. The letters 'UIMP' are printed in white, bold, sans-serif font across the center of the arrow.

UIMP

Table 5.1 Aspect ratio of model versus thickness in every angle of loading

Model	Angle of Loading (°)	Aspect Ratio														
		Thickness			EA			SEA			MCF			CFE		
		t ₁₂ / t ₀₆	t ₁₈ / t ₁₂	t ₁₈ / t ₀₆	EA ₁₂ / EA ₀₆	EA ₁₈ EA ₁₂	EA ₁₈ EA ₀₆	SEA ₁₂ SEA ₀₆	SEA ₁₈ SEA ₁₂	SEA ₁₈ SEA ₀₆	MCF ₁₂ MCF ₀₆	MCF ₁₈ MCF ₁₂	MCF ₁₈ MCF ₀₆	CFE ₁₂ CFE ₀₆	CFE ₁₈ CFE ₁₂	CFE ₁₈ CFE ₀₆
Circular	0				3.21	1.69	5.44	1.61	1.13	1.82	3.29	1.78	5.84	1.29	1.05	1.35
	10	2	1.5	3	2.96	1.38	4.09	1.48	0.92	1.37	2.91	1.87	5.44	1.15	1.09	1.25
	20				2.93	1.18	3.46	1.47	0.78	1.15	2.78	1.86	5.17	1.36	1.12	1.52
	30				2.81	1.55	4.35	1.41	1.03	1.46	2.89	1.90	5.50	1.05	1.05	1.11
Hexagon	0				2.78	1.73	4.81	1.39	1.16	1.60	2.92	1.91	5.59	1.00	0.96	0.96
	10	2	1.5	3	2.85	1.82	5.20	1.42	1.21	1.73	2.87	1.78	5.10	1.31	0.89	1.16
	20				2.93	1.88	5.51	1.47	1.25	1.84	2.91	1.86	5.42	1.01	1.00	1.01
	30				2.75	1.94	5.34	1.37	1.30	1.78	2.80	1.91	5.36	0.92	1.04	0.96
Multicell	0				2.93	1.86	5.46	1.47	1.24	1.81	2.91	1.86	5.40	0.88	1.05	0.93
	10	2	1.5	3	2.84	1.88	5.34	1.43	1.25	1.78	2.83	1.89	5.35	1.04	0.98	1.02
	20				3.24	1.74	5.66	1.62	1.17	1.89	3.22	1.76	5.67	1.06	0.96	1.02
	30				2.85	1.97	5.61	1.43	1.31	1.86	2.78	1.99	5.52	0.90	0.97	0.87
		Average:			2.93	1.72	5.02	1.46	1.15	1.67	2.93	1.86	5.45	1.08	1.01	1.10
		Maximum:			3.24	1.97	5.66	1.62	1.31	1.89	3.29	1.99	5.84	1.36	1.12	1.52
		Minimum:			2.75	1.18	3.46	1.37	0.78	1.15	2.78	1.76	5.10	0.88	0.89	0.87

5.3 Highlights and Contributions of Work

The major contributions of this thesis thus can be summarized as follows:

- Designation of energy absorber in concept of energy dissipating energy absorbing device.
- Energy absorbing device impacted by various angle of loading.
- Extensive dynamic analysis of the proposed design.
- A study of honeycomb fillers made from different size, geometry, thickness and angle of loading. Hence enriching the databank on the axial and oblique crush response of honeycomb fillers by dynamic impact loading.

5.4 Future Work

The recommendations for future works are suggested below:

Dynamic impact test: It is suggested to improve the dynamic impact on crush response of honeycomb filler. Various impact mass and impact velocities are to be investigated. Different angles of loading also are investigated since not all impact.

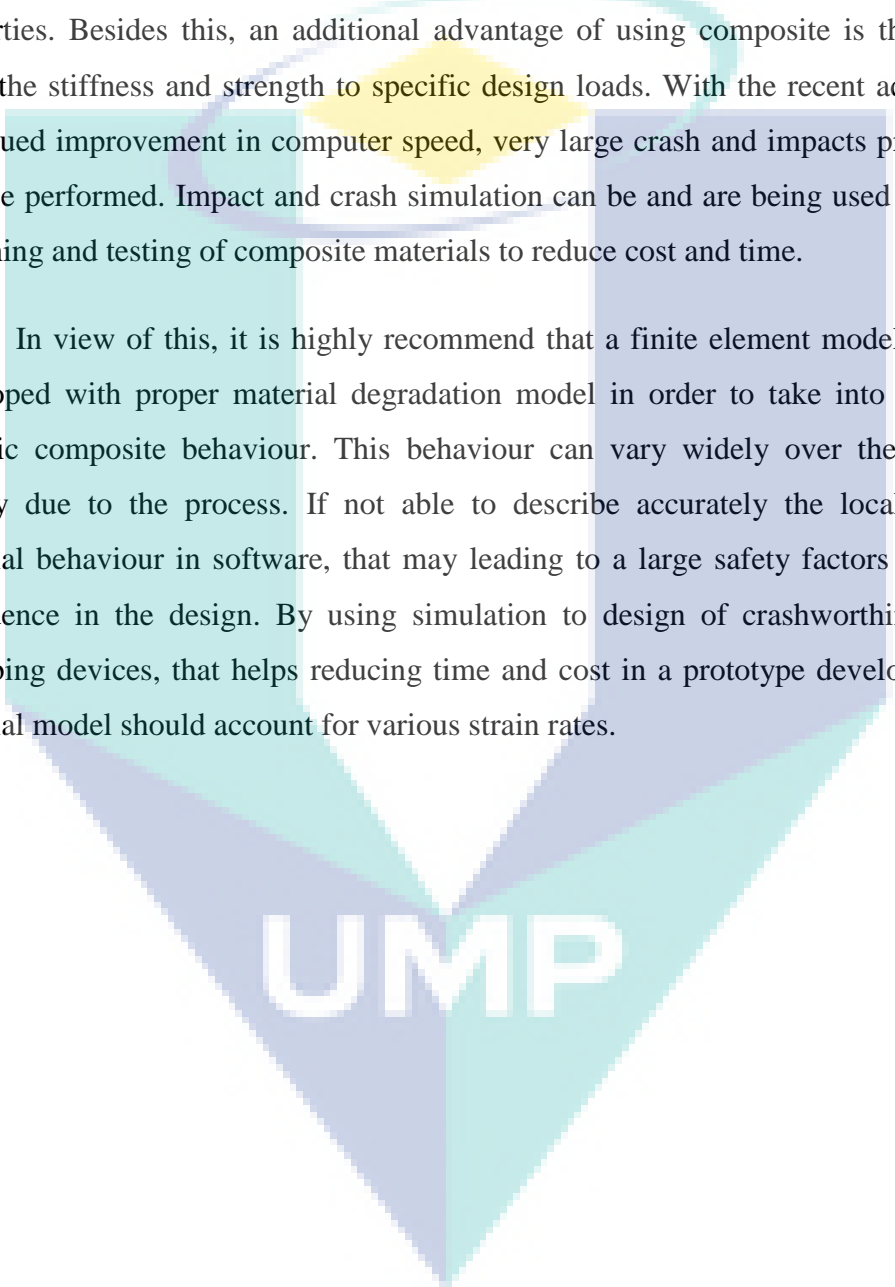
Optimization study: To optimize the current proposed design with respect to its thickness, dimension of single cell and various geometry design. Trigger mechanism design could be an alternative to enhance the overall performance of the honeycomb filler. Trigger mechanisms are “design faults” within a structure that will fail first and promote progressive crushing. It is usually designed into structure.

Finite Element Analysis on composite material: Finite element analysis is the way of the future since it is the part of the virtual prototype process chain. Most major design decisions are based on finite element because its robustness and well established performance. Many of the crashworthiness investigation models used conventional metals studied by software of FE such as NX NASTRAN, PAM CRASH ANSYS and LS DYNA. For such materials, there is a well-established non-linear material constitutive law that takes into account strain rates and strain hardening. These models

have been tested and verified and hence are widely used by automotive industries with high confidence.

Composite materials have been increasingly used in the military, automotive, aerospace and marine applications over the last two decades. The use of composite material is very attractive because their outstanding strength, stiffness and light weight properties. Besides this, an additional advantage of using composite is the ability to tailor the stiffness and strength to specific design loads. With the recent advances and continued improvement in computer speed, very large crash and impacts problems can now be performed. Impact and crash simulation can be and are being used as an aid in designing and testing of composite materials to reduce cost and time.

In view of this, it is highly recommend that a finite element model need to be developed with proper material degradation model in order to take into account the specific composite behaviour. This behaviour can vary widely over the entire part mainly due to the process. If not able to describe accurately the local composite material behaviour in software, that may leading to a large safety factors and lack of confidence in the design. By using simulation to design of crashworthiness energy absorbing devices, that helps reducing time and cost in a prototype development. The material model should account for various strain rates.



UMP

REFERENCES

- Aaron, V., Adibi-Sedeh, A. H., Nagarajan, H., and Bahr, B. (2003). Determination of strength characteristics of aluminum honeycomb material subjected to out-of-plane compression using finite element analysis. *Advances in Structures*, 427–432.
- Abaqus Analysis User's Manual 6.10. (2010). *Dassault Systèmes*. Retrieved from <https://www.sharcnet.ca/Software/Abaqus610/Documentation/docs/v6.10/books/usb/default.htm?startat=pt06ch26s06alm16.html>
- Abramowicz, W. (1981). Simplified crushing analysis of thin-walled columns and beams. *Engineering Transactions*, 29: 3–27.
- Abramowicz, W. (1983). The effective crushing distance in axially compressed thin-walled metal columns. *International Journal of Impact Engineering*, 1(3): 309–317.
- Abramowicz, W., and Jones, N. (1984). Dynamic axial crushing of square tubes. *International Journal of Impact Engineering*, 2(2): 179–208.
- Abramowicz, W., and Jones, N. (1986). Dynamic progressive buckling of circular and square tubes. *International Journal of Impact Engineering*, 4(4): 243–270.
- Abramowicz, W., and Wierzbicki, T. (1989). Axial crushing of multicorner sheet metal columns. *Journal of Applied Mechanics*, 56(1): 113–120.
- Ahmad, Z., and Thambiratnam, D. P. (2009). Dynamic computer simulation and energy absorption of foam-filled conical tubes under axial impact loading. *Computers & Structures*, 87(3–4): 186–197.
- Ahmad, Z., Thambiratnam, D. P., and Tan, A. C. C. (2010). Dynamic energy absorption characteristics of foam-filled conical tubes under oblique impact loading. *International Journal of Impact Engineering*, 37(5): 475–488.
- Akerstrom, T., and Wierzbicki, T. (1977). Dynamic crushing of strain rate sensitive box columns. In *SAE Technical Papers* (p. SAE Paper No. 770592). Southfield, Michigan, April 18-20: In Second International Conference on Vehicle Structural Mechanics.
- Aktay, L., Kröplin, B.-H., Toksoy, A. K., and Güden, M. (2008). Finite element and coupled finite element/smooth particle hydrodynamics modeling of the quasi-static crushing of empty and foam-filled single, bitubular and constraint hexagonal- and square-packed aluminum tubes. *Materials & Design*, 29(5): 952–962.
- Alexander, J. M. (1960). An approximate analysis of the collapse of thin cylindrical shells under axial loading. *Quarterly Journal of Mechanics and Applied Mathematics*, 13(1): 10–15.

- Alghamdi, A. A. A. (2001). Collapsible impact energy absorbers: An overview. *Thin-Walled Structures*, 39(2): 189–213.
- Asanjarani, A., Dibajian, S. H., and Mahdian, A. (2017). Multi-objective crashworthiness optimization of tapered thin-walled square tubes with indentations. *Thin-Walled Structures*, 116: 26–36.
- Avalle, M., Belingardi, G., and Montanini, R. (2001). Characterization of polymeric structural foams under compressive impact loading by means of energy-absorption diagram. *International Journal of Impact Engineering*, 25(5): 455–472.
- Baroutaji, A., Sajjia, M., and Olabi, A.-G. (2017). On the crashworthiness performance of thin-walled energy absorbers: Recent advances and future developments. *Thin-Walled Structures*, 118: 137–163.
- Bi, J., Fang, H., Wang, Q., and Ren, X. (2010). Modeling and optimization of foam-filled thin-walled columns for crashworthiness designs. *Finite Elements in Analysis and Design*, 46(9): 698–709.
- Carruthers, J. J., Kettle, A. P., and Robinson, A. M. (1998). Energy absorption capability and crashworthiness of composite material structures: A review. *Applied Mechanics Reviews*, 51(10): 635–649.
- Chen, W., and Wierzbicki, T. (2001). Relative merits of single-cell, multi-cell and foam-filled thin-walled structures in energy absorption. *Thin-Walled Structures*, 39(4): 287–306.
- Chou, C. (1998). *Honeycomb materials models for simulating responses of foams*. MD-48, AEC, Ford Motor Company.
- Chung, J., and Waas, A. M. (2000). The inplane elastic properties of circular cell and elliptical cell honeycombs. *Acta Mechanica*, 144(1–2): 29–42.
- Chung, Jaeung, and Waas, A. M. (2002)a. Compressive response of circular cell polycarbonate honeycombs under inplane biaxial static and dynamic loading. Part I: experiments. *International Journal of Impact Engineering*, 27(7): 729–754.
- Chung, Jaeung, and Waas, A. M. (2002)b. Compressive response of honeycombs Under in-plane uniaxial static and dynamic loading, part 2: Simulations. *AIAA Journal*, 40(5): 974–980.
- Corex-Honeycomb. (2018). Aluminium Honeycomb core material. Retrieved from <https://corex-honeycomb.co.uk/products-and-services/aluminium-honeycomb/>
- Costas, M., Morin, D., Langseth, M., Romera, L., and Díaz, J. (2016). Axial crushing of aluminum extrusions filled with PET foam and GFRP. An experimental investigation. *Thin-Walled Structures*, 99: 45–57.

- Cowper, G., and Symonds, P. (1957). Strain hardening and strain-rate effects in the impact loading of cantilever beam. *Brown University Division of Applied Mathematics*, 1–46.
- Crutzen, Y., Inzaghi, A., Mogilevsky, M., and Albertini, C. (1996). Computer modelling of the energy absorption process in box-type structures under oblique impact. *Automotive Automation Limited (UK)*, 1293–1298.
- Daneshi, G. ., and Hosseinipour, S. . (2002). Grooves effect on crashworthiness characteristics of thin-walled tubes under axial compression. *Materials & Design*, 23(7): 611–617.
- Deqiang, S., Weihong, Z., and Yanbin, W. (2010). Mean out-of-plane dynamic plateau stresses of hexagonal honeycomb cores under impact loadings. *Composite Structures*, 92(11): 2609–2621.
- Djamaluddin, F., Abdullah, S., and Ariffin, A. (2015). Multi objective optimization of foam-filled circular tubes for quasi-static and dynamic responses. *Latin American Journal*, 12(6): 1126–1143.
- Djamaluddin, F., Abdullah, S., Ariffin, A. K., and Nopiah, Z. M. (2015). Non-linear finite element analysis of bitubal circular tubes for progressive and bending collapses. *International Journal of Mechanical Sciences*, 99: 228–236.
- Eskandarian, A., Marzougui, D., and Bedewi, N. E. (1997). Finite element model and validation of a surrogate crash test vehicle for impacts with roadside objects. *International Journal of Crashworthiness*, 2(3): 239–258.
- Evans, L. (1989). Passive compared to active approaches to reducing occupant fatalities. In *12th international conference on experimental safety vehicles* (pp. 1–18).
- Evans, L. (2001). Causal influence of car mass and size on driver fatality risk. *American Journal of Public Health*, 91(7): 1076–1081.
- Fang, J., Gao, Y., Sun, G., Qiu, N., and Li, Q. (2015). On design of multi-cell tubes under axial and oblique impact loads. *Thin-Walled Structures*, 95: 115–126.
- Galib, D. A., and Limam, A. (2004). Experimental and numerical investigation of static and dynamic axial crushing of circular aluminum tubes. *Thin-Walled Structures*, 42(8): 1103–1137.
- Gameiro, C. P., and Cirne, J. (2007). Dynamic axial crushing of short to long circular aluminium tubes with agglomerate cork filler. *International Journal of Mechanical Sciences*, 49(9): 1029–1037.
- Guillow, S. R., Lu, G., and Grzebieta, R. H. (2001). Quasi-static axial compression of thin-walled circular aluminium tubes. *International Journal of Mechanical Sciences*, 43(9): 2103–2123.

- Han, D. C., and Park, S. H. (1999). Collapse behavior of square thin-walled columns subjected to oblique loads. *Thin-Walled Structures*, 35(3): 167–184.
- Hanssen, A. G., Langseth, M., and Hopperstad, O. S. (2000). Static and dynamic crushing of square aluminium extrusions with aluminium foam filler. *International Journal of Impact Engineering*, 24(4): 347–383.
- Hayduk, R. J., and Wierzbicki, T. (1984). Extensional collapse modes of structural members. *Computers & Structures*, 18(3): 447–458.
- He, Q., Feng, J., Zhou, H., and Tian, G. (2018). Numerical study on the dynamic behavior of circular honeycomb structure with concentrated filling inclusions defects. *Journal of Mechanical Science and Technology*, 32(8): 3727–3735.
- HKS. (2006). Getting Started with ABAQUS. *Hibbitt, Karlsson & Sorensen, Inc.* Retrieved from https://books.google.com.my/books/about/Getting_Started_with_ABAQUS_Standard.html?id=Qo4YAQAAMAAJ&redir_esc=y
- Hong, S.-T., Pan, J., Tyan, T., and Prasad, P. (2008). Dynamic crush behaviors of aluminum honeycomb specimens under compression dominant inclined loads. *International Journal of Plasticity*, 24(1): 89–117.
- Hou, S., Li, Q., Long, S., Yang, X., and Li, W. (2008). Multiobjective optimization of multi-cell sections for the crashworthiness design. *International Journal of Impact Engineering*, 35(11): 1355–1367.
- Hu, L. L., He, X. L., Wu, G. P., and Yu, T. X. (2015). Dynamic crushing of the circular-celled honeycombs under out-of-plane impact. *International Journal of Impact Engineering*, 75: 150–161.
- Hu, L. L., Yu, T. X., Gao, Z. Y., and Huang, X. Q. (2008). The inhomogeneous deformation of polycarbonate circular honeycombs under in-plane compression. *International Journal of Mechanical Sciences*, 50(7): 1224–1236.
- Hui, D. (1986). Design of beneficial geometric imperfections for elastic collapse of thin-walled box columns. *International Journal of Mechanical Sciences*, 28(3): 163–172.
- Ismail, A. (2008). Energy absorption of foam-filled steel extrusion under quasi-static oblique loading. *International Journal of Engineering and Technology*, 5(1): 11–24.
- Jacob, G. C., Fellers, J. F., Simunovic, S., and Starbuck, J. M. (2002). Energy absorption in polymer composites for automotive crashworthiness. *Journal of Composite Materials*, 36(7): 813–850.
- Jacob, G. C. G. C., Starbuck, J. M. M., Simunovic, S., and Fellers, J. F. J. F. (2003). Energy absorption in glass-reinforced continuous strand mat composites. *Journal of Applied Polymer Science*, 90(12): 3222–3232.

- Jensen, Ø., Langseth, M., and Hopperstad, O. S. (2004). Experimental investigations on the behaviour of short to long square aluminium tubes subjected to axial loading. *International Journal of Impact Engineering*, 30(8–9): 973–1003.
- Johnson, W., and Reid, S. R. (1978). Metallic energy dissipating systems. *Applied Mechanics Reviews*, 31(3): 277–287.
- Johnson, W., and Soden, P. (1977). Inextensional collapse of thin-walled tubes under axial compression. *The Journal of Strain*, 12(4): 317–330.
- Jusuf, A., Dirgantara, T., Gunawan, L., and Putra, I. S. (2015). Crashworthiness analysis of multi-cell prismatic structures. *International Journal of Impact Engineering*, 78: 34–50.
- Kecman, D. (1983). Bending collapse of rectangular and square section tubes. *International Journal of Mechanical Sciences*, 25(9–10): 623–636.
- Khan, M. K., Baig, T., and Mirza, S. (2012). Experimental investigation of in-plane and out-of-plane crushing of aluminum honeycomb. *Materials Science and Engineering: A*, 539: 135–142.
- Kim, H.-S. (2001). *Crash behavior of three dimensional thin-walled structures under combined loading*. Massachusetts Institute of Technology.
- Kim, H.-S. (2002). New extruded multi-cell aluminum profile for maximum crash energy absorption and weight efficiency. *Thin-Walled Structures*, 40(4): 311–327.
- Kim, H.-S., and Wierzbicki, T. (2000). Numerical and analytical study on deep biaxial bending collapse of thin-walled beams. *International Journal of Mechanical Sciences*, 42(10): 1947–1970.
- Kim, H.-S., and Wierzbicki, T. (2001). Crush behavior of thin-walled prismatic columns under combined bending and compression. *Computers & Structures*, 79(15): 1417–1432.
- Langseth, M., and Hopperstad, O. S. (1996). Static and dynamic axial crushing of square thin-walled aluminium extrusions. *International Journal of Impact Engineering*, 18(7–8): 949–968.
- Langseth, M., Hopperstad, O. S., and Berstad, T. (1999). Crashworthiness of aluminium extrusions: validation of numerical simulation, effect of mass ratio and impact velocity. *International Journal of Impact Engineering*, 22(9–10): 829–854.
- Li, Z., Rakheja, S., and Shangguan, W.-B. (2019). Study on crushing behaviors of foam-filled thin-walled square tubes with different types and number of initiators under multiple angle loads. *Thin-Walled Structures*, 145: 106376.
- Liang, S., and Chen, H. L. (2006). Investigation on the square cell honeycomb structures under axial loading. *Composite Structures*, 72(4): 446–454.

- Lin, T.-C., Chen, T.-J., and Huang, J.-S. (2012). In-plane elastic constants and strengths of circular cell honeycombs. *Composites Science and Technology*, 72(12): 1380–1386.
- Liu, L., Wang, H., and Guan, Z. (2015). Experimental and numerical study on the mechanical response of Nomex honeycomb core under transverse loading. *Composite Structures*, 121: 304–314.
- Liu, Ying, and Zhang, X.-C. (2009). The influence of cell micro-topology on the in-plane dynamic crushing of honeycombs. *International Journal of Impact Engineering*, 36(1): 98–109.
- Liu, Yucheng. (2008). Crashworthiness design of multi-corner thin-walled columns. *Thin-Walled Structures*, 46(12): 1329–1337.
- Lu, G., and Yu, T. (2003). Energy absorption of structures and materials, CRC Press.
- Mahmoodi, A., Shojaeefard, M. H., and Saeidi Googarchin, H. (2016). Theoretical development and numerical investigation on energy absorption behavior of tapered multi-cell tubes. *Thin-Walled Structures*, 102: 98–110.
- Malaysia New Vehicles Registered - Road Transport Department Malaysia. (2019). *Trading Economics*. Retrieved from <https://tradingeconomics.com/malaysia/car-registrations>
- Mantena, P. R., and Mann, R. (2003). Impact and dynamic response of high-density structural foams used as filler inside circular steel tube. *Composite Structures*, 61(4): 291–302.
- Mellquist, E. C., and Waas, A. M. (2004). Size effects in the crushing of honeycomb structures. In *Collection of Technical Papers - AIAA/ASME/ASCE/AHS/ASC Structures, Structural Dynamics and Materials Conference* (Vol. 2, pp. 1388–1401). Reston, Virginia: American Institute of Aeronautics and Astronautics.
- Ministry of Transport Malaysia. (2017). Annual Transport Statistics. Retrieved from <http://www.mot.gov.my/en/resources/yearly-statistic>
- Mirfendereski, L., Salimi, M., and Ziaei-Rad, S. (2008). Parametric study and numerical analysis of empty and foam-filled thin-walled tubes under static and dynamic loadings. *International Journal of Mechanical Sciences*, 50(6): 1042–1057.
- Mohammadiha, O., Beheshti, H., and Aboutalebi, F. H. (2015). Multi-objective optimisation of functionally graded honeycomb filled crash boxes under oblique impact loading. *International Journal of Crashworthiness*, 20(1): 44–59.
- Mozafari, H., Khatami, S., Molatefi, H., Crupi, V., Epasto, G., and Guglielmino, E. (2016). Finite element analysis of foam-filled honeycomb structures under impact loading and crashworthiness design. *International Journal of Crashworthiness*, 21(2): 148–160.

- Nagel, G. M., and Thambiratnam, D. P. (2004). A numerical study on the impact response and energy absorption of tapered thin-walled tubes. *International Journal of Mechanical Sciences*, 46(2): 201–216.
- Nagel, G. M., and Thambiratnam, D. P. (2006). Dynamic simulation and energy absorption of tapered thin-walled tubes under oblique impact loading. *International Journal of Impact Engineering*, 32(10): 1595–1620.
- Najafi, A., and Rais-Rohani, M. (2011). Mechanics of axial plastic collapse in multi-cell, multi-corner crush tubes. *Thin-Walled Structures*, 49(1): 1–12.
- National Highway Traffic Safety Administration - NHTSA. (2015). Traffic Safety Facts 2014: A Compilation of Motor Vehicle Crash Data from the Fatality Analysis Reporting System and the General Estimates System. Retrieved from <https://crashstats.nhtsa.dot.gov/Api/Public/Publication/812261>
- Nia, A. A., and Parsapour, M. (2013). An investigation on the energy absorption characteristics of multi-cell square tubes. *Thin-Walled Structures*, 68: 26–34.
- Nia, A. A., and Sadeghi, M. Z. (2013). An experimental investigation on the effect of strain rate on the behaviour of bare and foam-filled aluminium honeycombs. *Materials & Design (1980-2015)*, 52: 748–756.
- Ohkubo, Y., Akamatsu, T., and Shirasawa, K. (1974). Mean crushing strength of closed-hat section members. In *SAE Technical Papers* (p. 740040). Detroit: SAE Technical Paper.
- Olabi, A. G., Morris, E., Hashmi, M. S. J., and Gilchrist, M. D. (2008). Optimised design of nested circular tube energy absorbers under lateral impact loading. *International Journal of Mechanical Sciences*, 50(1): 104–116.
- Oruganti, R. K., and Ghosh, A. K. (2008). FEM analysis of transverse creep in honeycomb structures. *Acta Materialia*, 56(4): 726–735.
- Paik, J. K., Thayamballi, A. K., and Kim, G. S. (1999). The strength characteristics of aluminum honeycomb sandwich panels. *Thin-Walled Structures*, 35(3): 205–231.
- Pirmohammad, S., and Marzdashti, S. E. (2016). Crushing behavior of new designed multi-cell members subjected to axial and oblique quasi-static loads. *Thin-Walled Structures*, 108: 291–304.
- Pletschen, B., Herrmann, R., Kallina, I., and Zeidler, F. (1990). The significance of frontal offset collisions in real world accidents. In *SAE Technical Papers* (p. 900411).
- Qin, Q. H., and Wang, T. J. (2009). A theoretical analysis of the dynamic response of metallic sandwich beam under impulsive loading. *European Journal of Mechanics, A/Solids*, 28(5): 1014–1025.

- Qin, Q. H., Wang, T. J., and Zhao, S. Z. (2009). Large deflections of metallic sandwich and monolithic beams under locally impulsive loading. *International Journal of Mechanical Sciences*, 51(11–12): 752–773.
- Qiu, N., Gao, Y., Fang, J., Feng, Z., Sun, G., and Li, Q. (2015). Crashworthiness analysis and design of multi-cell hexagonal columns under multiple loading cases. *Finite Elements in Analysis and Design*, 104: 89–101.
- Reid, S. R., and Reddy, T. Y. (1986). Static and dynamic crushing of tapered sheet metal tubes of rectangular cross-section. *International Journal of Mechanical Sciences*, 28(9): 623–637.
- Reyes, A., Hopperstad, O. S., and Langseth, M. (2004). Aluminum foam-filled extrusions subjected to oblique loading: experimental and numerical study. *International Journal of Solids and Structures*, 41(5–6): 1645–1675.
- Reyes, A., Langseth, M., and Hopperstad, O. S. (2002). Crashworthiness of aluminum extrusions subjected to oblique loading: experiments and numerical analyses. *International Journal of Mechanical Sciences*, 44(9): 1965–1984.
- Reyes, A., Langseth, M., and Hopperstad, O. S. (2003). Square aluminum tubes subjected to oblique loading. *International Journal of Impact Engineering*, 28(10): 1077–1106.
- Robinson, S. (1997). Simulation model verification and validation: Increasing the users' confidence. In *Winter Simulation Conference Proceedings* (pp. 53–59). IEEE Computer Society.
- Salehghaffari, S., Tajdari, M., Panahi, M., and Mokhtarnezhad, F. (2010). Attempts to improve energy absorption characteristics of circular metal tubes subjected to axial loading. *Thin-Walled Structures*, 48(6): 379–390.
- Santosa, S. P., Wierzbicki, T., Hanssen, A. G., and Langseth, M. (2000). Experimental and numerical studies of foam-filled sections. *International Journal of Impact Engineering*, 24(5): 509–534.
- Seitzberger, M., Rammerstorfer, F. G., Gradinger, R., Degischer, H. P., Blaimschein, M., and Walch, C. (2000). Experimental studies on the quasi-static axial crushing of steel columns filled with aluminium foam. *International Journal of Solids and Structures*, 37(30): 4125–4147.
- Shariatpanahi, M., Masoumi, A., and Ataei, A. (2008). Optimum design of partially tapered rectangular thin-walled tubes in axial crushing. *Proceedings of the Institution of Mechanical Engineers, Part B: Journal of Engineering Manufacture*, 222(2): 285–291.
- Sheriff, N. M., Gupta, N. K., Velmurugan, R., and Shanmugapriyan, N. (2008). Optimization of thin conical frusta for impact energy absorption. *Thin-Walled Structures*, 46(6): 653–666.

- Shiravand, A., and Asgari, M. (2019). Hybrid metal-composite conical tubes for energy absorption; theoretical development and numerical simulation. *Thin-Walled Structures*, 145: 106442.
- Singace, A. ., El-Sobky, H., and Petsios, M. (2001). Influence of end constraints on the collapse of axially impacted frusta. *Thin-Walled Structures*, 39(5): 415–428.
- Song, J., and Guo, F. (2013). A comparative study on the windowed and multi-cell square tubes under axial and oblique loading. *Thin-Walled Structures*, 66: 9–14.
- Stucki, S. L., Hollowell, W. T., and Fessahaie, O. (1998). Determination of frontal offset test conditions based on crash data. *National Highway Traffic Safety Administration*, (208).
- Summers, S. M., Prasad, A., and Hollowell, W. T. (2001). NHTSA's Research Program for Vehicle Aggressivity and Fleet Compatibility. *NHTSA Research and Development Web site*. Retrieved from <https://www.nrd.nhtsa.dot.gov/pdf/esv/esv17/Proceed/00179.pdf>
- Sun, G., Jiang, H., Fang, J., Li, G., and Li, Q. (2016). Crashworthiness of vertex based hierarchical honeycombs in out-of-plane impact. *Materials & Design*, 110: 705–719.
- Tabacu, S. (2016). Analysis of circular tubes with rectangular multi-cell insert under oblique impact loads. *Thin-Walled Structures*, 106: 129–147.
- Tang, Z., Liu, S., and Zhang, Z. (2013). Analysis of energy absorption characteristics of cylindrical multi-cell columns. *Thin-Walled Structures*, 62: 75–84.
- Tani, M., and Funahashi, A. (1978). Energy absorption by the plastic deformation of body structural members. In *SAE Technical Papers*.
- Tarlochan, F. (2007). *Design, fabrication and evaluation of composite sandwich panels for crashworthiness*. Universiti Putra Malaysia, Malaysia.
- Tho, C. H. (2006). Crashworthiness design optimization using surrogate models, (August).
- Tisza, M., and Czinege, I. (2018). Comparative study of the application of steels and aluminium in lightweight production of automotive parts. *International Journal of Lightweight Materials and Manufacture*, 1(4): 229–238.
- Tolouei, R., Maher, M., and Titheridge, H. (2013). Vehicle mass and injury risk in two-car crashes: A novel methodology. *Accident Analysis and Prevention*, 50: 155–166.
- Tran, T. (2017). Crushing analysis under multiple impact loading cases for multi-cell triangular tubes. *Thin-Walled Structures*, 113: 262–272.

- Triantos, D., and Michaels, M. (1999). Design and fabrication of an aluminum engine cradle for a general motors vehicle. In *SAE Technical Papers* (p. 9). SAE Technical Paper Series.
- Usta, F., and Turkmen, H. S. (2017). Crash behavior of nested tube structures with various cross sections. In *2017 8th International Conference on Recent Advances in Space Technologies (RAST)* (pp. 23–27). IEEE.
- Wallentowitz, H., and Adam, H. (1996). Predicting the crashworthiness of vehicle structures made by lightweight design materials and innovative joining methods. *International Journal of Crashworthiness*, 163–180.
- Wierzbicki, T., and Abramowicz, W. (1983). On the crushing mechanics of thin-walled structures. *Journal of Applied Mechanics, Transactions ASME*, 50(4): 727–734.
- Wierzbicki, Tomasz. (1983). Crushing analysis of metal honeycombs. *International Journal of Impact Engineering*, 1(2): 157–174.
- Wierzbicki, Tomasz, and Abramowicz, W. (1989). *The Mechanics of Deep Plastic Collapse of Thin-walled Structures. Structural Failure*. New York: Wiley.
- Wierzbicki, Tomasz, and Bhat, S. (1986). A moving hinge solution for axisymmetric crushing of tubes. *International Journal of Mechanical Sciences*, 28(3): 135–151.
- Wierzbicki, Tomasz, Bhat, S., and Abramowicz, W. (1992). Alexander revisited—a two folding elements model of progressive crushing of tubes. *International Journal of Solids and Structures*, 29(24): 3269–3288.
- Wierzbicki, Tomasz, Recke, L., Abramowicz, W., Gholami, T., and Huang, J. (1994). Stress profiles in thin-walled prismatic columns subjected to crush loading-II. Bending. *Computers & Structures*, 51(6): 625–641.
- Witteman, W. J. (1999). *Improved Vehicle Crashworthiness Design by Control of the Energy Absorption for Different Collision Situations*.
- World Health Organization. (2015). *Global status report on road safety 2015*. World Health Organization. World Health Organization.
- Wu, E. (1995). Plastic buckling of metallic honeycombs. *Journal of Chinese Society of Mechanical Engineers*, 16(1): 11–20.
- Wu, E., and Jiang, W.-S. (1997). Axial crush of metallic honeycombs. *International Journal of Impact Engineering*, 19(5–6): 439–456.
- Xiang, J., and Du, J. (2017). Energy absorption characteristics of bio-inspired honeycomb structure under axial impact loading. *Materials Science and Engineering: A*, 696: 283–289.

- Xu, S., Beynon, J. H., Ruan, D., and Yu, T. X. (2012). Strength enhancement of aluminium honeycombs caused by entrapped air under dynamic out-of-plane compression. *International Journal of Impact Engineering*, 47: 1–13.
- Xu, Shanqing, Beynon, J. H., Ruan, D., and Lu, G. (2012). Experimental study of the out-of-plane dynamic compression of hexagonal honeycombs. *Composite Structures*, 94(8): 2326–2336.
- Yasui, Y. (2000). Dynamic axial crushing of multi-layer honeycomb panels and impact tensile behavior of the component members. *International Journal of Impact Engineering*, 24(6–7): 659–671.
- Yin, H., Wen, G., Hou, S., and Chen, K. (2011). Crushing analysis and multiobjective crashworthiness optimization of honeycomb-filled single and bitubular polygonal tubes. *Materials & Design*, 32(8–9): 4449–4460.
- Zarei, H., and Kröger, M. (2008). Optimum honeycomb filled crash absorber design. *Materials & Design*, 29(1): 193–204.
- Zarei, H. R., and Kröger, M. (2006). Multiobjective crashworthiness optimization of circular aluminum tubes. *Thin-Walled Structures*, 44(3): 301–308.
- Zarei, H. R., and Kröger, M. (2008). Bending behavior of empty and foam-filled beams: Structural optimization. *International Journal of Impact Engineering*, 35(6): 521–529.
- Zhang, J., and Ashby, M. F. (1992). The out-of-plane properties of honeycombs. *International Journal of Mechanical Sciences*, 34(6): 475–489.
- Zhang, X., and Cheng, G. (2007). A comparative study of energy absorption characteristics of foam-filled and multi-cell square columns. *International Journal of Impact Engineering*, 34(11): 1739–1752.
- Zhang, X., Cheng, G., You, Z., and Zhang, H. (2007). Energy absorption of axially compressed thin-walled square tubes with patterns. *Thin-Walled Structures*, 45(9): 737–746.
- Zhang, X., Cheng, G., and Zhang, H. (2006). Theoretical prediction and numerical simulation of multi-cell square thin-walled structures. *Thin-Walled Structures*, 44(11): 1185–1191.
- Zhang, X., and Zhang, H. (2013). Energy absorption of multi-cell stub columns under axial compression. *Thin-Walled Structures*, 68: 156–163.
- Zhang, Y., Lu, M., Wang, C. H., Sun, G., and Li, G. (2016). Out-of-plane crashworthiness of bio-inspired self-similar regular hierarchical honeycombs. *Composite Structures*, 144: 1–13.

Zhang, Z., Liu, S., and Tang, Z. (2009). Design optimization of cross-sectional configuration of rib-reinforced thin-walled beam. *Thin-Walled Structures*, 47(8–9): 868–878.

Zhou, J., Qin, R., and Chen, B. (2019). Energy absorption properties of multi-cell thin-walled tubes with a double surface gradient. *Thin-Walled Structures*, 145: 106386.

Zhou, W., Craig, J., and Hanagud, S. (1991). Crashworthy behavior of graphite/epoxy composite sine wave webs. In *32nd Structures, Structural Dynamics, and Materials Conference*. Reston, Virginia: American Institute of Aeronautics and Astronautics.

